

**Artificial Intelligence in Quantum Intramolecular Dynamics
with Application to a Heavy Central Mass Problem**

by

Steven Mark Lederman

In Partial Fulfillment of the Requirements
for the Degree of
Doctor of Philosophy

California Institute of Technology
Pasadena, California
1988

(Submitted November 23, 1987)

Acknowledgments

It is difficult to thank all of the wonderful people I have had the pleasure of knowing during my time at Caltech. To my advisor, Rudy Marcus, I express my appreciation for his patience when we disagreed on science, his warm and kind nature, and the time he spent with me. I am indebted to Vicente Lopez and Victor Fairen for our fruitful collaborations, which helped make my thesis work both possible and pleasurable. Another enjoyable aspect of working in the Marcus group is the members of that group. I am indebted to Paul Siders, Dave Wardlaw, Bob Cave, Joyce Lundstead, Greg Voth, Vasil Babamov, Stephen Klippenstein, Hitoshi Sumi, Lee Marshal and Walter Nadler, for your help and especially for your friendship. For all the many other people, who are too numerous to list individually, whose paths crossed mine during my stay at Caltech, there is a warm place in my heart for each of you.

My parents, Leonard and Florence, have over my years influenced and supported my educational endeavors. Because of my memory of long nights as a child being *forced* to learn to read and more recent recollections of support in my long academic career, my parents have my thanks and my deepest love.

Finally, I want to thank my original chemistry teacher, Robert George. He, more than anyone, is the reason I became a chemist rather than entering one of the many allied fields. He inspired me to enjoy chemistry as a field which can be both challenging and stimulating. He taught me to question the accepted, accept the questioned, but do so in an intelligent way.

Abstract

This dissertation consists in effect, of three parts, each involving some aspect of intramolecular vibrational relaxation. The first section contains simple approximate statistical formulas for the density of vibrational and rovibrational states by symmetry type for non-linear molecules. A modified Whitten-Rabinovitch estimate of the density of states by symmetry type for linear molecules is also derived. Sample calculations are given, which serve to demonstrate the accuracy of all formulas given. In the second section, a 4-coordinate model is presented and is used to treat the vibrational energy redistribution in a molecule with a heavy central metal atom. Local group modes are identified using perturbation theory, and their dynamical separation and importance in analyzing energy redistribution is noted. A comparison of classical and quantum calculations on the model system is also given. In the third section, artificial intelligence methods are used to treat the time-evolution of intramolecular quantum dynamics. Comparison is made of several AI search algorithms and of evaluation functions, proposed here, in an application to the study of quantum intramolecular vibrational relaxation. The methods developed are applied to an 11-coordinate heavy central mass problem and are used to treat both vibrational quantum beats and "dissipative" intramolecular energy transfer.

Table of Contents

Acknowledgments	ii
Abstract	iii
Introduction	1
Chapter 1: Densities of Vibrational States of Given Symmetry Species and Their Use in Statistical Estimates Involving Coriolis and Anharmonic Effects	8
Chapter 2: Densities of Vibrational States of Given Symmetry Species. Linear Molecules and Rovibrational States of Nonlinear Molecules	13
Chapter 3: Local Group Modes and the Dynamics of Intramolecular Energy Transfer Across a Heavy Atom	21
Chapter 4: Quantum and Classical Energy Transfer Between Ligands of a Heavy Metal Atom	32
Chapter 5: The Use of Artificial Intelligence Methods in Studying Quantum Intramolecular Vibrational Relaxation	39

Introduction

The common theme throughout this dissertation is the study of intramolecular vibrational relaxation (IVR). The thesis can be regarded as divided into three sections, each involving different aspects of IVR. Chapters 1 and 2 contain discussions of approximate density of states by symmetry type. In the second section, which comprises Chapters 3 and 4, a model is developed to investigate the problem of laser selective chemistry for the specific problem of a heavy central mass. Finally, in Chapter 5, a method is presented for using artificial intelligence for the solution of high-dimensional, quantum mechanical IVR problems.

The first chapter of this thesis is concerned with simple, statistical estimates of the density of vibrational states by symmetry type for non-linear molecules. The formulas derived are for harmonic and separable degrees of freedom in the limit of at least several quanta in each mode. (Subsequently, this work was supplemented by a clever group theoretical proof in the high temperature limit by Pechukas,¹ and by the treatment of non-separable degrees of freedom using a Monte Carlo integration and involving a solution by computer simulation.²) Since the formulas derived in Chapter 1 represent the density of vibrational states of a given symmetry type as a fraction of the total density of states, previous estimates for the total density of states, such as that of Whitten-Rabinovitch, could easily be used to estimate the density of states by symmetry type. The results presented in Chapter 1 show that the approximate, statistical formulas are accurate even at relatively low energies of vibrational excitation.

The results of Chapter 1 are extended in Chapter 2 to vibrational state densities of linear molecules and to rovibrational state densities of non-linear molecules. Non-linear rovibrational states show the same fraction of the total density of rovibrational states in each symmetry type as vibrational states. However, the statistical estimates of the rovibrational density of states proved to be more accurate at the

same excess energy than for vibrational states alone. Also, linear molecules are discussed, where the density of states by each angular momentum or symmetry type, is given in the form of a modified Whitten-Rabinovitch formula.

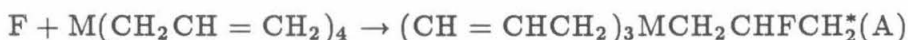
The interest in density of states by symmetry type arrives from the many types of matrix elements for which forbidden transitions can be classified by symmetry selection rules. For example, a coupling by Fermi resonance must have a component of total symmetry in the product of the two coupled states or the coupling will be zero. Thus, if only a pure Fermi resonance is involved, the number of states involved in the couplings and redistribution of energy would be the subset of the total number of states that are of the proper symmetry. Clearly, realistic coupling in multidimensional systems is more complex and may have fewer symmetry selection rules. However, in many systems, the simply symmetry selection rules serve as a good first-order approximation, which can lead to important physical insights.

Our work on the density of states of specific symmetry types has already found use in several chemical applications. For example, an estimate of the vibrational density of states by symmetry type in p-difluorobenzene leads to the conclusion that coupling of the vibrational states to the rotational manifold was probably present, since the experimental results indicated participation by a higher density of states.³ Also, the vibrational density of states by symmetry type was used to conclude that Coriolis forces were playing a role in the energy redistribution in formaldehyde.⁴ Furthermore, by using density of vibrational states by symmetry type and Fermi's Golden Rule, it was shown that the rate of IVR in anthracene was consistent with the redistribution occurring in a subset of states defined by symmetry.⁵

The second section of this thesis is ultimately related to the possibility of laser-selective chemistry when a heavy central atom is present in a molecular system. The goal of intramolecular laser-selective chemistry is to produce chemical reactions by laser excitation of molecules such that the products formed are not statistically distributed. The hope is that the short-time pulse and narrow bandwidth of lasers

can produce such specific excitations of a molecule that only the excited degrees of freedom would be involved in a chemical reaction. However, thus far this hope has not been realized for chemically interesting reactions because of the redistribution of energy occurring on a time scale that is faster than that of the reaction. The difficulty in performing laser-selective chemistry is consistent with the success of the statistical RRKM theory in predicting reaction rates.

In this context, two interesting and somewhat contradictory experiments were performed approximately five years ago. Both experiments were of the chemical activation type in which an atom was added to a double bond in a metal ligand system. This produced a vibrationally hot-free radical, and the rate of its chemical reaction was studied to see if the energy redistributed across the heavy central metal atom. In one experiment,⁶ the reaction performed was



where the rate of chemical reaction was faster than that predicted by an RRKM theory, in which the full molecular system was assumed to be involved in redistribution. This result was used to conclude that the energy remained trapped in the ligand where the initial excitation occurred. In a different experiment,⁷ the chemical reaction

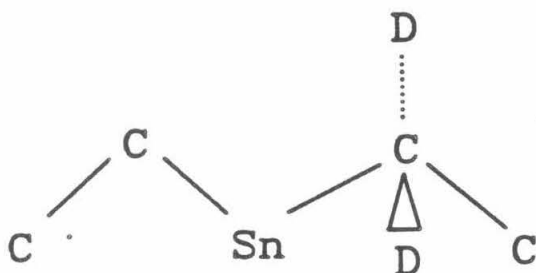


was studied. The decomposition rate observed was consistent with an RRKM calculation in which the energy was redistributed throughout the molecule, and thus no heavy central atom blockage of energy transfer across the metal atom was observed.

Several theoretical studies, the first initially in our laboratory,⁸ had been performed previously, to probe the question of blockage of energy redistribution by a

heavy central metal atom because of the experimental motivation. In the first of these, classical trajectories were used to treat the dynamics of a linear, seven-atom model $C - C - C - Sn - C - C - C$.⁸ The results showed that the amount of energy transfer depended upon the type of potential and energy of excitation. Another classical trajectory study⁹ was performed using a model $M(-C - C = C)_4$, where M was either tin or carbon. In the results, both blockage and redistribution across the central atom (M) were found, depending on the type of potential energy surface used.

In Chapters 3 and 4 of this thesis, a modification of the numerical classical mechanical, seven-atom model of Lopez and Marcus is investigated. It involves the five-atom model $C - C - Sn - C - C$, for which an analytic classical analysis was possible because of the presence of only a few degrees of freedom. The variables of the system can be separated approximately into those involving the left ($C - C - Sn$) and right ($Sn - C - C$) ligands, because of the presence of the heavy central metal atom. In our study of this model, the existence of two type of motions was found to occur in each ligand. They were termed the X and Y modes. The X mode consisted mainly of the $C - C$ motion in each ligand, whereas the Y mode was predominantly the vibration of the $C - C$ center of mass relative to the Sn. These two "local group modes" were found to be approximately dynamically separable. Excitation of the X mode was shown to cause only a slow "transfer" of energy across the central atom, whereas excitation of the Y mode showed, in contrast, a rapid energy transfer across the metal atom. These analytic results were shown to agree with the classical and quantum calculations. On the basis of these results, a model



was developed. Its intramolecular classical and quantum dynamics will be discussed in a future article. Several quantum results for this model are presented in Chapter 5.

In the final chapter of this thesis, Chapter 5, the question of accurate quantum mechanical calculations of IVR in high-dimensional systems is addressed. A commonly encountered problem in performing quantum calculations in IVR is the treatment of the very large number of states that must be considered. However, of the large number of states that are present in many molecules, only a small subset might be involved in any particular excitation of the system. This subset is determined, in part, by energetics, and in part, by couplings. Thus, a crucial question in accurate quantum mechanical modeling of large molecules is determining the important subset of zeroth order states.

The redistribution of a vibrational excitation can be viewed as a sequential process where the probability flows from one state to another via various paths. Each state involved in the flow is often crucial, such that if any state in a path were removed from the description of the process, the outcome would be dramatically changed. Artificial Intelligence (AI) search methods for finding important paths are particularly well suited to this problem. The use of AI had already been used successfully in the field of multiphoton dynamics.¹⁰

Two important questions in applying AI search methods to quantum IVR problems are the search algorithm and evaluation function. The search algorithm determines in what order the possible states are found, and the evaluation function determines how an estimate of the importance of different paths is assigned. Several different search algorithms and evaluation functions are investigated in Chapter 5 and applied to the latest heavy mass model for quantitative comparisons. These results show the accuracy and dramatic reduction in the number of states needed to be considered through the use of AI search methods. The development of AI methods for solving quantum IVR problems could represent a significant step for-

ward in the study of high dimension IVR problems because it is a reliable, efficient, and easily implemented technique.

References

- ¹ P. Pechukas, J. Phys. Chem., **88**, 828 (1984).
- ² See, for example, J.R. Barker, J. Phys. Chem., **91**, 3849 (1987).
- ³ R.A. Coveleskie, D.A. Dolson and C.S. Parmenter, J. Phys. Chem., **89**, 655 (1985).
- ⁴ H.L. Dai, C.L. Korpa, J.L. Kinsey and R.W. Field, J. Chem. Phys., **82**, 1688 (1985).
- ⁵ P.M. Felker and A.H. Zewail, Chem. Phys. Lett., **108**, 303 (1984).
- ⁶ P. Rogers, D.C. Montague, J.P. Frank, S.C. Tyler and F.S. Rowland, Chem. Phys. Lett., **89**, 9 (1982); P.J. Rogers, J.I. Selco and F.S. Rowland, Chem. Phys. Lett., **97**, 313 (1983).
- ⁷ S.P. Wrigley and B.S. Rabinovitch, Chem Phys. Lett., **98**, 386 (1983); S.P. Wrigley, D.A. Oswald and B.S. Rabinovitch, Chem. Phys. Lett., **104**, 521 (1984).
- ⁸ V. Lopez and R.A. Marcus, Chem. Phys. Lett., **93**, 232 (1982).
- ⁹ K.N. Swamy and W.L. Hase, J. Chem. Phys., **82**, 123 (1985).
- ¹⁰ J.V. Tietz and S.-I. Chu, Chem. Phys. Lett., **101**, 446 (1983); J. Chang and R.E. Wyatt, Chem. Phys. Lett., **121**, 307 (1985); *ibid.*, J. Chem. Phys., **85**, 1826 (1986).

**Chapter 1: Densities of Vibrational States of Given Symmetry Species
and Their Use in Statistical Estimates Involving Coriolis
and Anharmonic Effects**

[The text of this chapter appeared in: S. M. Lederman, J. H. Runnels and R. A. Marcus, *J. Phys. Chem.*, **87**, 4364 (1983).]

Densities of Vibrational States of Given Symmetry Species and Their Use in Statistical Estimates Involving Coriolis and Anharmonic Effects

Steven M. Lederman, John H. Runnels, and R. A. Marcus*

Arthur Amos Noyes Laboratory of Chemical Physics,¹ California Institute of Technology, Pasadena, California 91125
(Received: August 24, 1983)

A simple approximate statistical formula for densities of vibrational states of given symmetry is presented. The formula becomes increasingly exact at higher vibrational energies. Application to Coriolis and anharmonic effects is discussed.

1. Introduction

The symmetry of a vibrational quantum state affects its coupling to other vibrational states via anharmonic and Coriolis forces, and thereby can influence intramolecular relaxation. In recent experiments on vibronic excitation of molecules, specific vibrational modes of given symmetry have been excited in an electronically excited state and their spectroscopic behavior has been investigated. Coriolis coupling between degenerate or nearly degenerate states¹⁻⁴ and between nondegenerate states⁵⁻⁸ has been invoked.

It is of interest to know the density of vibrational states of the desired symmetry for such coupling to a particular vibrational state. For example, a statistical theory of density of states of a given symmetry has been used as a possible explanation of the disappearance, via Coriolis coupling, of certain spectral lines.^{2,3} This statistical approach involved direct counting of combination and overtone states having the specified symmetry. In the course of our study we noticed a striking regularity in this counting of states. We present here a simple statistical approximation for the density of states of any specified symmetry species, eq 2. We first illustrate it for several molecules of different symmetry types (section 2) and then give an approximate derivation in section 3. Equation 2 becomes increasingly exact with increasing vibrational energy. Applications are noted in section 4.

2. Results

All exact results were determined by precise computer counting of harmonic states. The number of states of a given symmetry species was determined by allowing any combination of overtones (and fundamentals). All quantum states were considered with equal a priori probability and standard rules were used to determine the symmetry species of the various resultant states.⁹ Degeneracy was allowed for, but all energy splittings due to perturbations were ignored and energies were assigned their unperturbed values. The sum of the number of states of each symmetry species with this counting method represents the total number of states at any energy. A check of values was performed by comparing this total number of states to the semiclassical Whitten-Rabinovitch approximation.¹⁰ At the energies investigated the total density of states (removing scatter and oscillations) was negligibly different from the Whitten-Rabinovitch estimate.

Tables I-III list the results for several representative molecules for various energies ϵ in excess of the zero-point energy. The values reported are the actual number $N(\Gamma)$ of harmonic states of each symmetry species Γ (equivalently, of each irreducible representation) with excess en-

TABLE I: Numbers and Ratio of States of Benzene for Each Representation at Various Excess Energies^a

Γ	$\epsilon = 2004$ cm ⁻¹		$\epsilon = 4009$ cm ⁻¹		$\epsilon = 6013$ cm ⁻¹	
	$N(\Gamma)$	$24\gamma(\Gamma)$	$N(\Gamma)$	$24\gamma(\Gamma)$	$N(\Gamma)$	$24\gamma(\Gamma)$
a _{1g}	99	1.39	10 759	1.03	508 350	1.00
a _{2g}	67	0.94	10 304	0.99	504 540	1.00
b _{1g}	47	0.66	10 122	0.97	503 872	1.00
b _{2g}	71	1.00	10 499	1.01	507 273	1.00
a _{1u}	73	1.03	10 387	1.00	506 161	1.00
a _{2u}	81	1.14	10 533	1.01	507 388	1.00
b _{1u}	71	1.00	10 425	1.00	506 267	1.00
b _{2u}	62	0.87	10 292	0.99	505 311	1.00
e _{1g}	236	3.32	41 210	3.96	2 022 314	4.00
e _{2g}	330	4.64	42 124	4.04	2 025 738	4.00
e _{1u}	262	3.69	41 440	3.98	2 023 098	4.00
e _{2u}	306	4.31	41 836	4.02	2 027 070	4.00

^a The symbols are defined in the text: $\gamma(\Gamma)$ equals $N(\Gamma)/N$. The zero-point energy is 20 034 cm⁻¹. The number 24 is introduced to make clearer the relations among the γ 's.

TABLE II: Numbers and Ratio of States of Methane for Each Representation at Various Excess Energies^a

Γ	$\epsilon = 9883$ cm ⁻¹		$\epsilon = 19 766$ cm ⁻¹		$\epsilon = 29 648$ cm ⁻¹	
	$N(\Gamma)$	$24\gamma(\Gamma)$	$N(\Gamma)$	$24\gamma(\Gamma)$	$N(\Gamma)$	$24\gamma(\Gamma)$
a ₁	83	1.52	3 131	1.12	41 114	1.05
a ₂	38	0.70	2 545	0.91	37 687	0.96
e	236	4.33	11 326	4.06	157 536	4.02
t ₁	408	7.49	24 063	8.64	346 749	8.85
t ₂	543	9.96	25 812	9.26	356 985	9.11

^a See footnote to Table I. Zero-point energy is 9882 cm⁻¹.

TABLE III: Numbers and Ratio of States of Formaldehyde at Various Excess Energies^a

Γ	$\epsilon = 11 293$ cm ⁻¹		$\epsilon = 22 586$ cm ⁻¹		$\epsilon = 45 157$ cm ⁻¹	
	$N(\Gamma)$	$4\gamma(\Gamma)$	$N(\Gamma)$	$4\gamma(\Gamma)$	$N(\Gamma)$	$4\gamma(\Gamma)$
a ₁	322	1.32	6508	1.16	210 880	1.08
a ₂	172	0.70	4724	0.84	179 835	0.92
b ₁	215	0.88	5073	0.90	183 701	0.94
b ₂	268	1.10	6098	1.09	206 653	1.06

^a See footnote to Table I. Zero-point energy = 5644 cm⁻¹. The number multiplying $\gamma(\Gamma)$ is now 4 instead of 24.

energy equal or less than ϵ . Also given is $\gamma(\Gamma)$, namely, the ratio $N(\Gamma)/N$, N being the total number of states with

¹ Contribution No. 6900.

TABLE IV: Groups of Molecular Symmetries, Rules, and R Values

molecular symmetry	multiplication rules ^a	averaged overtone rules	R_A , R_E , R_T
Group 1			
O_h, O_h, T_h T_d, T_h	$A \times T = T$ $E \times E = 2A + E$ $E \times T = 2T$ $T \times T = A + E + 2T$	$A^v \equiv A$ $E^v \equiv A + E$ $T^v \equiv A + E + 3T$	1, 1, 3
Group 2			
C_{2v}, C_{3h}, C_{3v} D_{2v}, D_{3d}, D_{3h} C_{4v}, C_{6h}, C_{6v} D_{6h}, D_{6h}, S_6	$E \times E = 2A + E$	$A^v \equiv A$ $E^v \equiv A + E$	1, 1, 0
Group 3			
C_{4v}, C_{4v}, C_{4h} D_{2d}, D_{2d} D_{4h}, S_4	$E \times E = 4A$	$A^v \equiv A$ $E^v \equiv 2A + E$	2, 1, 0

^a There are also the rules, $A \times A = A$ and $A \times E = E$, which are the same for groups 1, 2, and 3.

energy equal or less than ϵ . Throughout, we suppress the ϵ in the notation for brevity. The sum of $\gamma(\Gamma)$ over all Γ equals unity.

The results in Table I are for benzene, an example of the D_{6h} point group.¹¹ One sees that the populations of the nondegenerate symmetry species rapidly become equal as ϵ increases, as do those of the doubly degenerate symmetry species. One also sees that the ratio of the number of states for any nondegenerate symmetry species to that for any double degenerate one rapidly converges to 1:4.

The results in Table II are for methane,¹² an example of the T_d point group. As the energy increases, the ratio of the number of states for any nondegenerate to the doubly degenerate to any triply degenerate symmetry species approaches 1:4:9. Higher energies are needed to reach the limiting ratio than was needed in Table I, for reasons evident from the derivation in section 3.¹³

The results in Table III are for a C_{2v} molecule, formaldehyde, for which Coriolis coupling has been discussed, e.g., ref 4, 5, and 7. Only nondegenerate symmetry species occur and these populations become equal. We have also studied molecules in the point groups $D_{4h}, D_{3h}, D_{3d}, C_{4v}$, and O_h and in every case have found, as ϵ becomes large,

that the numbers of states of each symmetry species with the same degeneracy become equal, and that the ratio of states of nondegenerate to doubly degenerate to triply degenerate symmetry species approaches a constant value.

These results for specific molecules can be generalized into three broad classes of molecular point groups listed in Table IV. We shall show that the ratio of the numbers of states of any nondegenerate to any doubly degenerate to any triply degenerate symmetry species $N(A):N(E):N(T)$, is given by eq 1, with increasing accuracy as ϵ increases

$$N(A):N(E):N(T) = R_A/n_A:2R_E/n_E:3R_T/n_T \quad (1)$$

where R_A, R_E , and R_T are given in Table IV for the various types of molecular symmetry point groups. n_A is the total number of nondegenerate symmetry species from a character table of the relevant point group; n_E and n_T are the analogous quantities for the doubly and triply degenerate symmetry species, respectively. Equation 1 is derived in section 3, together with the values of the R 's listed in Table IV. Using eq 1 we also show in section 3 that the density of states $\rho(\Gamma)$ for any particular symmetry species is given, with increasing accuracy as ϵ increases, by

$$\rho(\Gamma) = \rho g_\Gamma R_\Gamma / (R_A + 2R_E + 3R_T) n_\Gamma \quad (2)$$

where ρ is the total density of states at the excess energy ϵ ; g_Γ is 1, 2, or 3, R_Γ is R_A, R_E , or R_T , and n_Γ is n_A, n_E , or n_T , according as the Γ belongs to a nondegenerate, doubly degenerate, or triply degenerate symmetry species. Equations 1 and 2 are the principal results of this paper. Equations 1 and 2 assume that all n_Γ symmetry species are accessible. If some symmetry species are not accessible, n_Γ refers only to the accessible species. However, for all real molecules we have studied thus far, all symmetry species in a point group have been accessible. When the vibrations are anharmonic, the use of different symmetry types remains valid (ref 9, p 146).

In applications of eq 2 to molecules such as CH_2O , which have only nondegenerate representations, we have $R_A = 1$ and $R_E = R_T = 0$.

3. Derivation of Eq 1 and 2

To simplify the derivation of eq 1 and 2, two assumptions will be made:

The first assumption is that in building up various combinations of overtones of the various fundamentals there is randomization of the numbers of states between symmetry species having the same degeneracy (e.g., among the four E-symmetry species in Table I). The tendency to randomization is indeed evident in the exact multiplication rules given in ref 9.

The second assumption is that the energy is sufficiently high that frequently some degenerate fundamental has several quanta in it. This causes representations of overtones of degenerate fundamentals to obey the averaged overtone rules given in the third column of Table IV.

The first assumption is seen to be true in Tables I-III within statistical deviations, for the three molecules given there. Consistent with this assumption, we adopt a notation such that all nondegenerate symmetry species are grouped together and each is called A (which now includes all A and B representations), each doubly degenerate symmetry species is called E (i.e., irrespective of whether it is e_{1g}, e_{2g}, e_{1u} , etc.), and each triply degenerate one is called T . Each E label contains two states and T contains three states. The first assumption simplifies the multiplication rules and, after examining Table X-12 of ref 9, led to the three sets of groups in Table IV. Within each set the now simplified multiplication rules have become similar. The overtone rules of ref 9 also became simple

(1) Riedle, E.; Neusser, H. J.; Schlag, E. W. *J. Phys. Chem.* 1982, 86, 4847.

(2) Runnels, J. H. M.S. Thesis, California Institute of Technology, 1983.

(3) Riedle, E.; Neusser, H. J.; Schlag, E. W. *Faraday Discuss. Chem. Soc.*, in press.

(4) Dai, H. L.; Korpa, C. L.; Kinsey, J. L.; Field, R. W., to be submitted.

(5) Tang, K. Y.; Fairchild, P. W.; Lee, E. K. C. *J. Chem. Phys.* 1977, 66, 3303.

(6) Forch, B. E.; Chen, K. T.; Saigusa, H.; Lim, E. C. *J. Phys. Chem.* 1983, 87, 2280. Chen, K. T.; Forch, B. E.; Lim, E. C. *Chem. Phys. Lett.* 1983, 99, 98.

(7) Garland, N. L.; Lee, E. K. C. *Faraday Discuss. Chem. Soc.*, in press.

(8) E.g., Mills, I. M. *Pure Appl. Chem.* 1965, 11, 325.

(9) Wilson, E. B.; Decius, J. C.; Cross, P. C. "Molecular Vibrations"; McGraw-Hill: New York, 1955; pp 331 ff.

(10) Robinson, P. J.; Holbrook, K. A. "Unimolecular Reactions"; Wiley-Interscience: New York, 1972; pp 131 ff.

(11) Robey, M. J.; Schlag, E. W. *J. Chem. Phys.* 1977, 67, 2775.

(12) Gray, D. L.; Robiette, A. G. *Mol. Phys.* 1979, 37, 1901.

(13) The exact recursion relation for the representation of triply degenerate overtones has a longer recursion cycle. Further, the approximation used in section 3 (Table IV) for the triply degenerate overtone rule is less accurate than the others at low energies, though it becomes increasingly exact at high energies.

after introducing the two assumptions, and represent averages, e.g. over the variable q in Table X-13, ref 9. (In the case of the overtone rule for a triply degenerate fundamental, the result in Table IV is an approximate average over q and over even and odd ν in ref 9 and becomes increasingly exact as p in ref 9 becomes large.)

We illustrate the first assumption using a combination level in D_{6h} , such as $a_{1g} + a_{2g} + a_{1u} + a_{2u} + e_{1g} + e_{2g} + e_{1u} + e_{2u}$. Because of the first assumption this representation can be rewritten as $4A + 4E$. Because we are mainly interested in ratio of labels, we introduce an equivalency symbol =:

$$4A + 4E = A + E \quad (3)$$

Thus, the representation of the cited combination level in D_{6h} is, in this sense, equivalent to $A + E$. Its ratio of A labels to E labels is 1:1.

The following derivation of eq 1 and 2 is first given for group 1 type molecular point group symmetries in Table IV. We order the vibrational fundamentals of a molecule so that the first k of them are of the A type, the next m are of the E type, and the final n are of the T type, $k + 2m + 3n$ being therefore the total number of normal modes. We let A^{ν_i} signify that the i th nondegenerate fundamental contains ν_i quanta, and use an analogous notation for the other (E and T) fundamentals. The representation of any given vibrational excitation can be written as

$$\Gamma = A^{\nu_1} \dots A^{\nu_k} E^{\nu_{k+1}} \dots E^{\nu_{k+m}} T^{\nu_{k+m+1}} \dots T^{\nu_{k+m+n}} = \Gamma_A \Gamma_E \Gamma_T \quad (4)$$

where Γ_A denotes the product of the A factors, etc. We evaluate Γ_A , Γ_E , and Γ_T separately. We shall assume in the following that at least one ν_i in Γ_E and at least one in Γ_T exceeds unity.

We have

$$\Gamma_A = A^{\nu_1} \dots A^{\nu_k} \quad (5)$$

From Table IV we know that $A^{\nu} = A$ for any ν , so that

$$\Gamma_A = A \dots A = A \quad (6)$$

independently of k , using the multiplication rules for group 1 in Table IV.

Using the same method for combinations of overtones of E -type fundamentals, Γ_E is given by

$$\Gamma_E = E^{\nu_{k+1}} \dots E^{\nu_{k+m}} \quad (7)$$

From Table IV one sees that

$$E^{\nu} = A + E \quad (\nu > 1) \quad E^{\nu} = E \quad (\nu = 1) \quad (8)$$

From the multiplication rules in Table IV

$$(A + E)(A + E) = A + E \quad E(A + E) = A + E \quad (9)$$

Application of eq 8 and 9 to eq 7 yields¹⁴

$$\Gamma_E = A + E \quad (10)$$

as long as at least one $\nu_i > 1$. For Γ_T we have

$$\Gamma_T = T^{\nu_{k+m+1}} \dots T^{\nu_{k+m+n}} \quad (11)$$

From the overtone rules in Table IV we have $T^{\nu} = A + E$

+ $3T$ or T , according as $\nu > 1$ or $\nu = 1$. The multiplication rules in Table IV yield

$$\begin{aligned} (A + E + 3T)(A + E + 3T) &= A + E + 3T \\ T(A + E + 3T) &= A + E + 3T \end{aligned} \quad (12)$$

Application of eq 12 to 11 yields 13, as long as at least one $\nu_i > 1$.

$$\Gamma_T = A + E + 3T \quad (13)$$

Equations 4, 6, 10, and 13 plus the multiplication rules in Table IV then yield

$$\begin{aligned} \Gamma &= A(A + E)(A + E + 3T) = \\ &= 3A + 3E + 9T = A + E + 3T \end{aligned} \quad (14)$$

The ratio of labels given by eq 14 is seen to be independent of the specific vibrational excitation level. Therefore, the ratio of the total number of A labels to E labels to T labels is always 1:1:3. These numbers provide the R values listed as in the last column of Table IV.

To obtain eq 1 we now note that the ratio of labels is $R_A:R_E:R_T$, and so the ratio of states is $R_A:2R_E:3R_T$ when degeneracy is included. Since there are n_A symmetry species of the A type which share this R_A , n_E which share this $2R_E$, and n_T sharing the $3R_T$, eq 1 for ratios of numbers of states of specific symmetry species immediately follows.

We turn next to group 2 in Table IV, for which $R_A = 1$ and $R_E = 1$. Since the multiplication and overtone rules for group 2 are identical with those for group 1 except that there are no triply degenerate symmetry species, one finds that the representation of a combination of overtones is now given by

$$\Gamma = A^{\nu_1} \dots A^{\nu_k} E^{\nu_{k+1}} \dots E^{\nu_{k+m}} = A(A + E) = A + E \quad (15)$$

Once again, the ratio of A to E labels is independent of the vibrational excitation, namely, 1:1. One thus has $R_A = 1$ and $R_E = 1$, as reported in the last column of Table IV. Equation 1 again follows.

For group 3 one uses the same logic, except that now the rules for the E representations are different, as seen in Table IV. For the A overtones we have $\Gamma_A = A$ as before. However, we have $E^{\nu} = 2A + E$ or E , according as $\nu > 1$ or $\nu = 1$. Use of multiplication rules in Table IV yields

$$\begin{aligned} (2A + E)(2A + E) &= 2A + E \\ E(2A + E) &= 2A + E \end{aligned} \quad (16)$$

Application to eq 7 gives $2A + E$ for Γ_E . Hence

$$\Gamma = A(2A + E) = 2A + E \quad (17)$$

Thus, the ratio of A labels to E labels is 2:1 for group 3 symmetries, independently of the vibrational excitation. Hence, one obtains the $R_A = 2$, $R_E = 1$ in the last column of Table IV and eq 1 follows.

To obtain eq 2 we note that the total number of states N with excess energy equal to or less than ϵ is $n_A N(\Gamma_A) + n_E N(\Gamma_E) + n_T N(\Gamma_T)$, where Γ_A is a Γ of type A , etc. Equation 1 can be rewritten as $n_A N(\Gamma_A) = cR_A$, $n_E N(\Gamma_E) = 2cR_E$, and $n_T N(\Gamma_T) = 3cR_T$, where c is constant. Summing yields $N = c(R_A + 2R_E + 3R_T)$ and hence yields $N/(R_A + 2R_E + 3R_T)$ for c . One thus obtains (using the definition of g_{Γ} given earlier)

$$N(\Gamma) = N g_{\Gamma} R_{\Gamma} / (R_A + 2R_E + 3R_T) n_{\Gamma} \quad (18)$$

Differentiation of this equation with respect to ϵ yields eq

(14) The associative law converts a multiplication such as $(E \times E \times E) \times (A + E)$ to $(E \times E) \times (E \times (A + E))$ and hence successive applications of eq 9 may be used to obtain eq 10.

2, since the R 's, n_r 's, and g_r 's in eq 18 are independent of ϵ .

4. Discussion

Coriolis Coupling. To illustrate an application of eq 2 we consider benzene and parallel type Coriolis coupling. Riedle et al.¹³ measured the Doppler-free rotationally resolved two-photon spectrum of the $14_0^1 1_0^1$ bands of benzene ($n = 1, 2$). They excited an electronic state of B_{2u} symmetry and a vibrational state of b_{2u} symmetry, and examined the fluorescence excitation spectrum of the Q branch. Only the $K = 0$ levels remained when $n = 2$, plus some residual structure from the $K \neq 0$ states. One of the possible explanations involves Coriolis effects.¹⁵

The b_{2u} vibrational state couples by parallel Coriolis interactions to b_{1u} states,¹⁻³ giving new levels $1/2(E_1 + E_2) \pm [(H_{12})^2 + (\Delta E/2)^2]^{1/2}$. H_{12} is the Coriolis interaction energy and $\Delta E (= E_2 - E_1)$ is the energy difference of the b_{1u} and b_{2u} states. When $\Delta E = 0$ there is extensive transfer of the oscillator strength from the b_{2u} level (50%), while when $|H_{12}/\Delta E| \ll 1$ there is little. There can be further splitting due to Coriolis effects, yielding a further reduction in intensity of $K \neq 0$ lines and still further irregularities in the spectrum. If the b_{1u} states to which the original b_{2u} state is coupled have large nonradiative rates, the total fluorescence intensity is also decreased,³ in agreement with the experiment.¹³

The transfer of oscillator strength due to Coriolis coupling is significant for states within an energy ΔE of about, say, H_{12} . H_{12} equals $\pm 2C\zeta Kl$, where $C (= \hbar^2/2I_z)$ is¹⁷ 0.09 cm^{-1} , K and l are the z rotational and z vibrational angular momentum quantum numbers ($K > 0$), and ζ is a Coriolis interaction constant. If the maximum ζ is¹⁸ about 0.8, H_{12} is about $\pm 0.15Kl \text{ cm}^{-1}$ or less. (Any unfavorable vibrational overlap¹⁹ decreases this ζ .) For comparison it may be noted

that the separation of adjacent K states in the Q branch is about $0.008K \text{ cm}^{-1}$, according to available rotational constants.¹⁷

One sees that if there is sufficient parallel Coriolis coupling (sufficient proximity of suitable b_{1u} states to the original b_{2u} state) the fluorescence excitation spectrum will contain the $K = 0$ lines, which are unaffected by parallel Coriolis coupling, plus some residual irregular structure from the $K \neq 0$ lines. To create this Coriolis coupling the density of suitable vibrational states of the b_{1u} symmetry species would have to be about 6 per cm^{-1} ($\sim 1/H_{12}$) when $K = l = 1$. The total density of b_{1u} states (suitable and unsuitable) is given by eq 2 and by the R values in Table IV. It is approximately 1/24 the total density of states. In order for the total density of b_{1u} states to reach 6 per cm^{-1} , the total density of states would therefore have to be 144 per cm^{-1} . This density corresponds to an energy, determined from the Whitten-Rabinovitch approximation or from direct counting, of about 3370 cm^{-1} . This energy also corresponds roughly to the energy where disappearance of the $K \neq 0$ lines occurs in experimental measurements by Riedle et al.,¹ and so one has a possible statistical^{2,3} explanation of the results. However, consistency of argument would require that one examine the effect of perpendicular Coriolis interactions¹⁵ on the $K = 0$ state, using assumptions analogous to those used above, and vibrational overlap^{19,20} aspects should also be explored.

Anharmonic Coupling. Other questions which can be addressed by use of eq 2 involve other types of coupling. For example, if a zeroth-order state (wavepacket) of some given symmetry species is excited, one can use eq 2 to calculate the density of vibrational states of the same symmetry species with which the wavepacket can be associated.

Acknowledgment. We are pleased to acknowledge the support of this research by a grant from the National Science Foundation. J.H.R. also acknowledges a fellowship from the Fannie and John Hertz Foundation.

(15) An alternative mechanism which still distinguishes $K = 0$ states is given by Callomon, J. H. *Faraday Discuss. Chem. Soc.*, in press (discussion comment).

(16) E.g., Hougen, J. T. *J. Chem. Phys.* 1963, 38, 1167. Hougen, J. T. In "Physical Chemistry: An Advanced Treatise"; Henderson, D.; Ed.; Academic Press: New York, 1970; Vol. IV, p 346. Mills, I. M. In "Molecular Spectroscopy: Modern Research"; Rao, K. N.; Mathews, C. W., Ed.; Academic Press: New York, 1972; pp 128 ff. Reference 9, p 367.

(17) Riedle, E.; Neusser, H. J.; Schlag, E. W. *J. Chem. Phys.* 1981, 75, 4231.

(18) We used the larger ones calculated in ref 11.

(19) E.g., for harmonic states one requires¹⁶ $\Delta v_1 = -\Delta v_2 = \pm 1$, $\Delta v_3 = 0$. Sufficient anharmonicity would distribute the original vibrational parentage of the harmonic states more widely over the anharmonic states, and so the state-by-state requirement would then be less severe.

(20) E.g., if as a minimal requirement one added the supplementary conditions on the b_{1u} states that $v_{1a} = 0$ and that $v_1 = 1$ or 2, the density of such b_{1u} states at $\epsilon = 3370 \text{ cm}^{-1}$ is found by using eq 2 and calculating ρ . One distributes among the remaining 28 modes an energy (3370-923) cm^{-1} when $v_1 = 1$, yielding $\rho(b_{1u}) = 0.65$ per cm^{-1} , and an energy (3370-1846) cm^{-1} when $v_1 = 2$, yielding $\rho(b_{1u}) = 0.05$ per cm^{-1} . The total density of such b_{1u} states is about 0.7 per cm^{-1} at 3370 cm^{-1} instead of 6 per cm^{-1} .

**Chapter 2: Densities of Vibrational States of Given Symmetry Species.
Linear Molecules and Rovibrational States of Nonlinear
Molecules**

[The text of this chapter appeared in: S. M. Lederman and R. A. Marcus, J. Chem. Phys., **81**, 5601 (1984).]

Densities of vibrational states of given symmetry species. Linear molecules and rovibrational states of nonlinear molecules

Steven M. Lederman and R. A. Marcus
Arthur Amos Noyes Laboratory of Chemical Physics¹
California Institute of Technology, Pasadena, California 91125

(Received 24 May 1984; accepted 6 August 1984)

A simple statistical expression is given for the density of states of any symmetry species for linear molecules. Molecules with one and two pairs of doubly degenerate bending modes are considered. The results of our previous paper for vibrational states of nonlinear molecules are also extended to include density of rotational-vibrational states by symmetry species. The various expressions are tested by comparing with exact counts of states.

I. INTRODUCTION

In a recent paper,¹ we derived a simple statistical expression for the density $\rho(\Gamma)$ of vibrational states with symmetry species Γ for nonlinear molecules, or for the number $N(\Gamma)$ of states of symmetry Γ with energy less than or equal to E in terms of the total number of states N with energy less than or equal to E :

$$\rho(\Gamma) = \rho f_{\Gamma}, \quad N(\Gamma) = N f_{\Gamma}, \quad (1a)$$

where the fraction of states of symmetry Γ is

$$f_{\Gamma} = g_{\Gamma} R_{\Gamma} / (R_A + 2R_E + 3R_T) n_{\Gamma}. \quad (1b)$$

Here, ρ is the total density of states, determined by exact count or by use of an approximate formula such as that of Whitten-Rabinovitch. [In using a formula such as Eq. (1a) one is often interested in the case of high energies, where Whitten-Rabinovitch is applicable.] g_{Γ} is 1, 2, or 3 according as Γ is of an A , E , or T (non, doubly, or triply degenerate) species, the R 's are small integers whose values for the various types of molecular point groups are given in Ref. 1 and n_{Γ} is the number of symmetry species of type A , E , or T . An equivalent equation appears in the general work by Quack² on group representations: in scattering theory and most recently by Pechukas³ in his nice treatment of molecular symmetry point groups. For any given symmetry species the number of scattering channels (Quack) or fraction of vibrational states (Pechukas) is written in their notation as $[\Gamma_m] W(E, J) / g$ or n_m^2 / g , respectively. In each case the result excluded the symmetry associated with rotation about the C_{∞} symmetry axis of linear molecules.

Exact counts were given to test the accuracy of the formula in Ref. 1. Sinha and Kinsey⁴ have recently presented a fast computational method for an exact count.

In Sec. II of the present paper we develop statistical formulas for the density of vibrational states by symmetry species for linear molecules. In the process we first consider the purely classical density of states, using the vibrational angular momentum component as a representation of symmetry species. The formulas are then converted to a "semi-classical" form (to agree better with the exact quantum count) by introducing an expression analogous to that of

Whitten and Rabinovitch⁵ for unrestricted counts of states. Comparisons with exact quantum counts are given in Sec. III.

The density of rovibrational states by symmetry species is treated for nonlinear molecules in Sec. IV. Such systems are of interest because coupled rovibrational states have been invoked to explain the onset of intramolecular vibrational relaxation at energies where the density of vibrational states alone is too small to explain the data.⁶ A simple formula, analogous to that which we derived in Ref. 1, is obtained for these rovibrational states. The formula is compared with an exact quantum count of rovibrational states. The results are discussed in Sec. V.

II. DENSITY OF VIBRATIONAL STATES OF LINEAR MOLECULES BY SYMMETRY SPECIES

In the case of nonlinear molecules there are a finite number of symmetry species. With increasing energy, the partitioning of states among symmetry species became energy independent and was given by a simple formula [Eq. (1)]. In the case of linear molecules, however, there are an infinite number of symmetry species, each characterized by the projection of the angular momentum along the internuclear axis.⁷ The partitioning of states by symmetry species no longer approaches a constant value with increasing energy, and so the formula derived in the present paper is no longer quite as simple.

Two cases are considered below: (A) linear molecules with one degenerate pair of bending modes (e.g., CO_2); and (B) linear molecules with two degenerate pairs of bending modes (e.g., C_2H_2). The case of more than two degenerate modes can be treated similarly, but is rarer and is omitted here.

A. One degenerate pair of modes

We use the symbol l to denote quantum number for the (signed) component of angular momentum along the internuclear axis of the molecule. We first show that the classical number of vibrational states with energy less than or equal to E for a molecule with s vibrations and with a given value of l is $N'_l(E)$:

$$N'_l(E) = (E - |l| h\nu)^{s-1} / 2(s-1)! h\nu \prod_i h\nu_i, \quad (2)$$

¹Contribution No. 7026.

where ν is the vibration frequency of the degenerate bending mode ($i = 1, 2$) and in the present section the ν_i ($i = 3$ to s) are vibration frequencies of the remaining $s-2$ modes.

The derivation of Eq. (2) is given in Appendix A. It involves consideration of the partitioning of the energy E among all vibrational modes subject to the constraint that the (signed) component of the vibrational angular momentum along the internuclear axis is specified. Incidentally, integration of Eq. (2) over the limits of l , namely from $-E/h\nu$ to $E/h\nu$ (Appendix A), for a given E yields $E^s/s!(h\nu)^2\Pi_i h\nu_i$, the conventional expression for the classical number of states of s oscillators with energy less than or equal to E .

The accuracy of Eq. (2) can be improved by converting to an expression which parallels that used by Whitten and Rabinovitch⁵ for the unrestricted number of states (cf. Appendix A)

$$N_s^l(\epsilon) = (\epsilon + aE_{z,s} - |l| h\nu)^{s-1} / 2(s-1)! h\nu \Pi_i h\nu_i, \quad (3a)$$

where

$$\epsilon = E - E_{z,s} \quad (3b)$$

and $E_{z,s}$ is the zero-point energy of the set of s oscillators; a is a factor given by Whitten and Rabinovitch, which we calcu-

$$N_s^l(E) = \frac{h\nu_2[E - |l| h\nu_1]^{s-1} - h\nu_1[E - |l| h\nu_2]^{s-1} \theta(E/h\nu_2 - |l|)}{(s-1)! 2h\nu_1 h\nu_2 [(h\nu_2)^2 - (h\nu_1)^2] \Pi_i h\nu_i} \quad (6)$$

where $\nu_2 > \nu_1$. Here, the product Π_i is from $i = 5$ to s throughout this section and $\theta(x)$ is 0 if $x < 0$ and 1 if $x > 0$. Integration of Eq. (6) over all l from $-E/h\nu_1$ to $E/h\nu_1$, yields the conventional classical expression for the number of states, namely, $E^s/s!(h\nu_1)^2(h\nu_2)^2\Pi_i h\nu_i$.

Once again, a Whitten-Rabinovitch⁵ type of modification is introduced to convert the expression in Eq. (6) to one which better approximates the quantum results, namely,

$$N_s^l(\epsilon) = \frac{h\nu_2(\epsilon + a_1 E_{z,s} - |l| h\nu_1)^{s-1} - h\nu_1(\epsilon + a_2 E_{z,s} - |l| h\nu_2)^{s-1} \theta(E/h\nu_2 - |l|)}{2(s-1)! h\nu_1 h\nu_2 [(h\nu_2)^2 - (h\nu_1)^2] \Pi_i h\nu_i}, \quad (7)$$

where ϵ is again given by Eq. (3b), a_1 is computed at a reduced energy $(\epsilon - |l| h\nu_1)/E_{z,s}$, and a_2 at a reduced energy of $(\epsilon - |l| h\nu_2)/E_{z,s}$ and in each case for s oscillators.

The density of states, obtained by differentiating Eq. (7) is

$$\rho_s^l(\epsilon) = \frac{h\nu_2(\epsilon - a_1 E_{z,s} - |l| h\nu_1)^{s-2} (1 + \zeta_1) - h\nu_1(\epsilon - a_2 E_{z,s} - |l| h\nu_2)^{s-2} (1 + \zeta_2) \theta(E/h\nu_2 - |l|)}{2(s-2)! h\nu_1 h\nu_2 [(h\nu_2)^2 - (h\nu_1)^2] \Pi_i h\nu_i}, \quad (8)$$

where $\zeta_i = (da_i/d\epsilon)E_{z,s}$.

Once again, when $+l$ and $-l$ states are grouped together to represent the symmetry species we have

$$N_s^{l \pm} = 2N_s^l(l \neq 0) \quad (9a)$$

$$= N_s^l(l = 0), \quad (9b)$$

where N_s^l is given by Eq. (7) and with analogous remarks for $\rho_s^{l \pm}(\epsilon)$.

III. RESULTS FOR LINEAR MOLECULES

In this section we give the quantum count $N(\Gamma)$ of harmonic vibrational states by symmetry species Γ with energy less than or equal to ϵ . Standard tables were used for computing the symmetry of overtone and combination states.⁸

The Σ states are those for which $|l| = 0$, the E_2 states (or Π states) are those for which $|l| = 1$, etc.⁷ When two degenerate pairs of modes are present both Σ^+ and Σ^- states occur. In applying Eqs. (7) and (9) we assume a randomness

late at a reduced⁵ energy $(E - |l| h\nu)/E_{z,s}$ and for the given s frequencies.

The density of states by angular momentum is found by differentiating Eq. (3):

$$\rho_s^l(\epsilon) = \frac{(\epsilon + aE_{z,s} - |l| h\nu)^{s-2}}{2(s-2)! h\nu \Pi_i h\nu_i} \left[1 + \frac{da}{d\epsilon} E_{z,s} \right]. \quad (4)$$

When $+l$ and $-l$ states are grouped together, to form the Π, Δ, \dots states,⁷ we have as their number

$$\begin{aligned} N_s^{l \pm} &= 2N_s^l \quad (l \neq 0) \\ &= N_s^l \quad (l = 0), \end{aligned} \quad (5)$$

where N_s^l is given by Eq. (3). Similar remarks are applicable in obtaining $\rho_s^{l \pm}(\epsilon)$ from the $\rho_s^l(\epsilon)$ in Eq. (4).

B. Two degenerate pairs of modes

The derivation for this case parallels the previous one, but involves more complicated limits. If ν_1 and ν_2 are the vibration frequencies of the two degenerate pairs of modes ($i = 1-4$), the classical expression for the number of states with a specified (signed) l and with an energy less than or equal to E is shown in Appendix B to be

among these states and so to count each of the symmetry species Σ^+ and Σ^- we divide Eq. (7) for $l = 0$ by a factor of 2. In examples of molecules with an inversion center, g and u states occur, but Eqs. (3), (5), (7), and (9) refer to the sum of the (g,u) pairs. We assume a randomness among this type of pair and so also divide these equations by a factor of 2. Thus, when one has $\Sigma_g^-, \Sigma_u^+, \Sigma_g^+$, and Σ_u^- states, the equations for $l = 0$ are divided by a factor of 4.

Results for four representative linear molecules are given in Tables I to IV. Results for HCN,⁹ a $C_{\infty v}$ molecule with one degenerate pair of normal modes, are given in Table I. R is the ratio of the exact $N(\Gamma)$ to the approximate number given by Eq. (3) and (5). In the last row ("total") the item labeled $N(\Gamma)$ is really the total number of states [i.e., $\Sigma N(\Gamma)$, summed over all Γ , even those that are not listed]. The " R " in this row is the ratio of this $\Sigma N(\Gamma)$ to the standard Whitten-Rabinovitch expression⁵ for the total number of states. We also note that Σ^- states are not allowed for a molecule with

TABLE I. Number of vibrational states of HCN by Symmetry type at various excess energies and ratio R of exact number to approximate formulas.^a

Γ	$\epsilon = 10\,250\text{ cm}^{-1}$		$\epsilon = 20\,250\text{ cm}^{-1}$		$\epsilon = 40\,250\text{ cm}^{-1}$	
	$N(\Gamma)$	R	$N(\Gamma)$	R	$N(\Gamma)$	R
Σ^-	41	0.98	221	1.00	1 404	1.00 ^b
E_1^+	70	0.99	404	1.00	2 672	1.00
E_2^-	60	1.01	368	1.00	2 544	1.00
E_3	50	1.01	332	1.00	2 416	1.00
E_4	40	0.99	300	1.00	2 294	1.00
E_5	34	1.04	270	1.00	2 176	1.00
E_6	26	1.00	242	1.00	2 062	1.00
E_7	20	0.98	216	1.00	1 952	1.00
E_8	16	1.04	192	1.00	1 846	1.00
E_9	12	1.05	170	1.00	1 744	1.00
E_{10}	8	0.99	150	1.00	1 646	1.00
E_{11}	6	1.10	130	1.00	1 550	1.00
E_{12}	4	1.16	114	1.00	1 460	1.00
E_{13}	2	0.94	98	1.00	1 372	1.00
E_{14}	2	2.35	84	1.00	1 288	1.00
E_{15}			70	0.98	1 208	1.00
E_{16}			60	1.00	1 132	1.00
E_{17}			50	1.00	1 058	1.00
E_{18}			40	0.98	988	1.00
E_{19}			34	1.03	922	1.00
E_{20}			26	0.99	856	1.00
E_{21}			20	0.97	796	1.00
E_{22}			16	1.02	738	1.00
Total	391	0.99	3 641	0.99	42 952	1.00

^a Zero-point energy is 3412.5 cm^{-1} .^b As in Ref. 7, E_1 is a Π state, E_2 is a Δ state, etc.^c In this and other tables the formulas in Ref. 4 were used in some cases outside the suggested range of accuracy, but we still, as the results show, found the formula of Ref. 4 to be quite accurate.

only one pair of degenerate modes¹⁰ and hence we did not divide Eq. (7) for $l = 0$ by the factor of 2 mentioned in the preceding paragraph.

Results for CO_2 ,¹¹ a $D_{\infty h}$ molecule with one degenerate pair of modes, are given in Table II. Here, there are g and u states due to the inversion center and $N_g(\Gamma)$ and $N_u(\Gamma)$ represent the exact quantum number of states with g and u symmetry, respectively, with the cited value of $|l|$. Thus, R_g and R_u denote the ratios of exact counts to those based on the right-hand side of Eq. (5) divided by 2, as discussed above. R in the last column represents the ratio of $N_g(\Gamma) + N_u(\Gamma)$ to the number of states given by Eqs. (3) and (5).

Table III contains results for C_2BrCl ,¹² a $C_{\infty v}$ molecule with two degenerate pairs of modes. R is the ratio of exact count $N(\Gamma)$ to the number given by Eq. (9a) when $l \neq 0$. When $l = 0$ (i.e., $\Gamma \equiv \Sigma$), R is the ratio of the sum of $N(\Gamma)$'s for Σ^+ and Σ^- to the number given by Eq. (9b).

Table IV contains results for C_2H_2 ,¹³ a $D_{\infty h}$ molecule with two degenerate modes. Here, there are both g and u states and Σ^+ and Σ^- states occur. Thus, for $l \neq 0$, one divides the right-hand side of Eq. (9a) by a factor of 2 to calculate R_g and R_u . When computing R_g and R_u for the four Σ states one divides the right-hand side of Eq. (9b) by a factor of 4, as already noted. When $l = 0$, R is the ratio of the sum of $N(\Gamma)$ for Σ_g^+ , Σ_g^- , Σ_u^+ , and Σ_u^- , to the number given by Eq. (9b).

TABLE II. Number of vibrational states for CO_2 by symmetry type at (A) $\epsilon = 20\,250\text{ cm}^{-1}$ and (B) $\epsilon = 40\,250\text{ cm}^{-1}$ and ratio of exact number to approximate formula.^a

Γ	$N_g(\Gamma)$	R_g	$N_u(\Gamma)$	R_u	R
(A)					
Σ^+	276	1.18	194	0.83	1.01
E_1	346	0.81	500	1.17	0.99
E_2	466	1.20	320	0.82	1.01
E_3	282	0.80	418	1.18	0.99
E_4	388	1.21	260	0.81	1.01
E_5	226	0.78	346	1.20	0.99
E_6	320	1.23	208	0.80	1.01
E_7	178	0.76	282	1.21	0.99
E_8	260	1.25	164	0.79	1.02
E_9	138	0.75	226	1.22	0.98
E_{10}	208	1.27	126	0.77	1.02
E_{11}	104	0.72	178	1.23	0.98
E_{12}	164	1.30	94	0.75	1.02
E_{13}	76	0.69	138	1.26	0.98
E_{14}	126	1.33	68	0.72	1.03
E_{15}	54	0.67	104	1.28	0.97
E_{16}	94	1.37	48	0.70	1.03
E_{17}	36	0.62	76	1.31	0.97
E_{18}	68	1.41	32	0.66	1.04
E_{19}	22	0.56	54	1.36	0.96
E_{20}	48	1.49	20	0.62	1.06
E_{21}	12	0.47	36	1.41	0.94
E_{22}	32	1.60	12	0.60	1.10
Total	7926				1.00
(B)					
Σ^+	1 706	1.10	1417	0.91	1.01
E_1	2 684	0.91	3250	1.10	1.00
E_2	3 114	1.10	2568	0.91	1.01
E_3	2 428	0.90	2958	1.10	1.00
E_4	2 832	1.11	2320	0.91	1.01
E_5	2 188	0.90	2684	1.10	1.00
E_6	2 568	1.11	2088	0.90	1.01
E_7	1 964	0.89	2428	1.11	1.00
E_8	2 320	1.11	1872	0.90	1.01
E_9	1 756	0.89	2188	1.11	1.00
E_{10}	2 088	1.12	1672	0.90	1.01
E_{11}	1 564	0.89	1964	1.11	1.00
E_{12}	1 872	1.12	1486	0.89	1.01
E_{13}	1 386	0.88	1756	1.12	1.00
E_{14}	1 672	1.13	1314	0.89	1.01
E_{15}	1 222	0.88	1564	1.12	1.00
E_{16}	1 486	1.13	1156	0.88	1.01
E_{17}	1 072	0.87	1386	1.13	1.00
E_{18}	1 314	1.14	1012	0.88	1.01
E_{19}	934	0.86	1222	1.13	1.00
E_{20}	1 156	1.14	880	0.87	1.01
E_{21}	808	0.86	1072	1.14	1.00
E_{22}	1 012	1.15	760	0.87	1.01
Total	99 757				1.00

^a Zero-point energy is 2510 cm^{-1} .

IV. DENSITY OF ROVIBRATIONAL STATES FOR NONLINEAR MOLECULES

Just as the vibrational states in Ref. 1 were characterized by symmetry species, the rotational and the rovibrational states are similarly characterized. It is shown in Appendix C that the fraction of rovibrational states of a given symmetry species is the same as that of vibrational states alone and is therefore equal to the f_r given by Eq. (1b).

TABLE III. Number of vibrational states for C₂BrCl by symmetry type at various excess energies and ratio of exact number to approximate formula.*

Γ	$\epsilon = 3050 \text{ cm}^{-1}$		$\epsilon = 6050 \text{ cm}^{-1}$		$\epsilon = 9050 \text{ cm}^{-1}$	
	$N(\Gamma)$	R	$N(\Gamma)$	R	$N(\Gamma)$	R
Σ^+	393	1.07	6317	1.03	40594	1.01
Σ^-	216	1.06	4405	1.02	31313	1.01
E_1	1170		21110		142760	
E_2	1096	1.07	20564	1.03	140632	1.01
E_3	962	1.06	19562	1.02	136936	1.01
E_4	848	1.08	18512	1.03	132642	1.01
E_5	702	1.07	17156	1.02	127216	1.01
E_6	586	1.09	15886	1.03	121580	1.01
E_7	460	1.08	14414	1.02	115148	1.01
E_8	368	1.11	13100	1.03	108804	1.01
E_9	274	1.09	11668	1.02	101928	1.01
E_{10}	210	1.13	10436	1.03	95364	1.01
E_{11}	148	1.10	9132	1.03	88464	1.01
E_{12}	108	1.14	8054	1.04	82040	1.01
E_{13}	72	1.12	6932	1.03	75416	1.01
E_{14}	50	1.17	6034	1.04	69374	1.01
E_{15}	30	1.12	5110	1.03	63236	1.01
E_{16}	20	1.26	4396	1.05	57734	1.02
E_{17}	10	1.15	3662	1.04	52202	1.01
E_{18}	6	1.43	3118	1.06	47322	1.02
E_{19}	2	1.24	2554	1.04	42458	1.02
E_{20}	2	4.19	2152	1.06	38232	1.02
E_{21}			1734	1.05	34038	1.02
E_{22}			1446	1.08	30464	1.02
Total	7733	0.99	232508	1.00	2177519	1.00

*Zero-point energy is 2245.5 cm⁻¹.

In the exact counts of rovibrational states listed in Tables V to VIII each harmonic vibrational state was coupled to each of the $2J + 1$ rotational states, where J was assigned various values. The coupling was assumed weak and the new states were assumed to have the sum of the energies of the separated states. The symmetry of the rotational states was found within the full molecular point group using the method given by Hougen.¹⁴ The tables of the symmetry of rotational states for the molecular groups D_{nd} , D_{nh} , C_{nv} , and C_{nh} by Weber¹⁵ were useful, as were the symmetries for methane.¹⁶

Results for benzene,¹⁷ a symmetric top, are given in Table V. $N_{\text{VR}}(\Gamma)$ denotes the exact quantum number of rovibrational states of energy less than or equal to ϵ for symmetry species Γ , ϵ being the total rovibrational energy above the zero-point energy and $\gamma(\Gamma)$ is the ratio $N_{\text{VR}}(\Gamma)/f_{\Gamma} \sum_{\Gamma} N_{\nu}(\Gamma)$, where $N_{\nu}(\Gamma)$ is the exact number of vibrational states of symmetry Γ . The results are given for several values of J , where $J = 30$ is close to the room temperature value. One sees that for the rovibrational states the ratio of any nondegenerate symmetry species to any double degenerate symmetry species is 1:4, just as it was for the vibrational states.

We explore three approximations for the number of rovibrational states from a knowledge of the number of vibrational states:

(i) In this first approximation the rotational energy is neglected in the approximate formula for the number of states, i.e., we assume in this approximation that

$$N_{\text{VR}}(\Gamma; \epsilon) = (2J + 1)f_{\Gamma}N_{\nu}(\epsilon), \quad (10)$$

TABLE IV. Number of vibrational states for C₂H₂ by symmetry type at (A) $\epsilon = 9900 \text{ cm}^{-1}$ and (B) $\epsilon = 19\,900 \text{ cm}^{-1}$ and ratio of exact number to approximate formulas.*

Γ	$N_{\nu}(\Gamma)$	R	$N_{\nu}(\Gamma)$	R_{ν}	R
(A)					
Σ^+	223	1.49	171	1.14	1.04
Σ^-	97	0.65	131	0.88	1.05
E_1	608	1.05	608	1.05	
E_2	578	1.07	544	1.01	1.04
E_3	508	1.05	506	1.04	1.05
E_4	448	1.07	424	1.01	1.04
E_5	372	1.05	368	1.04	1.05
E_6	308	1.07	294	1.02	1.05
E_7	244	1.07	242	1.07	1.07
E_8	188	1.08	178	1.02	1.05
E_9	144	1.12	138	1.07	1.10
E_{10}	98	1.07	92	1.01	1.04
E_{11}	70	1.14	64	1.04	1.09
E_{12}	44	1.13	40	1.03	1.08
E_{13}	28	1.12	26	1.04	1.08
E_{14}	14	1.17	12	1.00	1.09
E_{15}	8	1.68	6	1.26	1.48
E_{16}	2	1.70	0	0.00	0.85
Total	7 826				1.00
(B)					
Σ^+	3 979	1.23	3 600	1.12	1.02
Σ^-	2 612	0.90	2 895	0.90	1.01
E_1	12 922	1.01	12 964	1.02	
E_2	12 678	1.02	12 510	1.01	1.01
E_3	12 042	1.01	12 078	1.01	1.01
E_4	11 488	1.02	11 342	1.00	1.01
E_5	10 644	1.01	10 678	1.01	1.01
E_6	9 928	1.02	9 798	1.01	1.01
E_7	9 006	1.01	9 034	1.02	1.01
E_8	8 228	1.02	8 120	1.01	1.01
E_9	7 314	1.01	7 340	1.02	1.01
E_{10}	6 562	1.02	6 468	1.01	1.01
E_{11}	5 710	1.01	5 736	1.02	1.02
E_{12}	5 032	1.02	4 952	1.01	1.01
E_{13}	4 282	1.01	4 310	1.02	1.02
E_{14}	3 700	1.03	3 636	1.01	1.02
E_{15}	3 078	1.01	3 098	1.02	1.02
E_{16}	2 602	1.03	2 556	1.01	1.02
E_{17}	2 112	1.02	2 124	1.02	1.02
E_{18}	1 740	1.04	1 706	1.02	1.03
E_{19}	1 370	1.02	1 376	1.03	1.02
E_{20}	1 092	1.04	1 074	1.02	1.03
E_{21}	830	1.03	832	1.03	1.03
E_{22}	638	1.05	628	1.03	1.04
Total	281 302				1.00

*Zero-point energy is 5860.5 cm⁻¹.

where $N_{\text{VR}}(\Gamma; \epsilon)$ denotes the number of vibrational states of symmetry Γ with total energy less than or equal to ϵ and $N_{\nu}(\epsilon)$ is the number of vibrational states for this ϵ , regardless of symmetry. ϵ is the total energy in excess of the zero-point energy, as before. To test the approximation given by Eq. (10) we calculate a quantity $\alpha(\Gamma)$ defined by

$$\alpha(\Gamma) = N_{\text{VR}}(\Gamma; \epsilon) / (2J + 1)f_{\Gamma}N_{\nu}(\epsilon). \quad (11)$$

(ii) In this second approximation the rotational energy E_{rot} of the molecule (as a symmetric top) is averaged over the K quantum number assuming a uniform distribution in K . Instead of Eq. (10) we now use

$$N_{\text{VR}}(\Gamma; \epsilon) = (2J + 1)f_{\Gamma}N_{\nu}(\epsilon - \langle E_{\text{rot}} \rangle). \quad (12)$$

TABLE V. Number and ratio of rotational-vibrational states $N_{VR}(J)$ for benzene at $\epsilon = 3004.8 \text{ cm}^{-1}$ for various J 's.^a

Γ	$J = 1$		$J = 20$		$J = 30$	
	$N_{VR}(\Gamma)$	$\gamma(\Gamma)$	$N_{VR}(\Gamma)$	$\gamma(\Gamma)$	$N_{VR}(\Gamma)$	$\gamma(\Gamma)$
a_{1g}	3 100	1.00	36 545	1.00	44 682	1.00
a_{2g}	3 024	0.97	36 430	1.00	44 582	1.00
b_{1g}	3 100	1.00	36 334	1.00	44 562	1.00
b_{2g}	3 200	1.03	36 431	1.00	44 648	1.00
a_{1u}	3 066	0.99	36 464	1.00	44 544	1.00
a_{2u}	3 108	1.00	36 506	1.00	44 584	1.00
b_{1u}	3 150	1.01	36 424	1.00	44 557	1.00
b_{2u}	3 118	1.00	36 387	1.00	44 531	1.00
e_{1g}	12 586	1.01	145 538	1.00	178 402	1.00
e_{2g}	12 262	0.98	145 958	1.00	178 544	1.00
e_{1u}	12 528	1.01	145 654	1.00	178 148	1.00
e_{2u}	12 356	1.00	145 918	1.00	178 278	1.00

^a Zero-point energy is 20034 cm^{-1} . Note that $\gamma(\Gamma)$ is defined differently than in paper I to include the degeneracy.

The rotational energy E_{rot} of a symmetric top having moments of inertia I_B and $I_A = I_C$ is

$$E_{rot}(K) = BJ(J+1) + K^2(C-B), \quad (13)$$

where the rotational constant $C > B$ for an oblate and $C < B$ for a prolate, symmetric top. Thus, $\langle E_{rot} \rangle$ depends on the $\langle K^2 \rangle$. For a given J , we have

$$\langle K^2 \rangle = \sum_{K=-J}^J K^2 / (2J+1) = \frac{1}{3} J(J+1). \quad (14)$$

Thereby,

$$\langle E_{rot} \rangle = BJ(J+1) + \frac{1}{3} J(J+1)(C-B). \quad (15)$$

The expression for a spherical top is obtained by setting $C = B$ in Eqs. (13) and (15). To test Eq. (12) we define a ratio $\beta(\Gamma)$:

$$\beta(\Gamma) = N_{VR}(\Gamma; \epsilon) / (2J+1) f_{\Gamma} N_v(\epsilon - \langle E_{rot} \rangle). \quad (16)$$

(iii) In this third approximation we calculate an $N_v(\Gamma)$ at $\epsilon - E_{rot}(J, K)$ and then average this over K . Thus, now

$$K_{VR}(\Gamma; \epsilon) = (2J+1) f_{\Gamma} N_v', \quad (17)$$

TABLE VI. Ratio of exact to three approximate results for benzene at various J 's^a and $\epsilon = 3004.8 \text{ cm}^{-1}$.

Γ	$J = 1$			$J = 20$			$J = 30$		
	$\alpha(\Gamma)$	$\beta(\Gamma)$	$\Delta(\Gamma)$	$\alpha(\Gamma)$	$\beta(\Gamma)$	$\Delta(\Gamma)$	$\alpha(\Gamma)$	$\beta(\Gamma)$	$\Delta(\Gamma)$
a_{1g}	1.00	1.00	1.00	0.86	1.00	1.00	0.71	1.01	1.00
a_{2g}	0.97	0.98	0.98	0.86	1.00	1.00	0.71	1.00	1.00
b_{1g}	1.00	1.00	1.00	0.86	1.00	1.00	0.71	1.00	1.00
b_{2g}	1.03	1.03	1.03	0.86	1.00	1.00	0.71	1.00	1.00
a_{1u}	0.99	0.99	0.99	0.86	1.00	1.00	0.71	1.00	1.00
a_{2u}	1.00	1.00	1.00	0.86	1.00	1.00	0.71	1.00	1.00
b_{1u}	1.01	1.02	1.02	0.86	1.00	1.00	0.71	1.00	1.00
b_{2u}	1.00	1.01	1.01	0.86	1.00	1.00	0.71	1.00	1.00
e_{1g}	1.02	1.01	1.01	0.86	1.00	1.00	0.71	1.00	1.00
e_{2g}	0.99	0.99	0.99	0.86	1.00	1.00	0.71	1.00	1.00
e_{1u}	1.01	1.01	1.01	0.86	1.00	1.00	0.71	1.00	1.00
e_{2u}	0.99	1.00	1.00	0.86	1.00	1.00	0.71	1.00	1.00

^a The total number of all vibrational states is 24 866. When $J = 1$, $\langle E_{rot} \rangle = 0.3 \text{ cm}^{-1}$; when $J = 20$, $\langle E_{rot} \rangle = 63.5 \text{ cm}^{-1}$; when $J = 30$, $\langle E_{rot} \rangle = 140.6 \text{ cm}^{-1}$.

TABLE VII. Ratio of exact to two approximate results for formaldehyde at various excess energies.^a

Γ	$\epsilon = 5640 \text{ cm}^{-1}$		$\epsilon = 11 280 \text{ cm}^{-1}$		$\epsilon = 22 572 \text{ cm}^{-1}$	
	$\beta(\Gamma)$	$\Delta(\Gamma)$	$\beta(\Gamma)$	$\Delta(\Gamma)$	$\beta(\Gamma)$	$\Delta(\Gamma)$
a_1	1.03	1.00	1.02	1.01	1.01	1.01
a_2	1.05	1.01	1.00	0.99	1.00	1.00
b_1	1.03	1.00	1.01	1.00	1.00	1.00
b_2	1.04	1.00	1.02	1.01	1.01	1.00
	$\sum_{\Gamma} N_v(\Gamma) = 73$		$\sum_{\Gamma} N_v(\Gamma) = 976$		$\sum_{\Gamma} N_v(\Gamma) = 22 392$	

^a $J = 15$, $\langle E_{rot} \rangle = 946.72 \text{ cm}^{-1}$, zero-point energy is 5644 cm^{-1} .

where

$$N_v' = \sum_{K=-J}^J N_v[\epsilon - E_{rot}(J, K)] / (2J+1). \quad (18)$$

To test this approximation we define a ratio $\Delta(\Gamma)$:

$$\Delta(\Gamma) = N_{VR}(\Gamma) / (2J+1) f_{\Gamma} N_v'. \quad (19)$$

Equations (10), (12), and (17) are tested for benzene, by calculating the $\alpha(\Gamma)$, $\beta(\Gamma)$, and $\Delta(\Gamma)$ using Eqs. (11), (16), and (19), respectively. The results are given in Table VI for several J 's. Equations (12) and (16) are tested for formaldehyde,¹⁸ a near symmetric top, in Table VII and for methane,¹⁹ a spherical top, in Table VIII. The closer the values of α , β , or Δ to unity the better, of course, the approximation.

V. DISCUSSION

Examination of Table I for linear molecules shows that the approximate formula [Eqs. (3) and (5)] for linear molecules agrees well with the exact results at the given energies. The deviations at very high $|l|$ at the lowest energy are due to poor statistics. Comparison of the R 's calculated at each l with the R in the last line shows that our Whitten-Rabinovich type expression by angular momentum [Eq. (3)] is virtually as accurate as the standard total Whitten-Rabinovich expression (except at large enough $|l|$'s). Similar remarks apply to its use for the sum of g and u states in Table II, but even for the counting of g states or u states alone it is seen to agree quite well. The remarks about Table I apply also to Table III, though there is less randomization between the Σ^+ and Σ^- than between g and u states. Equations (7) and (9) are seen to agree well with the exact count. A similar remark applies to Table IV.

TABLE VIII. Ratio of exact to two approximate results for methane.^a

Γ	$\epsilon = 4940 \text{ cm}^{-1}$		$\epsilon = 9880 \text{ cm}^{-1}$		$\epsilon = 19 760 \text{ cm}^{-1}$	
	$\beta(\Gamma)$	$\Delta(\Gamma)$	$\beta(\Gamma)$	$\Delta(\Gamma)$	$\beta(\Gamma)$	$\Delta(\Gamma)$
a_1	0.88		0.95		0.99	
a_2	1.05		1.03		1.01	
e	0.98		0.99		1.00	
t_1	1.03		1.02		1.00	
t_2	0.99		0.99		1.00	
	$\sum_{\Gamma} N_v(\Gamma) = 79$		$\sum_{\Gamma} N_v(\Gamma) = 1308$		$\sum_{\Gamma} N_v(\Gamma) = 66 877$	

^a $J = 5$, $\langle E_{rot} \rangle = 157.56 \text{ cm}^{-1}$, zero-point energy is 9883 cm^{-1} .

In Table V for rovibrational states, $\gamma(l')$ for benzene is even closer to unity than it was in Ref. 1 at the same number of states, perhaps due to the extra number of degrees of freedom. The three approximations for counting rovibrational states of nonlinear molecules of any symmetry species are embodied in Eqs. (10), (12), and (17). The results in Table VI for benzene show that even Eq. (10) is a good approximation except at high J . Equation (12) is seen to be even better than Eq. (10) and it agrees so closely with the exact results as not to make the use of Eq. (17) worthwhile for the present results. The tests in Table VII of Eqs. (12) and (17) for formaldehyde shows them to be satisfactory for the energy and J tested. Once again Eq. (17) contributes a negligible improvement over Eq. (12). Since methane is a spherical top, E_{rot} is independent of K and Eqs. (12) and (17) give identical results in Table VIII.

ACKNOWLEDGMENT

We are pleased to acknowledge the support of this research by the National Science Foundation.

APPENDIX A: DERIVATION OF EQS. (2) AND (3)

We let ν be the vibration frequency of each member of the degenerate pair and let $n^a h\nu$ and $n^b h\nu$ be the amounts of energy present in each member of the degenerate pair. Thereby $n^a h$ and $n^b h$ are the values of the classical action. Classically, n^a and n^b are continuous variables with a minimum value of zero. Quantum mechanically, n^a and n^b are half-integers, $1/2, 3/2, \dots$. For any pair of values (n^a, n^b) the component of angular momentum $|l|$ along the molecular axis is $|n^a - n^b|$.

We define a variable l' equal to $n^a - n^b$ and note that it can be positive or negative. We also define a principal vibrational "quantum number" n (the corresponding classical action being $n h$) for the degenerate pair

$$l' = n_1 - n_2, \quad n = n_1 + n_2. \quad (\text{A1})$$

l' is the quantum number for a signed angular momentum component along the internuclear axis. The classical number of states $N'_s(E)$ with a particular value of l' , and with energy less than or equal to E , is

$$N'_s(E) = \int_{n_2=0}^{E/h\nu} dn_2 \int_{n_1=0}^{E/h\nu - n_2} dn_1 \\ \times N_{s-2}(E - n_1 h\nu - n_2 h\nu) \delta(n_1 - n_2 - l'), \quad (\text{A2})$$

where s is the total number of vibrations and $N_{s-2}(x)$ is the number of vibrational states of $s-2$ oscillators with energy equal or less than x :

$$N_{s-2}(x) = \frac{x^{s-2}}{(s-2)! \Pi_i h\nu_i}. \quad (\text{A3})$$

Here, the product over i is from $i=3$ to s , oscillators 1 and 2 being the pair of degenerate bending vibrations. Using the transformation in Eq. (A1), the area element $dn_1 dn_2$ in Eq. (A2) becomes $dn' dl'$ and the delta function becomes $\delta(l' - l)$. We consider first the case of $l' > 0$. Here, because of the delta function, only the domain of $l' > 0$ need be considered. Equation (A2) then becomes

$$N'_s(E) = \frac{1}{2} \int_0^{E/h\nu} dl' \int_{l'}^{E/h\nu} dn N_{s-2}(E - nh\nu) \delta(l' - l). \quad (\text{A4})$$

[The limits on n and l' follows from those in Eq. (A2) and from the transformation given by Eq. (A1).] Integration over n yields

$$N'_s(E) = \left[\int_0^{E/h\nu} dl' (E - l' h\nu)^{s-1} \delta(l' - l) / 2(s-1)! h\nu \Pi_i h\nu_i \right]. \quad (\text{A5})$$

Integrating over l' yields Eq. (2) of the text. A similar argument applies to the case $l' < 0$. One then uses in Eq. (A4) the limits $(-l', E/h\nu)$ for n and $(-E/h\nu, 0)$ for l' . For $l=0$, the delta function occurs at an endpoint in Eq. (A5) and in a corresponding expression for $l' < 0$. Integrals over the $l' < 0$ and $l' > 0$ domains each yield $1/2$ and so Eq. (2) of the text is once again obtained.

In modifying Eq. (2) so as to yield Eq. (3) we have done so in a way which permits the standard Whitten-Rabinovitch expression⁵ to be recovered from Eq. (3) with only a minor approximation. If we integrate the right-hand side of Eq. (3) over all l , we first reexpress $(\epsilon + aE_{2,2} - lh\nu)^{s-1} dl$ for all l positive as $-d[(\epsilon + aE_{2,2} - lh\nu)^s / sh\nu [1 + E_{2,2}(da/d\epsilon)]]$. [We have used the fact that $da/d(-lh\nu)$ equals $da/d\epsilon$]. An analogous change is made in the domain of l negative. We then note that the dominant contribution of the original integrand occurs at $l=0$ and then replace the $da/d\epsilon$ by its value at $l=0$, i.e., at the "reduced energy" of $\epsilon/E_{2,2}$. This derivative is negligible at the E 's we have investigated (a is close to unity there) and so the standard⁵ Whitten-Rabinovitch expression is obtained after integration over l .

APPENDIX B: DERIVATION OF EQ. (6)

Let $n_1 h\nu_1$ and $n_2 h\nu_2$ denote the classical energies in the two pairs of degenerate modes, and let $n_1^a h\nu_1$ and $n_1^b h\nu_1$ denote the classical energies of each member of the first pair and similarly for the second pair. We define

$$l'_1 = n_1^a - n_1^b, \quad l'_2 = n_2^a - n_2^b, \\ n_1 = n_1^a + n_1^b, \quad n_2 = n_2^a + n_2^b. \quad (\text{B1})$$

As independent variables in the integration domain we use n_1, n_2, l'_1 , and l'_2 (instead of l'_1 and l'_2), where l' equals $l'_1 l'_2$. The volume element $dn_1^a dn_1^b dn_2^a dn_2^b$ becomes $dl'_1 dn_1 dl'_2 dn_2 / 4$.

The equation analogous to Eq. (A2) is found to be

$$N'_s(E) = \frac{1}{4} \iiint \int dl'_1 dl'_2 dn_1 dn_2 \\ \times N_{s-4}(E - n_1 h\nu_1 - n_2 h\nu_2) \delta(l' - l) \quad (\text{B2})$$

where $N_{s-4}(x)$ is the number of states of the $s-4$ oscillators with energy equal to or less than x :

$$N_{s-4}(x) = x^{s-4} / (s-4)! \Pi_i h\nu_i. \quad (\text{B3})$$

Here, i goes from 5 to s throughout, the oscillators $i=1-4$ being the two pairs of degenerate bending vibrations. The l in the delta function is a particular value of l' . The limits on the variables are as follows: n_1 goes from $|l'_1|$ to $(E - n_2 h\nu_2) / h\nu_1$,

and n_2 from $|l'_2|$ (i.e., $|l' - l'_1|$) to $(E - |l'_1| h\nu_1)/h\nu_2$. For example, the lower limit just cited for the n_1 integral $|l'_1|$ is seen by noting that $n_1 = l'_1 + 2n_1^0 = 2n_1^0 - l'_1$ and observing that when $l'_1 > 0$ the smallest value of n_1 is obtained by making $n_1^0 = 0$ and hence $n_1 = l'_1$, and that when l'_1 is negative, the smallest value of n_1 is obtained by making $n_1^0 = 0$ and hence making $n_1 = -l'_1$. That is, for both cases, we have $n_1 > |l'_1|$. The limits on l'_1 and l' in Eq. (B2) are given later:

$$N'_2(E) = \frac{\int \int (E - |l'| h\nu_1 - |l' - l'_1| h\nu_2)^{-2} \delta(l' - l) dl'_1 dl'}{4(s-2)h\nu_1 h\nu_2 \Pi_1 h\nu_1} \quad (\text{B4})$$

The limits on l'_1 and l' are found by noting that the quantity in parentheses in Eq. (B4) must be nonnegative. Because of the absolute value signs, it is convenient to divide the integration region into several subdomains, in each of which the integral over l'_1 can be easily evaluated. For example, we let $\nu_2 > \nu_1$ and let the most negative and most positive values of l'_1 for which the quantity in parentheses in Eq. (B4) is nonnegative be denoted by l'_1^{\min} and l'_1^{\max} . Then, for the domain with $l' > 0$, the l'_1 domains are found to be as follows:

When $l' < E/h\nu_2$, there are three subdomains of l'_1 , namely (l'_1^{\min} to 0) (0 to l') and (l' to l'_1^{\max}). Here, l'_1^{\min} is given by $E - l' h\nu_1 - (l' - l'_1^{\min}) h\nu_2 = 0$; and l'_1^{\max} is given by $E - l' h\nu_1 - (l'_1^{\max} - l') h\nu_2 = 0$. (We have used the fact that l'_1 can exceed l' since l'_2 can be negative.)

When $l' > E/h\nu_2$ (its maximum value is $E/h\nu_1$) one finds that the above l'_1^{\min} is positive rather than negative and so now there are only two subdomains of l'_1 ; namely (l'_1^{\min} to l') and (l' to l'_1^{\max}). Furthermore, when l is positive, we need only use the positive l' integration domain, because of the delta function. One thus finds, for $l > 0$, an expression identical with Eq. (6), but with $|l|$ replaced by l . Similar remarks apply for the case when l is negative, with an obvious change in limits, and once again obtains Eq. (6), but with $|l|$ replaced by $-l$. Equation (6) still applies when $l = 0$.

APPENDIX C: DERIVATION OF EQ. (1b) FOR ROVIBRATIONAL STATES

In what follows, we use the notation and method of paper I. For group I molecules (defined there) we showed that a vibrational state with several quanta in at least one degenerate mode has a ratio of 1:1:3 for A labels to E labels to T labels ("labels" defined there). This symmetry species of the vibrational state was represented as equivalent to $A + E + 3T$. If we couple this symmetry species for the vibrational state to a rotational state having a general symmetry species $lA + mE + nT$ in the molecular point group,

where l , m , and n are zeros or integers, the overall symmetry of the coupled state is

$$\begin{aligned} (A + E + 3T)(lA + mE + nT) \\ = (l + 2m + 3n)A + (l + 2n + 3n)E \\ + (3l + 6m + 9n)T \\ \equiv A + E + 3T. \end{aligned} \quad (\text{C1})$$

(The equivalent sign is defined in Ref. 1). Thus, the ratio of A labels to E labels to T labels of the coupled rovibrational state is 1:1:3, as it was for the vibrational state alone. If we assume a randomization of the labels among all of the symmetry species as in Ref. 1, the analysis is identical to that given for vibrational states alone there and yields the value of f_r given by Eq. (1b). It is of interest to note, though the results are independent of this, that if one averages over the rotational symmetry species given by Weber¹⁵ by averaging over all K 's, one obtains the same results as the averaged overtone rules given in Table I of Ref. 1 for vibrational state alone.

Similar arguments are applicable to groups 2 and 3 in Ref. 1, and so Eq. (1b) applies to rovibrational states of these molecular point groups as well.

¹S. M. Lederman, J. H. Runnels, and R. A. Marcus, *J. Phys. Chem.* **87**, 4364 (1983).

²M. Quack, *Mol. Phys.* **34**, 477 (1977), this pioneering work was called to our attention too late for citation in Ref. 1; M. Quack, *Stud. Phys. Theor. Chem.* **23**, 2355 (1983); M. Quack, Dissertation, ETH-Lausanne, 1975.

³P. Pechukas, *J. Phys. Chem.* **88**, 828 (1984).

⁴A. Sinha and J. L. Kinsey, *J. Chem. Phys.* **80**, 2029 (1984).

⁵G. Z. Whitten and B. S. Rabinovitch, *J. Chem. Phys.* **38**, 2466 (1963); cf. P. J. Robinson and K. A. Holbrook, *Unimolecular Reactions* (Wiley-Interscience, New York, 1972), p. 131 ff.

⁶D. A. Dolson, K. W. Holtzclaw, S. H. Lee, S. Munchak, C. S. Parmenter, and B. M. Stone, *Laser Chem.* **2**, 271 (1983).

⁷G. Herzberg, *Infrared and Raman Spectroscopy of Polyatomic Molecules* (Van Nostrand Reinhold, New York, 1945), p. 211.

⁸E. B. Wilson, J. C. Decius, and P. C. Cross, *Molecular Vibrations*, (McGraw-Hill, New York, 1955), pp. 331 ff.

⁹Data given in Ref. 6, pp. 174 and 279, were used.

¹⁰Reference 6, p. 140.

¹¹Data given in Ref. 6, pp. 173 and 274, were used.

¹²T. Shimanouchi, *J. Phys. Chem. Ref. Data* **6**, 1071 (1977).

¹³Data given in Ref. 6, pp. 180 and 290, were used.

¹⁴J. T. Hougen, *J. Chem. Phys.* **37**, 1433 (1962); **39**, 358 (1963).

¹⁵A. Weber, *J. Chem. Phys.* **73**, 3952 (1980); **76**, 3694 (1982).

¹⁶M. Quack, Dissertation, Ref. 2, gives results for T_u molecules and hence for methane, Table V; J. T. Hougen in *MTP International Review of Science, Physical Chemistry Series 2*, edited by D. A. Ramsay (Butterworths, London, 1976), Vol. 3, Chap. 3; P. R. Bunker, *Molecular Symmetry and Spectroscopy* (Academic, New York, 1979), p. 242.

¹⁷We use the data for the first electronically excited state, as in Ref. 1, using results given by M. J. Robey and E. W. Schlag, *J. Chem. Phys.* **67**, 2775 (1977), together with those in E. Riedle, H. J. Neusser, and E. W. Schlag, *ibid.* **75**, 4231 (1981).

¹⁸Data given by N. L. Garland and E. K. C. Lee, *Faraday Discuss. Chem. Soc.* **75**, 377 (1983) were used, together with those in Ref. 6, p. 437.

¹⁹Data given by D. L. Gray and A. G. Robiette, *Mol. Phys.* **37**, 1901 (1979) were used, together with those in Ref. 6, p. 456.

**Chapter 3: Local Group Modes and the Dynamics of Intramolecular
Energy Transfer Across a Heavy Atom**

[The text of this chapter appeared in: V. Lopez, V. Fairen, S. M. Lederman and R. A. Marcus, *J. Chem. Phys.*, **84**, 5494 (1986).]

Local group modes and the dynamics of intramolecular energy transfer across a heavy atom

Vicente Lopez

Departamento Química Física y Química Cuántica, Universidad Autónoma de Madrid, Cantoblanco, 28049 Madrid, Spain

Victor Fairen

Departamento de Termología, Facultad de Ciencias, Universidad de Valladolid, Valladolid, Spain and Departamento de Física Fundamental, UNED, 28003 Madrid, Spain

Steven M. Lederman and R. A. Marcus

Arthur Amos Noyes Laboratory of Chemical Physics, California Institute of Technology,^{a)} Pasadena, California 91125

(Received 29 August 1985; accepted 11 February 1986)

The dynamics of energy transfer is discussed for a model system in which two ligands are separated by a heavy atom. Numerical and analytical results are given for the case that each ligand is a CC. In the quasiperiodic regime, the dynamics are interpreted using perturbation theory. Local group modes involved in an intramolecular energy localization which can occur in this regime are identified. An approximate separation of the primarily ligand–ligand motions from the primarily ligand–metal–ligand ones occurs in the clearly quasiperiodic regime and also at an energy where the power spectra of the bond coordinates are “grassy.” The overall analysis is used to make predictions for systems with larger ligands, when the primarily metal atom–ligand modes are, as above, approximately separable from the primarily intraligand ones.

I. INTRODUCTION

In a previous paper¹ we considered the energy transfer between two ligands attached to a heavy atom M. Classical trajectories were calculated for model system C–C–M–C–C. While energy transfer occurred at low energies, there was only a restricted energy transfer when the energy of one ligand was high enough that the vibration frequencies in the two ligands were no longer “resonant.” More recently, calculations² were also reported for a system with more coordinates, including bending motions. For excitation energies of 50 kcal mol⁻¹, the energy transfer was restricted for the potential energy surface used.

In the present paper we treat the motion analytically for the five-atom system C–C–M–C–C. The extent of energy transfer in the quasiperiodic regime is analyzed in terms of the “local group modes”—the anharmonic modes for each ligand—using perturbation theory to calculate the properties of these modes. The perturbation theory is also tested by comparison of semiclassical and quantum eigenvalues of a ligand. At high energies a regime that may be partially chaotic occurs for the five-atom system and is discussed.

Based on the analytical and numerical findings in the present paper it is shown how certain features of the results can be extended to larger systems, provided an approximate separation condition is fulfilled.

II. EXCITATION ENERGY AND ENERGY TRANSFER

In this section the results of numerical trajectory calculations are described for the C–C–M–C–C system, where the bonds are, as before, Morse oscillators coupled by the stretching momenta cross terms and where the masses have been chosen to roughly reproduce the C/Sn mass ratio.¹

These calculations are aimed at exploring the range of behavior found in the previous model. Because of the smaller number of coordinates now, a perturbation analysis is simpler. Nevertheless, the qualitative numerical behavior is similar to that found¹ for the seven-atom chain. In the analysis we focus attention on local group modes of each metal–ligand subsystem, the present system being the simplest example where these group modes can be studied.

The model Hamiltonian used is

$$H = \frac{1}{2} \sum_{i,j=1}^4 g_{ij} p_i p_j + \sum_{i=1}^4 D_i [1 - e^{-a(r_i - r_i^0)}]^2, \quad (1)$$

where the g_{ij} 's are the usual Wilson G -matrix elements³ that couple adjacent bonds. The Morse potential parameters are the same as those in Ref. 1, namely, $D_i = 84.1$ kcal mol⁻¹, $a = 1.54 \text{ \AA}^{-1}$, and $r_i^0 = 1.54 \text{ \AA}$ (cf. Ref. 1 for precise values in a.u.). The r_i 's in Eq. (1) are the bond distances and the p_i 's denote their canonically conjugate momenta. In order to describe the energy transfer across the heavy atom, approximate energies E_L and E_R for both halves of the model chain (the left containing $i = 1, 2$ and the right containing $i = 3, 4$) are defined in such a way that the Hamiltonian (1) can be rewritten as

$$H = H_L + H_R + V_{LR}, \quad (2)$$

where

$$E_L = H_L = H_1 + H_2 + g_{12} p_1 p_2, \quad (3a)$$

$$E_R = H_R = H_3 + H_4 + g_{34} p_3 p_4, \quad (3b)$$

$$V_{LR} = g_{23} p_2 p_3, \quad (3c)$$

and H_i ($i = 1-4$) denotes the Hamiltonian of the i th Morse bond given by

$$H_i = \frac{1}{2} g_{ii} p_i^2 + D [1 - e^{-a(r_i - r_i^0)}]^2. \quad (4)$$

Equation (4) can be reduced to its normal form

^{a)} California Institute of Technology Contribution No. 7255.

$$H_i = J_i \omega_i^0 (1 - \chi_i J_i) \quad (5)$$

using the usual action-angle variables⁴ related to the bond coordinates and momenta according to

$$J_i = \frac{1}{2\chi_i} \left(1 - \left[2z_i - z_i^2 - \frac{g_{ii} p_i^2}{2D} \right]^{1/2} \right), \quad (6)$$

$$\phi_i = \cos^{-1} \left(\frac{z_i - 1 + (g_{ii} p_i^2 / 2\chi_i D)}{[1 - 2z_i + z_i^2 + (g_{ii} p_i^2 / 2D)]^{1/2}} \right), \quad (7)$$

Here,

$$\omega_i^0 = [2Da^2 g_{ii}]^{1/2}, \quad \chi_i = \omega_i^0 / 4D, \quad (8)$$

$$z_i = \exp[-a(r_i - r_i^0)].$$

The trajectories were calculated with an initial excitation energy E_1 of bond 1. All other bonds were taken to have, at time zero, the zero-point energy value with the action variable $J_i = \frac{1}{2}$ (in units of $\hbar = 1$), $r_i = r_i^0$ and $p_i > 0$. A predictor-corrector method⁵ with double precision arithmetic was first used to perform the numerical integration of Hamilton's equations of motion. All forward trajectories were back integrated to check their reliability and the initial conditions were found to be preserved for all but one trajectory, discussed later, that at $E_1 = 0.5 D$. To back integrate the latter it was necessary to go to the unusual step of using quadruple precision.⁵ All trajectory data given in the present paper are now quadruple precision, with initial conditions being preserved, on back integration, to within 0.01%.

In Fig. 1 the time evolution of E_L and E_R is depicted for an initial excitation of bond 1 to $E_1 = 0.3 D$. When averaged over an ensemble of trajectories with the same initial excitation energy E_1 and different phases for bond 1, the oscillating components in E_L and E_R disappear, while the nonequibrated final distribution of energy is preserved. There is an excess of energy in the originally excited left-hand side of the molecule. While the excitation is redistributed between the bonds 1 and 2 in less than a picosecond, no complete energy transfer is observed across the heavy atom for a time of integration as long as 0.25 ns for the cited initial energy E_1 . (Approximately 25 harmonic oscillations of each C-C bond occur per picosecond.) Results for only a portion of the total trajectory time are given in Fig. 1, the remaining portion being similar to that depicted there.

In Fig. 2 power spectra of the dynamical variable r_1 and its symmetric counterpart r_4 are given for the above trajec-

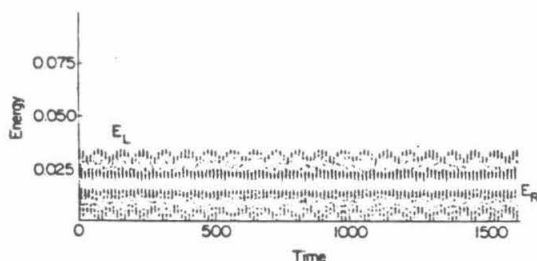


FIG. 1. Energy localization for $E_1 = 0.3 D$ and $\phi_1 = 0.5$. Figure depicts E_L and E_R (in a.u.) vs time. (One unit is $2\pi/\omega_i^0$ with ω_i^0 given by Eq. (8) and being about 0.038 ps.)

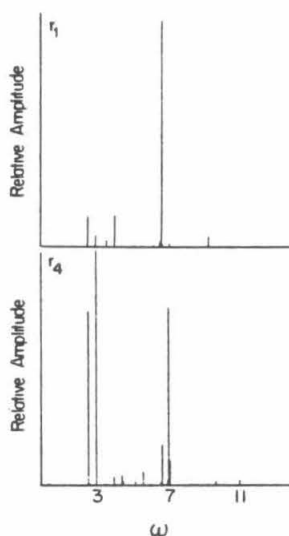


FIG. 2. Power spectra of bond distances r_1 and r_4 for $E_1 = 0.3 D$ and $\phi_1 = 0.5$. The unit of the angular frequency ω is the ω_i^0 given by Eq. (8).

tory. The spectra show that the motion is regular (quasiperiodic). The coordinates have the same frequencies, as they should in a coupled system, with a different intensity pattern as expected. The four fundamental frequencies should appear in pairs, due to the symmetry of the model chain. The fundamentals occur near $\omega = 3$ and 7 (units in caption).

The trajectory used for Fig. 1 is characteristic of a group of trajectories we will refer to as "localizing." They are prevalent for initial conditions corresponding to the energy range $E_1 = 0.15$ to $0.40 D$ (depending on initial phases, however). "Nonlocalizing" trajectories prevail for energies $E_1 < 0.1 D$. In the latter, energy equilibration between the two halves of the model chain is complete on the time scale of a C-C vibration. Power spectra for variables r_1 and r_4 for such trajectories are rather similar to the r_4 power spectrum displayed in Fig. 2.

When the excitation energy exceeds $0.4 D$, the behavior is different, although it is difficult to be precise about the energy range in which this new behavior appears. In Fig. 3 the time evolution of E_L is shown after an initial excitation of bond 1 to an energy of $0.5 D$. The trajectory is nonlocalizing and its power spectra (Fig. 4) have a number of grassy peaks; the model chain achieves a complete energy equilibra-

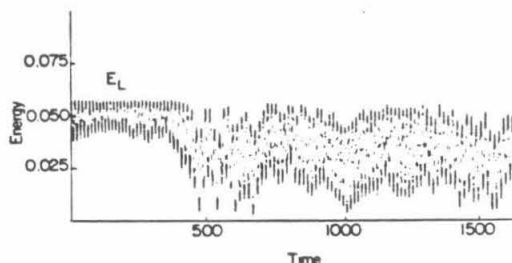


FIG. 3. E_L for a (possibly) chaotic trajectory for $E_1 = 0.5 D$ and $\phi_1 = 0.5$ (the same units as in Fig. 2).

tion across the heavy atom after some induction period has elapsed. In the corresponding power spectra for r_1 and r_4 in Fig. 4, a grasslike collection of lines appears that partially replaces the high frequency mode peak found in the previous quasiperiodic trajectories. On the other hand, the two low-frequency mode peaks, red shifted from their values in Fig. 2, still appear to be sharply defined. A combination band at an intermediate frequency has also become grassy.

Finally, at a still higher excitation energy of $E_1 = 0.7 D$, the seeming chaos has disappeared. A typical result is shown in Fig. 5 for the time evolution of E_L and E_R and in Fig. 6 for the power spectra of r_1 and r_4 . This result is an example of a localizing trajectory occurring for excitation energies E_1 near D . The intensity pattern in Fig. 6 differs from that in Fig. 1.

The above results summarize the different types of motion and energy transfer that we have encountered in this model system.

III. LOCAL GROUP MODE ANALYSIS

In this section the localization of energy described in Sec. II is analyzed in terms of resonances between the local group modes in each ligand, when the initial excitation of the left ligand is in the moderate energy range, namely for quasiperiodic trajectories in the range $E_1 < 0.4 D$. Local group modes involve a collective motion of the atoms of each ligand. The motion may be compared with that in a symmetric triatomic molecule ABA, with $m_B \gg m_A$. Here, the localization is due to nonlinear resonances between the two local bond modes^{6,7} AB and BA. A similar phenomenon is expected to occur in the present symmetric model chain, with a resonance now occurring between corresponding local group modes of each ligand. Only one of the two local group modes in each ligand, it will be shown, actively participates in the localization of energy in the present case.

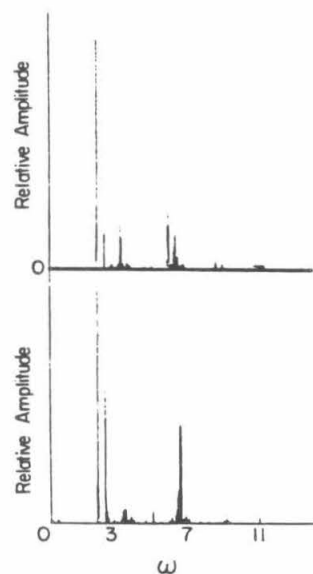


FIG. 4. Power spectra of bond distances r_1 and r_4 for $E_1 = 0.5 D$ and $\phi_1 = 0.5$ for the trajectory used for Fig. 3 (the same units as in Fig. 2).

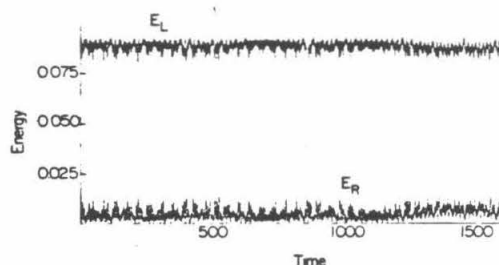


FIG. 5. Energy localization shown in the time evolution of E_L and E_R . $E_1 = 0.7 D$ and $\phi_1 = 0.5$ (the same units as in Fig. 1).

The analysis of results in Sec. II is performed by first identifying the local group modes of each ligand-metal subsystem. In the moderate to low energy range in which they occur ($E_1 < 0.4 D$), we will presume they are somewhat perturbed from the harmonic local group modes, i.e., from the standard normal modes of the ligand-metal subsystem. The corrections to normal modes are found in Appendix A using a Birkhoff-Gustavson perturbation scheme. In that analysis the Hamiltonians H_L and H_R in Eq. (3) are each cast into normal form [Eqs. (A11) and (A13)]. They are thereby expressed in terms of a polynomial in the local group mode actions, a polynomial generated here using terms up to and including fourth order analytically and sixth order numerically. The resulting H_L and H_R do not depend upon the new angle variables. The corresponding new action variables are thereby, within this order of approximation, constants of motion for $L-M$ and $M-R$, respectively. Physically, the two anharmonic local group modes in a ligand represent a primarily C-C stretching motion (termed the "X mode") and a primarily C-C group vs M motion (termed the "Y mode").⁸ The Y mode has a lower frequency of oscillation, due to a

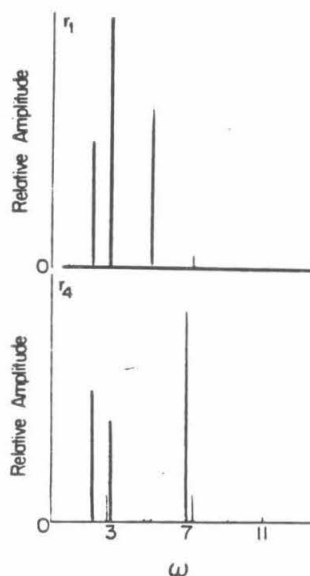


FIG. 6. Power spectra of bond distances r_1 and r_4 for $E_1 = 0.7 D$ and $\phi_1 = 0.5$ for the trajectory used for Fig. 5.

ngher effective mass. This perturbation scheme also yields the generating function needed to transform the original to the new action-angle variables.

Once an approximation to H_L and H_R has been constructed in terms of the actions of the local group modes, these expressions are introduced into Eq. (2), while the complicated expression for V_{LR} in terms of action-angle coordinates is expressed in terms of a Fourier series in the angle coordinates φ_x and φ_y for the X and Y modes for the left ligand and $\varphi_{x'}$ and $\varphi_{y'}$ for the equivalent X' and Y' modes for the right ligand. The resulting equation is

$$H = \sum_{n=1}^{\infty} \sum_{i+j=n} C_{ij} (J_x^i J_y^j + J_{x'}^i J_{y'}^j) + \sum_{k,l,m,n} V_{klmn} (J_x, J_{x'}, J_y, J_{y'}) \times \exp[i(k\varphi_x + l\varphi_y + m\varphi_{x'} + n\varphi_{y'})]. \quad (9)$$

In the standard Chirikov analysis^{9,10} of nonlinear resonances, only the leading terms of the expansion are usually taken into account. In the present problem we make the same approximation and see how well the results serve to interpret the trajectory results. From Eq. (A11) and leading terms of the Fourier expansion of V_{LR} , the resulting resonance Hamiltonian is¹¹

$$H = \omega_{0x} (J_x + J_{x'}) + \omega_{0y} (J_y + J_{y'}) - \lambda_x (J_x^2 + J_{x'}^2) - \lambda_y (J_y^2 + J_{y'}^2) - \lambda_{xy} (J_x J_y + J_{x'} J_{y'}) - \epsilon_x (J_x J_{x'})^{1/2} \cos(\varphi_x - \varphi_{x'}) - \epsilon_y (J_y J_{y'})^{1/2} \cos(\varphi_y - \varphi_{y'}). \quad (10)$$

where the λ 's are given in Eq. (A12) in Appendix A and the ϵ 's in Ref. 11. One omits thereby terms such as $\cos 2(\varphi_x - \varphi_{x'})$ and cross terms such as $\cos(\varphi_x - \varphi_{x'}) \cos(\varphi_y - \varphi_{y'})$. However, the omission does not decouple the (X, X') modes from the (Y, Y') ones, since there remain in Eq. (10) the λ_{xy} cross terms.

New variables are next introduced via a canonical transformation

$$\begin{aligned} I_x &= J_x + J_{x'}, & \theta_x &= (\varphi_x + \varphi_{x'})/2, \\ \bar{I}_x &= J_x - J_{x'}, & \bar{\theta}_x &= (\varphi_x - \varphi_{x'})/2, \\ I_y &= J_y + J_{y'}, & \theta_y &= (\varphi_y + \varphi_{y'})/2, \\ \bar{I}_y &= J_y - J_{y'}, & \bar{\theta}_y &= (\varphi_y - \varphi_{y'})/2. \end{aligned} \quad (11)$$

The new action variables \bar{I}_x and \bar{I}_y are particularly suited for monitoring the extent of energy transfer across the heavy atom. They describe what we shall call the \bar{X} and \bar{Y} motion of the molecular system. Equation (10) becomes

$$\begin{aligned} 2H &= 2\omega_{0x} I_x + 2\omega_{0y} I_y - \lambda_x (I_x^2 + \bar{I}_x^2) \\ &\quad - \lambda_y (I_y^2 + \bar{I}_y^2) - \lambda_{xy} (I_x I_y + \bar{I}_x \bar{I}_y) \\ &\quad - \epsilon_x (I_x^2 - \bar{I}_x^2)^{1/2} \cos 2\bar{\theta}_x \\ &\quad - \epsilon_y (I_y^2 - \bar{I}_y^2)^{1/2} \cos 2\bar{\theta}_y. \end{aligned} \quad (12)$$

As seen from the Hamiltonian in Eq. (12), I_x and I_y are constants of motion in this approximation. Including all the constants in a single term H_c , Eq. (12) may be rewritten as

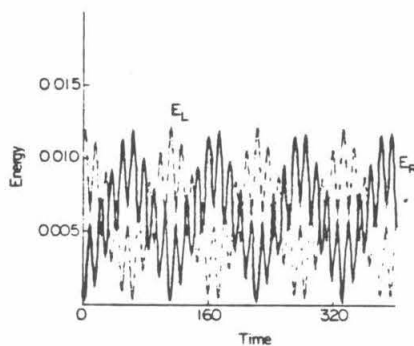


FIG. 7. Time evolution of E_L and E_R for nonlocalizing trajectory. $E_1 = 0.1$ D, $\phi_1 = 0.5$.

$$\begin{aligned} 2(H_c - E) &= \lambda_x \bar{I}_x^2 + \lambda_y \bar{I}_y^2 + \lambda_{xy} \bar{I}_x \bar{I}_y \\ &\quad + \epsilon_x (I_x^2 - \bar{I}_x^2)^{1/2} \cos 2\bar{\theta}_x \\ &\quad + \epsilon_y (I_y^2 - \bar{I}_y^2)^{1/2} \cos 2\bar{\theta}_y. \end{aligned} \quad (13)$$

The resulting Hamiltonian is equivalent to that of two coupled hindered rotors, each having a potential which is dependent on the action variables. Their momenta \bar{I}_x and \bar{I}_y represent differences between left and right local group mode actions, as in Eq. (11).

Numerical calculations for the energy and the actions are given in Figs. 7-14. They are made using the trajectory data for the conditions in Figs. 7 and 10 and using the sixth order actions (Appendix A) and the transformation equation (11). The time evolution of E_L and of E_R is depicted in Fig. 7 for a nonlocalizing group mode trajectory, and I_x and I_y for this trajectory are plotted vs time in Fig. 8. It is clear that both I_x and I_y are, as previously suggested, approximate constants of motion. On the other hand, it can be seen in Figs. 9 and 10 that both \bar{I}_x and \bar{I}_y each undergo a change of sign, i.e., they undergo an oscillatory motion. For the localizing trajectory whose energy in each ligand is plotted in

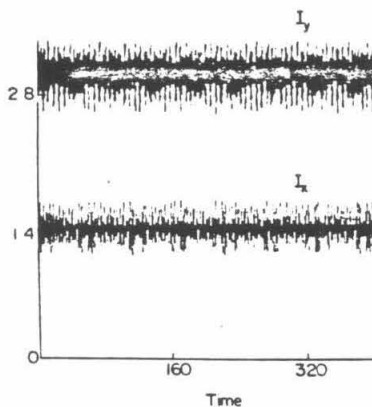


FIG. 8. Approximate invariants of the motion for the I_x and I_y (sixth order) modes of the molecule, corresponding to the trajectory used for Fig. 7.

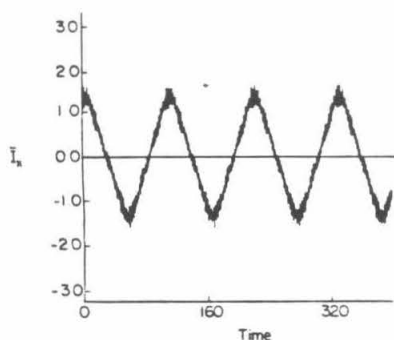


FIG. 9. Oscillating regime near the resonance for \bar{I}_x for the trajectory of Fig. 7.

Fig. 11, I_x and I_y are again approximate constants of motion (Fig. 12), \bar{I}_y still oscillates (Fig. 13), but the motion of \bar{I}_x has become "rotational", i.e., it no longer changes sign during the motion (Fig. 14). As a consequence there is no longer a complete equilibration of energy between the two ligands. That is, the \bar{X} motion (primarily an antisymmetric ligand-ligand motion) is responsible for the energy localization.

The above results and the behavior of the apparently only partially grassy spectrum in Fig. 4 indicate that the \bar{X} and \bar{Y} motions behave rather independently. They also indicate that although the \bar{Y} motion is only oscillatory in the examples given, the \bar{X} motion has two accessible possibilities, oscillation and rotation. A detailed understanding of this behavior is based on the following analysis.

When the frequency of the \bar{I}_y motion is significantly faster than that for \bar{I}_x as it is in Figs. 9 and 10 and Figs. 13 and 14, the λ_{xy} term tends to average to zero during the slow \bar{I}_x motion. Indeed, a subsequent numerical solution of the equations of motion based on the Hamiltonian (13) showed, for the conditions in Figs. 9 and 10, relatively little effect of the coupling term $\lambda_{xy}\bar{I}_x\bar{I}_y$. It produces the slow modulation of the amplitude of the \bar{I}_y motion noticeable in Fig. 10 and, to a lesser extent, in Fig. 14. For the solution based on Eq. (13), this modulation disappeared when λ_{xy} was set equal to zero. In what follows, we shall assume the \bar{I}_x and \bar{I}_y motions to be

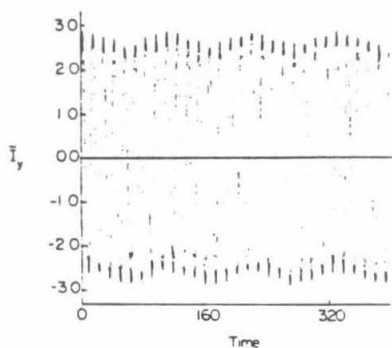


FIG. 10. Oscillating regime near the resonance for \bar{I}_y for the trajectory of Fig. 7.

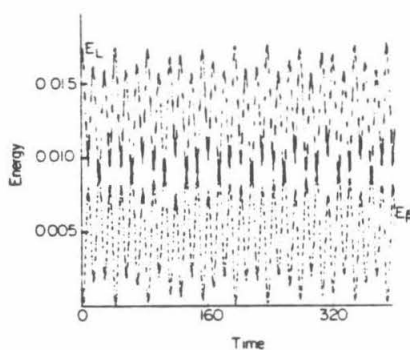


FIG. 11. Time evolution of E_L and E_R for a localizing trajectory. $E_1 = 0.15$ D, $\phi_1 = 0.5$.

largely decoupled by neglecting this λ_{xy} term. However, when the frequencies of those motions become comparable that term should be considered.

With the neglect of λ_{xy} , we may define an "energy" E_α , where α refers to X or Y :

$$2E_\alpha = \lambda_\alpha \bar{I}_\alpha^2 + \epsilon_\alpha (I_\alpha^2 - \bar{I}_\alpha^2)^{1/2} \cos 2\bar{\theta}_\alpha \quad (\alpha = X, Y). \quad (14)$$

The domain of interest in the phase space for φ_x and φ_y is $(0, 2\pi)$ and, as one sees from Eq. (11), the corresponding domain for $\bar{\theta}_x$ and for $\bar{\theta}_y$ is $(-\pi, \pi)$. The potential in Eq. (14) is periodic in $\bar{\theta}_\alpha$, with period π . Its maximum occurs at $\bar{\theta}_\alpha = 0$ and $\pm\pi$ and its minimum at $\bar{\theta}_\alpha = \pm\pi/2$. When the full $(-\pi, \pi)$ domain of $\bar{\theta}_\alpha$ is covered in the motion, the motion is "rotational"; when this domain is not fully explored $\bar{\theta}_\alpha$ oscillates about the point $\bar{\theta}_\alpha = \pi/2$ (or $-\pi/2$).

A separatrix in the $(\bar{I}_\alpha, \bar{\theta}_\alpha)$ phase plane separates the rotational from the oscillatory \bar{I}_α motion. The energy E_α^S for the separatrix found by noting that \bar{I}_α vanishes on the separatrix when $\cos 2\bar{\theta}_\alpha$ reaches its maximum $+1$. Thereby, from Eq. (14), we have

$$E_\alpha^S = \frac{1}{2}\epsilon_\alpha I_\alpha. \quad (15)$$

We next consider the conditions for \bar{I}_α to oscillate (i.e., that

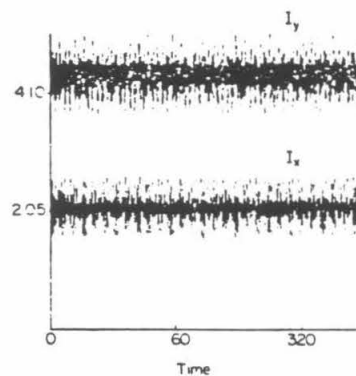


FIG. 12. Approximate invariants of the motion for I_x and I_y , modes of the molecule (sixth order), corresponding to the trajectory of Fig. 11.

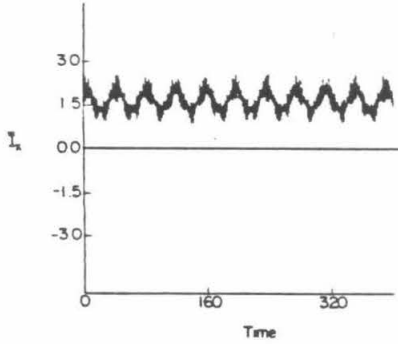


FIG. 13. Rotating regime for \bar{I}_x for the trajectory of Fig. 11.

$E_\alpha < E_\alpha^S$) or rotate ($E_\alpha > E_\alpha^S$), and to understand why the ease in attaining the "rotational" condition differs markedly for \bar{I}_x and \bar{I}_y (cf. Figs. 13 and 14).

We denote the maximum in \bar{I}_α during the motion by $\bar{I}_{\alpha,m}$. Since it occurs at $\cos 2\bar{\theta}_\alpha = -1$, Eq. (14) shows that

$$2E_\alpha = \lambda_\alpha \bar{I}_{\alpha,m}^2 - \epsilon_\alpha (I_\alpha^2 - \bar{I}_{\alpha,m}^2)^{1/2}. \quad (16)$$

In the particular case that the initial value of J_α ($\alpha = X$ or Y) is either small or if, due to energy transfer with $J_\alpha J_{\alpha'}$ becomes very small at some time during the motion, the maximum value of \bar{I}_α is seen from Eq. (11) to be close to I_α . In this case, Eq. (16) simplifies to

$$E_\alpha \approx \lambda_\alpha I_\alpha^2. \quad (17)$$

From Eqs. (15) and (17), one can easily determine the conditions for the \bar{I}_α motion to become localized on the hot ligand (i.e., for the motion of \bar{I}_α to become rotational), namely for $E_\alpha > E_\alpha^S$. Since E_α grows quadratically with I_α , as in Eq. (17), while E_α^S grows only linearly with I_α , as in Eq. (15), the condition $E_\alpha > E_\alpha^S$ is realized when I_α becomes large enough. When λ_α is small, as it is for the \bar{I}_y motion, the condition $E_\alpha > E_\alpha^S$ becomes difficult to attain and so the \bar{I}_y motion remains oscillatory, as in Figs. 10 and 14. From Eqs. (15) and (17), one sees that this condition $E_\alpha > E_\alpha^S$ is attained when I_α exceeds a critical value of I_α^C given by

$$I_\alpha^C = \epsilon_\alpha / \lambda_\alpha. \quad (18)$$

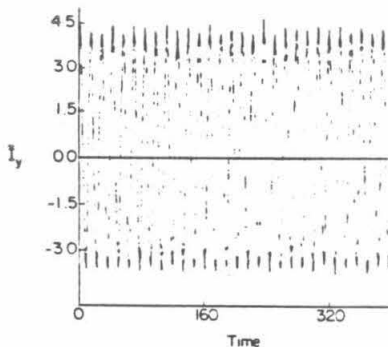


FIG. 14. Oscillating regime resonance for \bar{I}_y for the trajectory of Fig. 11.

For the values of the parameters considered in Sec. II, one finds $\lambda_x = 6.24$, $\epsilon_x = 11.44$, $\lambda_y = 0.99$, and $\epsilon_y = 65.98$, all in units of cm^{-1} . Thereby, $I_x^C \approx 1.83$ and $I_y^C \approx 66.6$. Examining the I_x 's and I_y 's in Figs. 8 and 12, it becomes clear why in both cases the motion of \bar{I}_α (Figs. 10 and 14) is oscillatory, why it should remain so even at much higher values of I_y , and why the \bar{I}_x motion is oscillatory in Fig. 9 (the I_x in the corresponding Fig. 8 is about 1.5), but rotational in Fig. 13 (I_x in the corresponding Fig. 12 is about 2.1).

Whether or not $\bar{I}_{\alpha,m}$ in Eq. (16) can attain a value nearly equal to I_α during the motion and hence permit use of the very simple Eq. (17), rather than requiring the use of Eq. (16), depends on the initial conditions. If J_α is made relatively small initially, as in the present examples, Eq. (17) becomes an increasingly good approximation to Eq. (16).

From Eq. (14), the frequency of the motion for \bar{I}_α can also be calculated, for any E_α and I_α . Equation (14) can be rearranged to give an equation containing second and zeroth powers of \bar{I}_α^2 , expressed as a function of powers of $\cos^2 2\bar{\theta}_\alpha$ and E_α . This quadratic equation for the variable \bar{I}_α^2 can be solved and the phase integral \bar{I}_α then calculated:

$$\bar{I}_\alpha = \oint \bar{I}_\alpha(\bar{\theta}_\alpha, E_\alpha) d\bar{\theta}_\alpha. \quad (19)$$

Here, the domain of $\bar{\theta}_\alpha$ is $(-\pi, \pi)$ for a rotational motion of \bar{I}_α and from turning point to turning point in the case that \bar{I}_α is oscillatory. The frequency $\bar{\omega}_\alpha$ of the \bar{I}_α motion is then calculated from the standard formula

$$\bar{\omega}_\alpha = dE_\alpha / d\bar{I}_\alpha = (d\bar{I}_\alpha / dE_\alpha)^{-1}. \quad (20)$$

We omit any further details of $\bar{\omega}_\alpha$, but merely note that a numerical solution of the equations of motion based on the Hamiltonian (13) gave good results for the frequency for the \bar{I}_y motion when there is a frequency gap of \bar{I}_x and \bar{I}_y motions, with or without the λ_{xy} term, at least if the system is not near the separatrix. The \bar{I}_x motion for the conditions in Fig. 13 is a very close to the separatrix and so whether or not it is localized (i.e., rotational) can also be sensitive to the initial conditions. A choice of the initial value of \bar{I}_x very close to I_x produced a rotational motion for the energy for Fig. 10.

We conclude this section by relating the preceding analysis to the matching or near matching of frequencies of the subsystems. The Hamiltonian (14) serves as a "resonance" Hamiltonian for transfer of action between the J_α and $J_{\alpha'}$ modes. It is more complicated than the standard Chirikov Hamiltonian,^{9,10} because the amplitude of this cosine term in Eq. (14) can vary markedly from nearly zero to some appreciable value, rather than being a nearly constant. The frequency ω_α of the J_α motion within a ligand is seen from Eq. (10), with the coupling terms λ_{xy} , ϵ_x , and ϵ_y set equal to zero, to be

$$\omega_\alpha = \partial H / \partial J_\alpha = \omega_{0\alpha} - 2\lambda_\alpha J_\alpha. \quad (21)$$

A resonance condition, and hence an extensive transfer of energy between the J_α and $J_{\alpha'}$ modes ($\alpha = X$ or Y), occurs when $\omega_\alpha \approx \omega_{\alpha'}$, i.e., when $J_\alpha \approx J_{\alpha'}$, for similar ligands. If the conditions are such that J_α and $J_{\alpha'}$ are sufficiently different, which may require a high value of $J_\alpha + J_{\alpha'}$ and an initially small J_α , ω_α and $\omega_{\alpha'}$ can be sufficiently different that a localization of the energy in the J_α mode can be achieved. We

have seen that this condition is difficult to achieve for the Y and Y' modes (i.e., for the \bar{I}_y motion)—there is too easy an energy transfer between the L - M and M - R modes—but it is achievable for the X and X' modes. Thereby, the restriction to the energy transfer is concentrated primarily in the intraligand modes J_x and $J_{x'}$.

IV. DISCUSSION

From the results of Secs. II and III, the following profile of the response of the system to increasing the excitation energy can be given: The local group modes involve collective motions of the ligands of the heavy central mass. A low-frequency mode in each ligand (the Y mode) has as its motion primarily that of the center of mass of a ligand vs the heavy atom; a high-frequency mode (the X mode) can be viewed as a relative motion of atoms within this ligand. Two key couplings occur in the local mode interaction: that between the modes of a particular ligand-metal atom subsystem, and that leading to the resonances between modes of the two subsystems. The rate and extent of energy transfer results from the interplay of both mechanisms. The former governs energy exchange within one ligand, while the latter regulates its flow between ligands.

At least for a moderate degree of excitation, the \bar{I}_x and \bar{I}_y motions appear to be approximately separable. Simultaneously, the ligand-ligand interaction may be explained as a 1:1 resonance between equivalent modes (J_x with $J_{x'}$ and J_y with $J_{y'}$). For very low excitations, namely for E_1 less than 0.1 D, the \bar{I}_x and \bar{I}_y motions are both oscillatory. The motion of the system is indeed expected to be largely that of somewhat perturbed normal modes of the whole chain. As the initial excitation energy is increased slightly, both the \bar{I}_x and the \bar{I}_y motion continue to be oscillatory, with the \bar{I}_y motion having the higher frequency of oscillation for the ligand to ligand energy transfer. There is no barrier to the energy flow in this region. Ultimately, the relatively small energy needed to exceed that of the separatrix of the resonance in the \bar{I}_x motion is responsible for the energy localization. Because of this small critical energy, the \bar{I}_x motion changes, for higher excitation, rapidly from oscillation about the resonance center to rotation, while the \bar{I}_y motion is still quasiharmonically oscillating. That is, the former, a primarily asymmetric ligand-ligand motion, serves to localize the energy while the other, a primarily asymmetric ligand-M-ligand motion, still transfers it.

The 1:1 resonance approximation used in Sec. II ceases to be valid when, at higher excitations, other X mode resonances become accessible to the system. These resonances arise from the neglected terms in the double Fourier expansion of the coupling term V_{LR} in Eq. (9). As is well known, the presence of several accessible resonances leads to an irregular ("chaotic") motion whenever the resonances begin to "overlap" (Chirikov theory), and power spectra then become grassy. With this aspect in mind we next consider the behavior in Figs. 3 and 4. A detailed analysis of this trajectory is beyond the scope of the present paper, which focuses instead on an analysis of the clearly quasiperiodic regime of $E_1 < 0.4$ D. However, a few remarks are in order. The most striking feature in Fig. 4 ($E_1 = 0.5$ D) is that the low fre-

quency peaks remain sharp while the high frequency ones and the combination band have become grassy. It follows that the approximate separation of the (X, X') motions from the (Y, Y') ones found at $E_1 < 0.4$ D continues at $E_1 = 0.5$ D. The sharp low frequency lines show that the motion of J_y and \bar{I}_y continues to be quasiperiodic. The grassy appearance of the other bands cannot be due to \bar{I}_x moving outside a resonance: A comparison of Fig. 9 with Fig. 13 shows that it already did so at an $E_1 = 0.15$ D and indeed such a move is expected to simplify the spectra. It could, of course, be due to \bar{I}_x moving into a new isolated resonance. Then to explain the grassy behavior in Fig. 4 one would presumably need to postulate that r_1 and r_4 are complicated functions of J_y, \bar{I}_y and of the (X, X') variables at $E_1 = 0.5$ D. (An isolated resonance yields a simple spectrum, a set of equally spaced lines in a single coordinate case, and hence the need to invoke complicated functions for r_1 and for r_4 , yielding many Fourier components.) Alternatively, the grassy appearance could be due to the onset of chaotic behavior¹² in the (X, X') motion. Indeed, the inability to back integrate this trajectory in double precision provides some evidence for this possibility. We shall not attempt to resolve this interesting question in the present paper.

Noting the above behavior of reducing to two separate two-coordinate problems for this five-atom system, one involving the X and X' motion and the other the Y and Y' motion, we briefly consider the induction period observed in Fig. 3. This induction period has been presumed in systems of two (chaotic) degrees of freedom to be related to the mean time¹³ needed to exit an area of phase space confined by the remnants of an invariant torus.¹⁴⁻¹⁶ Such a confinement need not occur in systems having a higher number of coupled anharmonic degrees of freedom.

At very high values of E_1 ($= 0.7$ D) a second clearly quasiperiodic regime for the entire system enters. We have not studied and attempted to characterize it as yet.

The \bar{I}_y motion was seen earlier to occur deep in a potential well, in virtue of the small value of λ_y and the large value for ϵ_y , for the given J_y . The \bar{I}_x motion was seen to be closer to the separatrix. Perhaps for this reason the \bar{I}_y motion appears to remain quasiperiodic in Figs. 3 and 4, while the \bar{I}_x motion showed a greater tendency to have a more complicated power spectrum (Fig. 4).

Using the above results, we next consider the behavior which might be predicted for system with many coordinates, i.e., for systems which approximate real molecules more closely. The Y and Y' modes were primarily the low frequency L vs M and M vs R motions, and are expected to remain so when L and R each become larger than a mere CC bond. For the conditions studied for Figs. 10 and 14, there was an easy energy exchange between these L vs M and M vs R modes. However, in large molecules this energy becomes typically only a small fraction of the total. The X and X' modes were primarily CC vibrations and now become primarily vibrations within L and R , respectively. At moderate energies they ceased to exchange energy significantly, but at energies where the power spectra became grassy they did so, though only after an induction period. A similar behavior can occur for the larger molecular system under certain conditions.

One condition for this energy localization in the excited ligand in larger systems is that there continue to be an approximate separation of the (X, X') from the (Y, Y') variables. In the present case, the frequency of the L vs M (and M vs R) motion was substantially less than that of the modes within L and R . Larger ligands will have some low frequency modes. If they are not coupled to the (Y, Y') variables, the approximate separation of variables can again occur. It is interesting to note therefore that in Ref. 2, which gave numerical results for larger systems, there was little energy transfer at moderate energies.

In the present analysis, attention has been focused for simplicity on the kinetic coupling in the C-M-C stretching motions. Potential energy coupling and a bending C-M-C coupling can also occur. This bond angle motion does not, however, appear to be involved in any major low order resonance (e.g., 1:1 or 1:2) with the C-M-C stretches, for the real molecules that we have examined. The results of Ref. 2, which included both of these additional couplings are thereby of added interest.

Perhaps the most striking finding in the present analysis is the approximate separation of variables in the primarily intraligand-intraligand motion from those in the primarily ligand-metal-ligand motion, a separation which appears in the clearly quasiperiodic regime for $E_1 < 0.4 D$ and in the new regime ($E_1 \sim 0.5 D$) whose power spectrum is grassy for certain lines and sharp for others.

The present calculations are classical. Some quantum mechanical calculations have been made in our group on the present system.¹⁷ We found that energy transfer occurs even when little occurred classically and hence that it occurred in that case by a tunneling mechanism and, thereby, at a reduced rate. Evidence is also obtained again for the approximate separation of variables. A detailed description of the results will be presented elsewhere.

ACKNOWLEDGMENTS

It is a pleasure to acknowledge the support of the National Science Foundation and of the U.S.-Spain Committee for Scientific and Technological Cooperation. We also acknowledge fruitful discussions with Dr. V. K. Babamov and invaluable computational assistance from Dr. D. W. Noid.

APPENDIX A: PERTURBATION HAMILTONIAN FOR METAL-LIGAND SUBSYSTEM

A perturbation technique is used in this appendix to find the approximate constants of the motion for H_L , and for H_R , and to examine the transition from nonlocalizing to localizing group mode trajectories at excitation energies $E_1 < 0.4 D$. For this range of energies, the vibrational modes in H_L and H_R cannot be too different from normal modes. Therefore, a perturbation scheme is used, the reference Hamiltonian being the one for which normal modes are valid. The Morse potentials are first expanded in a Taylor series around the equilibrium position

$$\sum_{i=1}^2 D(1 - e^{-a(r_i - r_i^0)})^2 = 2D \sum_{n=2}^{\infty} (-1)^n \frac{(2^{n-1} - 1)}{n!} a^n \times [(r_1 - r_1^0)^n + (r_2 - r_2^0)^n]. \quad (A1)$$

The Hamiltonian H_L is then divided into two parts

$$H_L = H_0 + V, \quad (A2)$$

where H_0 contains the quadratic terms

$$H_0 = \frac{1}{2} g_{11} p_1^2 + \frac{1}{2} g_{22} p_2^2 + g_{12} p_1 p_2 + Da^2 [(r_1 - r_1^0)^2 + (r_2 - r_2^0)^2] \quad (A3)$$

and V the anharmonic corrections

$$V = \sum_{n=3}^{\infty} 2Da^n V^{(n)},$$

where

$$V^{(n)} = \frac{(-1)^n (2^{n-1} - 1)}{n!} [(r_1 - r_1^0)^n + (r_2 - r_2^0)^n]. \quad (A4)$$

H_0 is an integrable Hamiltonian of a system that can be written as the sum of two independent harmonic oscillators of unit mass

$$H_0 = \frac{1}{2} (p_x^2 + p_y^2 + \omega_{0x}^2 x^2 + \omega_{0y}^2 y^2). \quad (A5)$$

where x and y are normal mode coordinates obtained from r_1 and r_2 by a linear transformation. In this notation x represents the high frequency normal mode and $s\omega_{0x} > \omega_{0y}$.

The anharmonic correction V has the following form in these new coordinates:

$$V = \sum_{n=3}^{\infty} \sum_{i+j=n} B_{ij} x^i y^j, \quad (A6)$$

where the B_{ij} are combinations¹⁸ of the g_{11} , g_{12} , and g_{22} appearing in Eq. (A3).

There is, therefore, a classical nonintegrable Hamiltonian

$$H = \frac{1}{2} (p_x^2 + \omega_{0x}^2 x^2) + \frac{1}{2} (p_y^2 + \omega_{0y}^2 y^2) + \sum_{n=3}^{\infty} \sum_{i+j=n} B_{ij} x^i y^j \quad (A7)$$

which for low energies can be approximated with a few terms and in which the nonintegrable part is a homogeneous polynomial in the coordinates.

An appropriate procedure for this case that permits the transformation of this Hamiltonian into a normal form, consisting of a power series of one dimensional uncoupled harmonic oscillators, has been given by Birkhoff¹⁹ and modified by Gustavson²⁰ to include systems with commensurable frequencies. This procedure has been reviewed elsewhere.²¹

The Birkhoff-Gustavson method was implemented with the aid of an automatic algebraic manipulator (SMP)²² to obtain H_L (H_R) in the normal form

$$H_L = \sum_n H^{(n)} = \sum_n \sum_{r+i=n} C_r^{(n)} [P_x^{(n)^2} + X^{(n)^2}]^r \times [P_y^{(n)^2} + Y^{(n)^2}]^i. \quad (A8)$$

This result can be achieved by successive canonical transfor-

TABLE I. Coefficients of the sixth order normal form of H_L (H_N).^a

C_{10}	1014.244 245	C_{20}	-6.235 703 968	C_{03}	-0.004 006 13
C_{01}	420.166 950 6	C_{02}	-0.985 135 279 6	C_{21}	-0.049 362 9
C_{11}	-4.567 716 084	C_{30}	0.004 999 26	C_{12}	0.038 390 3

^aUnits of the C_{ij} 's are cm^{-1} .

mations of the so called F_2 type, $F_2^{(m)}$ being the m th generating function:

$$F_2^{(m)} = P_x^{(m)} X^{(m-1)} + P_y^{(m)} Y^{(m-1)} + W(P_x^{(m)}, P_y^{(m)}, X^{(m-1)}, Y^{(m-1)}), \quad (\text{A9})$$

where $P_x^{(m)}$ and $P_y^{(m)}$ are a new momenta and $X^{(m-1)}$ and $Y^{(m-1)}$ are the old coordinates. The transformations equations are

$$\begin{aligned} X^{(m)} &= X^{(m-1)} + \frac{\partial W^{(m)}}{\partial P_x^{(m)}}, & Y^{(m)} &= Y^{(m-1)} + \frac{\partial W^{(m)}}{\partial P_y^{(m)}}, \\ P_x^{(m-1)} &= P_x^{(m)} + \frac{\partial W^{(m)}}{\partial X^{(m-1)}}, \\ P_y^{(m-1)} &= P_y^{(m)} + \frac{\partial W^{(m)}}{\partial Y^{(m-1)}}, \end{aligned} \quad (\text{A10})$$

where $X^{(m)}$ and $Y^{(m)}$ are new coordinates and $P_x^{(m-1)}$ and $P_y^{(m-1)}$ are the old momenta.

The generating function $W^{(m)}$ was obtained analytically up to and including $m = 4$. The normal form of H_L including terms up to $H^{(5)}$ is given by Eq. (A11) (the odd order terms vanish)

$$H_L = \omega_{0x} J_x + \omega_{0y} J_y - \lambda_x J_x^2 - \lambda_y J_y^2 - \lambda_{xy} J_x J_y, \quad (\text{A11})$$

where

$$\begin{aligned} \lambda_x &= -\frac{3}{2} b_{40} + \frac{15b_{30}^2}{4\omega_{0x}} + \frac{b_{21}^2 (8\omega_{0x}^2 - 3\omega_{0y}^2)}{4\omega_{0y} (4\omega_{0x}^2 - \omega_{0y}^2)}, \\ \lambda_y &= -\frac{3}{2} b_{04} + \frac{15b_{03}^2}{4\omega_{0y}} + \frac{b_{12}^2 (8\omega_{0y}^2 - 3\omega_{0x}^2)}{4\omega_{0x} (4\omega_{0y}^2 - \omega_{0x}^2)}, \\ \lambda_{xy} &= -b_{22} + \frac{3b_{03}b_{21}}{\omega_{0y}} + \frac{3b_{30}b_{12}}{\omega_{0x}} - \frac{2\omega_{0y}b_{12}^2}{(\omega_{0x}^2 - 4\omega_{0y}^2)} \\ &\quad - \frac{2\omega_{0x}b_{21}^2}{(\omega_{0y}^2 - 4\omega_{0x}^2)}. \end{aligned} \quad (\text{A12})$$

The b_{ij} 's are related to the coefficients appearing in Eq. (A7), $b_{ij} = B_{ij}/(\omega_{0x}'\omega_{0y}')^{1/2}$, and J_x and J_y in Eq. (A11) are the standard harmonic oscillator actions for the fourth order variables X , P_x , Y , and P_y .

These transformations have also been performed up to sixth order when the numerical values of the model system under study are used for ω_{0x} , ω_{0y} , and b_{ij} . The C_{ij} 's in the resulting Hamiltonian

$$H_L = \sum_{j=0}^3 C_{ij}^{(j)} J_x^{(6)} J_y^{(6)j} \quad (\text{A13})$$

are given in Table I for all (i, j) pairs whose sum lies between 1 and 3.

This approximate Hamiltonian is well suited²³ for EBK semiclassical quantization, and the accuracy of Eq. (A13) has been tested, by comparing the EBK semiclassical eigen-

values E_i^{SC} obtained from Eqs. (A11) and (A13) with the quantum eigenvalues E_i^Q obtained with a variational calculation using Morse wave functions as the basis set. In Table II we present numerical values of $E_i^Q - E_0^Q$ and of the $E_i^{\text{SC}} - E_0^{\text{SC}}$ obtained²⁴ with Eqs. (A11) and (A13) for $i < 30$, together with the number of quanta n_x and n_y in the X and Y modes, respectively. For eigenvalues with less than ten quanta in any mode, the quantity $E_i^{\text{SC}} - E_0^{\text{SC}}$ reproduces $E_i^Q - E_0^Q$ within 0.1%. Therefore, it can be expected that the actions $J_x^{(6)}$ and $J_y^{(6)}$ for the sixth order calculation represent with some accuracy the constants of the H_L motion for the range of energy containing at least up to the 30 quantum states in Table II. Thus, for sufficiently low energy, the motion of the C-C-Sn model system almost lies on the sur-

TABLE II. Comparison of variational eigenvalues E_i^Q of H_L and semiclassical values E_i^{SC} obtained with Eq. (A11).^a

n_x	n_y	$E_i^Q - E_0^Q$ (cm^{-1})	$E_i^{\text{SC}(4)} - E_0^{\text{SC}(4)}$ (cm^{-1})	$E_i^{\text{SC}(6)} - E_0^{\text{SC}(6)}$ (cm^{-1})
0	1	415.913	415.913	415.925
0	2	829.859	829.855	829.884
1	0	999.482	999.489	999.465
0	3	1241.81	1241.83	1241.85
1	1	1410.80	1410.83	1410.80
0	4	1651.75	1651.83	1651.80
1	2	1820.24	1820.21	1820.25
2	0	1986.49	1986.51	1986.45
0	5	2059.64	2059.86	2059.71
1	3	2227.76	2227.61	2227.78
2	1	2393.12	2393.28	2393.10
0	6	2465.46	2465.92	2465.55
1	4	2633.35	2633.05	2633.37
2	2	2797.92	2798.09	2797.94
3	0	2869.18	2870.01	2869.31
0	7	2961.05	2961.05	2961.00
1	5	3036.99	3036.51	3036.99
2	3	3200.90	3200.93	3200.93
0	8	3270.76	3272.13	3270.96
3	1	3362.88	3363.26	3362.86
1	6	3438.66	3438.00	3438.73
2	4	3602.03	3601.79	3602.06
0	9	3670.19	3672.29	3670.47
3	2	3762.96	3763.50	3762.98
1	7	3838.32	3837.53	3838.26
4	0	3923.22	3923.13	3923.13
2	5	4001.28	4000.69	4001.31
0	10	4067.42	4070.47	4067.82
3	3	4161.27	4161.67	4161.34
1	8	4235.96	4235.08	4235.86

^a n_x and n_y are the number of quanta in the X and Y modes. $E_i^{\text{SC}(4)}$ and $E_i^{\text{SC}(6)}$ are obtained to fourth order [Eq. (A11)] and sixth order, respectively. $E_0^Q = 715.084 \text{ cm}^{-1}$, $E_0^{\text{SC}(4)} = 714.258 \text{ cm}^{-1}$, $E_0^{\text{SC}(6)} = 714.257 \text{ cm}^{-1}$.

face of an invariant torus of radii given by $J_x^{(6)}$ and $J_y^{(6)}$. The $X^{(6)}$ motion in this torus mainly corresponds to the vibration of the C-C bond with a frequency $\partial H_L / \partial J_x^{(6)}$ or, using Eq. (A13),

$$\omega_x = \sum_{j=0}^3 i C_j^{(6)} J_x^{(6)j-1} J_y^{(6)j}, \quad (\text{A14})$$

whereas the $Y^{(6)}$ motion corresponds mostly to the vibration of the C-C center of mass against the Sn, with a lower frequency

$$\omega_y = \sum_{j=0}^3 j C_j^{(6)} J_x^{(6)j} J_y^{(6)j-1}. \quad (\text{A15})$$

Comparison of the numerical values of these frequencies using the $C_j^{(6)}$'s given in Table I shows the difference in anharmonicities between the two group modes. The X mode, with higher frequency, has also a larger anharmonicity ($C_{20} \approx 6.3 C_{02}$).

¹V. Lopez and R. A. Marcus, Chem. Phys. Lett. 93, 232 (1982). The masses used there and in the present paper 22 063.6065 and 218 027.596 a.u. are within a percent of the masses of C and Sn. In a.u., the D , a , and r' used in Eq. (1) are exactly 0.134, 0.815, and 2.91, respectively.

²K. N. Swamy and W. H. Hase, J. Chem. Phys. 82, 123 (1985).

³E. B. Wilson, J. C. Decius and P. C. Cross, *Molecular Vibrations* (McGraw-Hill, New York, 1955).

⁴C. C. Rankin and W. H. Miller, J. Chem. Phys. 55, 3150 (1971). This action variable is (in units of $\hbar = 1$) the classical equivalent of $n + 1/2$, where n is a continuous variable classically and an integer quantum mechanically. It is canonically conjugate to an angle variable which varies over an interval of 2π . The conventional action variable is instead $(n + 1/2)\hbar$ or, in units of $\hbar = 1, 2\pi(n + 1/2)$ and is conjugate to an angle variable which varies over a unit interval.

⁵M. K. Gordon, Sandia Laboratories Report, SAND 75-0211; L. F. Sham-pine and M. K. Gordon, *Computer Solution of Ordinary Differential Equations* (Freeman, San Francisco, 1975). We are particularly indebted to Dr. D. W. Noid of Oak Ridge National Laboratory for obtaining the quadruple-precision trajectories.

⁶C. Jaffé and P. Brumer, J. Chem. Phys. 73, 5646 (1980); C. Jaffé, *ibid.* 81, 616 (1984).

⁷E. L. Sibert III, W. P. Reinhardt, and J. T. Hynes, J. Chem. Phys. 77, 3583 (1982); R. M. Hedges and W. P. Reinhardt, *ibid.* 78, 3964 (1983); S. K. Gray and M. S. Child, Mol. Phys. 53, 961 (1984).

⁸The adiabatic separation between the slower motion along the Sn-CC coordinate and the faster motion along the C-C coordinate is analogous to the separation of the F-HH and the H-H motion in the collinear F-H-H system, first discussed by V. K. Babamov and A. Kuppermann [J. Chem. Phys. 77, 189 (1982)]. The latter is believed there to be responsible for the stability of the long lived states (resonances) in the collinear F + H₂ collision.

⁹B. V. Chirikov, Phys. Rep. 52, 263 (1979).

¹⁰A. J. Lichtenberg and M. A. Leiberman, *Regular and Stochastic Motion* (Springer, New York, 1983).

¹¹From Hamilton equations for the two independent oscillators of Hamiltonian (3a), it is easy to obtain frequencies ω_{0x} and ω_{0y} as those of the linearized motion around the minima of their potentials. From the coefficients of the linear transformation from local to normal mode momenta $P_2 = -a_x p_x + a_y p_y$, we get $\epsilon_x = \omega_{0x} a_x^2 / M$, $\epsilon_y = \omega_{0y} a_y^2 / M$, with M as the mass of the central atom.

¹²D. W. Noid, M. L. Koszykowski, and R. A. Marcus, J. Chem. Phys. 67, 404 (1977).

¹³J. C. Percival, AIP Conf. Proc. No. 57, 302 (1979); R. S. MacKay, J. D. Meiss, and I. C. Percival, Physica D 13, 55 (1984).

¹⁴S. Aubry, in *Solutions and Condensed Matter Physics*, edited by A. R. Bishop and T. Schneider (Springer, Berlin, 1978), p. 264.

¹⁵J. N. Mather, Topology, 21, 457 (1982); A. Katok, Ergodic Theory Dynam. Sys. 2, 185 (1982).

¹⁶R. B. Shirts and W. P. Reinhardt, J. Chem. Phys. 77, 5204 (1982).

¹⁷S. M. Lederman, V. Lopez, G. A. Voth, and R. A. Marcus, Chem. Phys. Lett. 124, 93 (1986).

¹⁸The B_j 's are the coefficients obtained upon substitution of the linear transformation from local to normal coordinates in Eq. (A6).

¹⁹G. D. Birkhoff, *Dynamical Systems* (American Mathematical Society, New York, 1966).

²⁰F. G. Gustavson, Astron. J. 71, 670 (1966).

²¹E.g., T. Uzer, D. W. Noid, and R. A. Marcus, J. Chem. Phys. 79, 4412 (1983), see Appendix A.

²²SMP is a symbolic manipulation program developed by the High Energy Physics group at Caltech.

²³R. T. Swimm and J. B. Delos, J. Chem. Phys. 71, 1706 (1979).

²⁴The numerical values of $\lambda_x, \lambda_y, \lambda_{xy}$ equal the $-C_{20}, -C_{02}$, and $-C_{11}$ given in Table I and $C_{10} = \omega_{0x}, C_{01} = \omega_{0y}$.

**Chapter 4: Quantum and Classical Energy Transfer Between Ligands
of a Heavy Metal Atom**

[The text of this chapter appeared in: S. M. Lederman, V. Lopez, G. A. Voth and R. A. Marcus, *Chem. Phys. Lett.*, **124**, 93 (1986).]

QUANTUM AND CLASSICAL ENERGY TRANSFER BETWEEN LIGANDS OF A HEAVY METAL ATOM

Steven M. LEDERMAN ^a, Vicente LOPEZ ^b, Gregory A. VOTH ^a and R.A. MARCUS ^a

^a Arthur Amos Noyes Laboratory of Chemical Physics ¹, California Institute of Technology, Pasadena, CA 91125, USA

^b Departamento Química Física y Química Cuántica, Universidad Autónoma de Madrid, Cantoblanco, 28049 Madrid, Spain

Received 25 October 1985

Quantum and classical vibrational energy transfer between two ligands separated by a heavy atom are compared for a model system, one ligand being vibrationally excited initially and the other unexcited. Similarities and differences of quantum and classical results are noted. The approximate separability of certain modes simplifies the interpretation.

1. Introduction

There has been recent interest in the effect of a heavy central atom on intramolecular vibrational redistribution [1-5]. Experimental studies on some organometallic compounds have suggested that a heavy metal atom may reduce the energy transfer between the ligands [1], while in another study on a somewhat different system this effect was not observed [2]. Several classical trajectory calculations on models of ligand-metal atom systems have also been reported [3-5]. Studies were made for a non-bending seven-atom chain C-C-C-M-C-C-C [3], an analogous five-atom chain [5], and a much larger system [4]. Analytical results were given for the five-atom system (four coupled Morse oscillators) [5] and compared with trajectory results. A condition that the analysis be applicable or extendable to larger and hence more realistic molecular systems was also described [5].

Quantum and classical dynamical calculations are presented and compared here for the model system studied in ref. [5], the initial state in each case being that of excited "local group modes" described below. The initial classical states are chosen by a semiclassical procedure to permit a direct comparison with the quantum results. The methods used for the calculations are outlined in section 2 and the preliminary

quantum and classical results for the model system are reported in section 3. In section 4 these results are discussed. Implications of the quantum-classical comparison for classical trajectory studies of unimolecular reactions are also noted.

2. Theory

We first recall several results obtained in our earlier study [5], where both the C-C-M-C-C system and the C-C-M subsystem were investigated. In this study the C-C bond in one ligand was initially excited (the other bonds had zero-point energy) and energy transfer to the other ligand was examined. The concept of anharmonic collective modes (local group modes) for the C-C-M subsystem was introduced. They were calculated using sixth-order Birkhoff-Gustavson perturbation theory, the unperturbed modes being the (harmonic) normal modes of the C-C-M subsystem. The resonant coupling of the C-C-M and M-C-C modes was then investigated analytically, supplementing the trajectory studies. The local group modes of the C-C-M ligand-metal subsystem were found to be of two quite different types. One such anharmonic group mode was largely, though not entirely, a ligand mode (termed the X mode). For the initial excitations studied it showed little energy transfer at moderate energies to the unexcited ligand but extensive exchange at low energies.

¹ Contribution No. 7298.

The other (termed the Y mode) was primarily, though not entirely, a C-C versus M vibration. It showed extensive energy exchange with the Y mode of the other ligand in both energy regions.

There are a number of advantages in introducing these X and Y local group modes: (1) There is an approximate separation of variables for these two modes, even when they are coupled to X and Y modes in the second (M-C-C) subsystem [5]. This approximate separation arises because of a frequency gap of the X and Y modes, and occurs except near the "separatrix" of the X motion in C-C-M-C-C [5]. (2) They facilitate the comparison of classical and quantum results, as described later. (3) Their use in the quantum calculation itself is advantageous: Initial quantum calculations using states of local bond mode Morse oscillators, instead of local group mode oscillators, as the basis functions showed convergence difficulties due to the large kinetic coupling between the zeroth-order bond mode Morse oscillator states. To avoid this difficulty, the eigenstates for each subsystem, C-C-M and M-C-C, were first obtained by "prediagonalizing" the couplings in these two subsystems. The new states thus obtained correspond to various excitations of the two local group modes of C-C-M (and similarly for M-C-C). Next, symmetrical and antisymmetrical products of the eigenstates of C-C-M and M-C-C were used as elements of a basis set to represent the Hamiltonian of the total system, which includes the kinetic energy coupling of the two subsystems across the heavy mass M. In this way convergence was obtained more readily for the full system, compared with that when the bond mode basis set was used.

In the quantum calculations the initial non-stationary wavefunction was chosen to be the product of two local group mode wavefunctions, one for each subsystem, which was then propagated in time. The identity of each eigenstate of a subsystem was determined using a classical analysis for local group modes and semiclassical methods. The Hamiltonian and the molecular parameters used were those in ref. [5]:

$$H = \frac{1}{2} \sum_{i,j=1}^4 g_{ij} p_i p_j + \sum_{i=1}^4 D \{1 - \exp[-a(r_i - r_i^e)]\}^2, \quad (1)$$

where the g_{ij} are the usual Wilson G -matrix elements [6] that couple adjacent bonds i and j . The Morse

potential parameters are the same as those in refs. [3,5], the r_i are the bond distances and the p_i are their canonically conjugate momenta. From the eigenvalues and eigenvectors of the system C-C-M-C-C and a knowledge of the initial state, all determined as above, the expectation value of the energy in the excited subsystem, C-C-M, was then determined as a function of time. (The kinetic energy coupling term $g_{23}p_2p_3$ across the heavy mass was small and was not included in the energy of the C-C-M subsystem displayed in figs. 1-4.)

Classical trajectories were also calculated to compare with the quantum results. The adiabatic switching method [7] was used to prepare an initial classical state having the desired quantized anharmonic local group mode action variables for the C-C-M and M-C-C subsystems. These initial action variables correspond semiclassically to the initial local group mode quantum numbers of the two uncoupled subsystems in the quantum calculation. Results for the eigenvalues of C-C-M obtained in this way are given in section 3.

Because of the absence of degeneracies, the adiabatic switching method gave excellent results. In particular, the final C-C-M-C-C energy, after the adiabatic switching but before the $g_{23}p_2p_3$ term was introduced, was independent of the initial phase of the trajectory. An initial zeroth-order (harmonic) classical state before adiabatic switching consisted of some excitation of the normal modes of C-C-M (M-C-C) in a harmonic Hamiltonian and had specified action variables. It was used to prepare by adiabatic switching an actual group mode state of C-C-M (M-C-C) having the same action variables. (The fourth- or sixth-order perturbation theory had established earlier the correspondence between the harmonic states of C-C-M and those of the anharmonic C-C-M [5].) The adiabatic switching thus involved the slow conversion of the harmonic potentials to the Morse bond potentials to obtain the desired anharmonic group mode trajectories. Switching times of 50, 100 and 200 C-C vibrational periods (1.9, 3.8 and 7.6 ps) were used and gave essentially the same results for the eigenvalues. The 100-period switching time was used in the calculations reported below.

An ensemble of these trajectories, each prepared by adiabatic switching and having the same initial action variables and a random selection of the four ini-

tial phases for the harmonic system, was then used to calculate the ensuing dynamics. Only forty such trajectories were used for the present preliminary calculations in each case. The average energy in the C-C-M subsystem was then computed as a function of time after this C-M-C coupling was initiated.

3. Results

The initial excitation is denoted by (n_X^L, n_Y^L) , where the n_X^L and n_Y^L denote the number of quanta in the X and Y group modes in the first subsystem (the "left subsystem") C-C-M. (This description of the states is the one used in table 2 of ref. [5].) The initial state assigned to the X and Y group modes in the second subsystem M-C-C was the ground state $[(n_X^R, n_Y^R) = (0,0)]$. Thus, the initial state of the entire system is a product of the (n_X^L, n_Y^L) state of C-C-M and the (0,0) state of M-C-C. In the figures the energy of the C-C-M in atomic units is plotted versus time in picoseconds. Results were obtained using initial C-C-M states of $(n_X^L, n_Y^L) = (4,0)$, (0,10), and (3,3).

We first report the results of the semiclassical quantization procedure used to identify the local group mode quantum numbers in the quantum calculations and to prepare the corresponding trajectories in the classical calculations. The semiclassical eigenvalues obtained by the adiabatic switching method for these states were 3923.16, 4067.60 and 4161.25 cm^{-1} , respectively, for energies in excess of the zero-point energy, while those obtained [5] by sixth-order Birkhoff-Gustavson perturbation theory were 3923.13, 4067.82 and 4161.34 cm^{-1} . The quantum mechanical eigenvalues which were closest to these semiclassical eigenvalues were 3923.21, 4067.42, and 4161.27 cm^{-1} , respectively [5], and this matching provided a simple identification of the local group mode quantum numbers of these states in the quantum mechanical calculations. The convergence of the quantum calculations themselves was tested by increasing the basis set for C-C-M-C-C from 1764 to 2500 basis functions, and no significant difference in eigenvalues, to twelve places, was found. In addition, no significant difference was found for the various expectation value plots in figs. 1-4.

The quantum and classical results for the

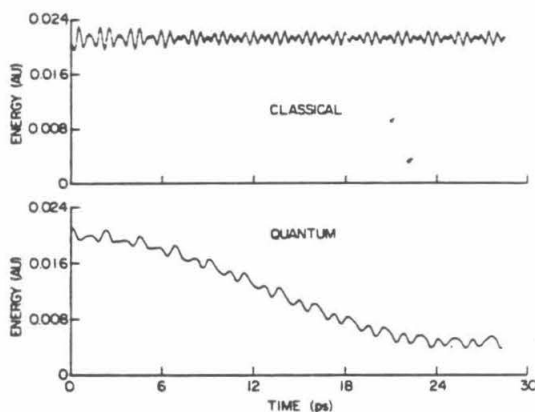


Fig. 1. Energy of C-C-M subsystem in C-C-M-C-C versus time, when the initial excitation is (4,0), and the M-C-C is initially in the state (0,0). Upper curve: classical. Lower curve: quantum.

C-C-M-C-C system with an initial state of (4,0) for C-C-M are given in fig. 1, and the quantum results for a longer time are given in fig. 2. This excitation represents one of an X-type group mode with a C-C-M energy of 0.021 au or 0.16 D. In figs. 1 and 2 it is seen that in the quantum case there is a periodic transfer of energy from one side of the molecule to the other. The corresponding classical results, also given in fig. 1, show no energy transfer.

In fig. 3 the energy of the C-C-M subsystem is

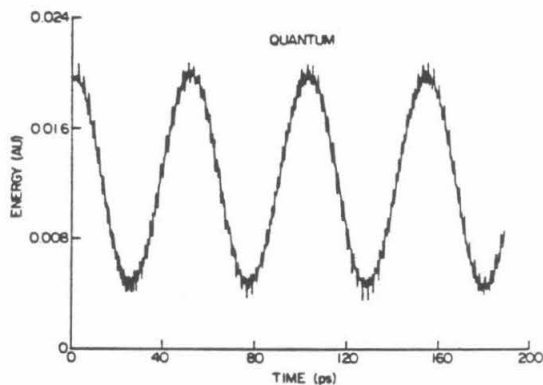


Fig. 2. Quantum results for conditions same as fig. 1 but plotted for a longer time.

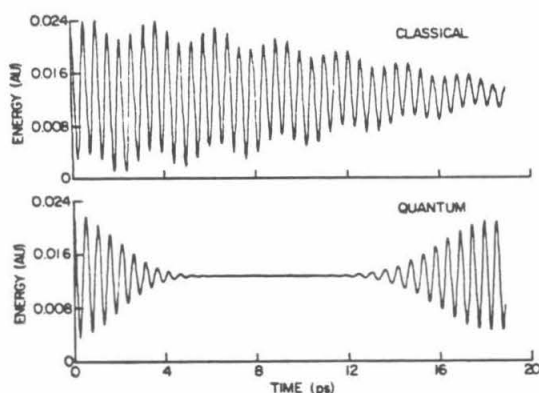


Fig. 3. Same as fig. 1 but for a (0,10) and (0,0) excitation of C-C-M and M-C-C, respectively.

plotted for an initial excitation of (0,10), which corresponds to the excitation of a Y-type group mode of C-C-M. The rate of transfer is much more rapid, both classically and quantum mechanically.

The time behavior of the energy of the C-C-M subsystem for an excitation of the initial state (3,3) is given in fig. 4. This state is a combination state of excited X- and Y-group modes, and shows a behavior characteristic of each (cf. figs. 2 and 3).

The mean energies $\langle H \rangle$ for the wavepackets describing the states with initial excitations of (4,0), (0,10) and (3,3) for C-C-M and (0,0) for M-C-C were

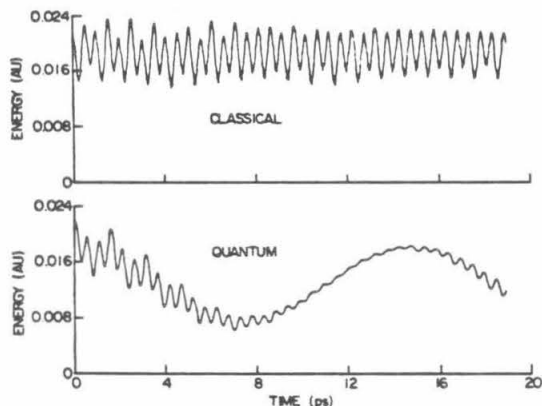


Fig. 4. Same as fig. 1 but for a (3,3) and (0,0) excitation of C-C-M and M-C-C, respectively.

calculated to be 2.44×10^{-2} , 2.50×10^{-2} , and 2.55×10^{-2} au, respectively. (H denotes the full Hamiltonian of C-C-M-C-C.) The root mean square deviation $(\langle H^2 \rangle - \langle H \rangle^2)^{1/2}$ of the energies of the initial wave packet was, in each case, relatively small, being 2.6×10^{-4} , 7.2×10^{-4} , and 4.5×10^{-4} , respectively.

4. Discussion

In the case of the excitation of the (4,0) state in fig. 1, no energy transfer occurs classically for the sample of trajectories used. In contrast, a periodic energy transfer (figs. 1 and 2) occurs quantum mechanically and is apparently due, therefore, to a classically forbidden process ("tunneling"). The period of the energy transfer is seen to be about 50 ps.

The behavior when the initial excitation is (0,10), namely of the Y mode, is seen in fig. 3 to be quite different, although the initial energy is approximately the same. The transfer of energy in both the classical and quantum cases occurs much more rapidly, each with the same period of about 0.5 ps for the high-frequency oscillation. This period agrees well with that computed numerically from the relatively simple classical resonance Hamiltonian derived using perturbation theory in ref. [5] (eq. (13)). The oscillation in energy of C-C-M is approximately from the initial excitation of the C-C-M subsystem to its zero-point energy and then back again. Also seen in the quantum plot in fig. 3 is a damping to a near-stationary value which corresponds to an equal energy on each side of the molecule. Subsequently the amplitude of oscillation again increases and ultimately the slow time behavior observed in this figure will repeat itself. A detailed comparison of the quantum and classical longer time behavior is not appropriate at this time, in virtue of the small sample of classical trajectories.

An initial excitation of the (3,3) state (fig. 4) yields a time dependence in the quantum case for the energy of the C-C-M subsystem whose qualitative appearance is that of a combination of that in figs. 2 and 3. It shows the rapid oscillations of energy found for a Y-mode excitation (fig. 3) and the slower oscillation seen for an X-mode excitation (fig. 2). The classical result itself does not show the slow energy oscillation found in the quantum result (nor did it for the

(4,0) case). The high-frequency oscillation is again similar for the two results. This behaviour for the (3,3) excitation, namely being approximately the superposition of that for the X-mode and for the Y-mode excitation, can be interpreted in terms of the approximate separation of variables used to analyze the classical results in ref. [5].

Further support for an approximate separation of variables in the energy regime examined in the present paper comes from a comparison of the quantum results with those obtained (but not cited in section 3) using smaller basis sets: To compare with the results for the (4,0) excitation in figs. 1 and 2, a basis set was used consisting purely of X-mode excitations for the left and right subsystems, and using the ground state for the Y mode. The results for the energy of C-C-M subsystem versus time were essentially the same as in fig. 2. Indeed, even a five-state basis set having $n_X^L + n_X^R = 4$ provided good agreement with this plot. A similar remark applies to an analogous calculation for an excitation of the (0,10) state in fig. 3 using purely Y-mode excitations and also such excitations with $n_Y^L + n_Y^R = 10$.

The lack of classical energy transfer when the X mode of C-C-M is excited, in contrast to the ready transfer when the Y mode is excited to about the same energy, was explained in ref. [5]: A classical resonance theory was described there and applied to those local group modes and to those of the M-C-C subsystem. The analysis also applies, semiclassically, to the quantum case. However, in the case of a high X-mode excitation, e.g., the (4,0) state, a classically forbidden transfer between two symmetrically related classical tori can occur and permits quantum mechanical energy transfer where it did not occur classically.

The present comparison of classical and quantum results also illustrates a potential shortcoming of classical trajectory calculations of unimolecular processes, a shortcoming sometimes overlooked in such studies when classical tori exist. In fig. 1 an example is given where there is essentially no energy transfer between two parts of a molecule classically (between two tori [5]), but there is a slow transfer quantum mechanically. In this way classical trajectories can give the appearance of less energy redistribution in an isolated molecule than would occur for a wave packet in a corresponding quantum mechanical and hence

more realistic calculation. This type of behavior is well known for ABA triatomic systems [8].

If there is an approximate separation of the intraligand and metal-ligand modes in a real molecule (X and Y modes, respectively), energy localization in a ligand may be obtained by an appropriate excitation of the X modes. For example, in the case of alkyl ligands, the X modes would involve the stretching and bending modes of the ligand's carbon and hydrogen atoms. Excitation of X modes of a particular ligand can then be made either via a single-photon high C-H stretching overtone excitation or via an infrared multiphoton excitation of CH bends. (The other ligands could contain D atoms rather than H atoms, to reduce their absorption at the relevant frequencies.) These methods for exciting X modes are suitable, unless some overtone of the metal-ligand Y mode has sufficiently large absorption in the excitation range. It may also be noted that the shorter the excitation pulse, for a given total integrated intensity, the more likely that a localized excitation would cause the excited ligand to react before its energy decays by classical or tunneling processes to the remaining ligands. A direct excitation of the metal-ligand (Y mode) states is perhaps possible using a suitable laser, but would not be useful for the purpose of energy localization and subsequent reaction within one ligand. The main question to be resolved, of course, is whether the Y-mode states are, in real molecules, resonantly coupled to X-mode states, thereby eliminating any separability of the two types of motion.

A more detailed paper amplifying and extending the present results will be submitted for publication, including the extension to larger systems.

Acknowledgement

It is a pleasure to acknowledge the support of the National Science Foundation and of the US-Spain Committee for Scientific and Technological Cooperation. We would also like to acknowledge helpful discussions with Dr. Victor Fahren.

References

- [1] P.J. Rogers, J.I. Selco and F.S. Rowland, *Chem. Phys. Letters* 97 (1983) 313;
P.J. Rogers, D.C. Montague, J.P. Frank, S.C. Tyler and F.S. Rowland, *Chem. Phys. Letters* 89 (1982) 9.
- [2] S.P. Wrigley and B.S. Rabinovitch, *Chem. Phys. Letters* 98 (1984) 386.
- [3] V. Lopez and R.A. Marcus, *Chem. Phys. Letters* 93 (1982) 2132.
- [4] K.N. Swamy and W.L. Hase, *J. Chem. Phys.* 82 (1985) 123.
- [5] V. Lopez, V. Fairen, S.M. Lederman and R.A. Marcus, *J. Chem. Phys.*, submitted for publication.
- [6] E.B. Wilson, J.C. Decius and P.C. Gross, *Molecular vibrations* (McGraw-Hill, New York, 1955) ch. 4.
- [7] E.A. Solov'ev, *Soviet Phys. JETP* 48 (1978) 635;
R.T. Skodje, F. Borondo and W.P. Reinhardt, *J. Chem. Phys.* 82 (1985) 4611;
B.R. Johnson, *J. Chem. Phys.* 83 (1985) 1204, and references therein.
- [8] E.L. Sibert III, J.T. Hynes and W.P. Reinhardt, *J. Chem. Phys.* 77 (1982) 3595;
J.S. Hutchinson, E.L. Sibert III and J.T. Hynes, *J. Chem. Phys.* 81 (1984) 1314.

Chapter 5: The Use of Artificial Intelligence Methods in Studying Quantum Intramolecular Vibrational Relaxation

[A modified version of the text of this chapter is being submitted to the Journal of Chemical Physics.]

The Use of Artificial Intelligence Methods in Studying Quantum Intramolecular Vibrational Relaxation

Steven M. Lederman and R. A. Marcus

*Arthur Amos Noyes Laboratory of Chemical Physics, † California Institute of
Technology, Pasadena, CA 91125*

Abstract

Artificial intelligence methods are used to treat the time evolution in intramolecular quantum dynamics. Comparison is made of several AI search algorithms and evaluation functions in an application to the study of quantum intramolecular vibrational relaxation. The methods developed are applied to an 11-coordinate heavy central mass problem and used to treat both quantum beats and “dissipative” intramolecular energy transfer.

I. Introduction

The quantum mechanical study of intramolecular vibrational relaxation (IVR) in complex molecules is often limited by the computational time associated with the use of a large number of states in high-dimensional systems. However, although a large number of vibrational states exist in the molecular system, only a small subset of these states might be involved in any particular excitation and ensuing dynamics of the molecule. This subset is limited, in part, by energetics and, in part, by couplings. The development of efficient and convenient methods that can identify the subset of important zeroth-order states should provide one approach to the practical solution of many IVR problems.

† Contribution No. 7694

In many IVR problems, a description of the redistribution of probability from an initial vibrational excitation is desired. This process can be viewed as the probability starting in an initial state and flowing through or between a series of states in the molecule. In this paper, AI techniques^{1,2} are used to find the most important subset of states from the many possible zeroth-order states. The states in the zeroth-order description can be ordered to form paths as illustrated in Fig. 1 and discussed in detail later. If any single state in a relevant path is excluded, the description of the dynamics can be dramatically changed. Thus, since entire paths are desired, the AI searching techniques, which generally find the most important paths first, are ideally suited as an aid in the solution of such quantum dynamics problems. Once the AI method finds the important subset of states, the dynamics can be analyzed, using this reduced block of states of the full Hamiltonian. With this subset of states, the specific search methods are designed to reproduce the important features of the dynamics of the full Hamiltonian.

Several papers have appeared that use a variety of AI techniques, for example, for solving multiphoton dynamics,³ vibrational eigenvalues,⁴ computational physics,⁵ and organic syntheses⁶ problems. These papers have shown the feasibility and success of a variety of AI methods in their respective applications. The strength of AI search methods lies in their ability to search efficiently many possible zeroth-order paths that could be important to the process. In the present case, the paths are found while utilizing the selection rules of the Hamiltonian which limit the possible non-zero coupled states, and a function is implemented that gives an estimate of the importance of each state in the actual dynamics.

In Sec. II, several search algorithms and their applicability to the IVR problem are discussed, while in Sec. III, a number of possible evaluation functions are examined for estimating the importance of possible zeroth-order states. An 11-dimensional model central mass IVR problem is described in Sec. IV and used in Sec. V for comparing the different search algorithms and evaluation functions.

The results of the different AI methods are discussed in Sec. VI, followed by some conclusions.

II. Search Algorithms

The use of AI methods in IVR combines the use of search algorithms and evaluation functions. The search algorithm determines the order in which possible zeroth-order paths are considered. The evaluation function is an estimate of the importance of the possible zeroth-order paths in the dynamics. The search algorithm will generally use the estimates of the evaluation function in deciding what path or paths to consider. Though these two concepts are not independent, the search algorithms are discussed in the present section and the evaluation functions are discussed in the next section.

There are a number of different types of search algorithms that have been proposed in the AI field; their efficiency and accuracy depends upon the type of problem to which they are applied.¹ In AI searching, the possible direct paths from an initial state (or states) are considered. Subsequent states in the possible paths are then considered, and in the process a *directed graph* or *tree* is formed in which each state is a *node* and the connections between the states are *directed arcs*. A path from an initial state can be found by following the directed arcs to a given destination state. One way to find the optimal path between these two states is to form the complete tree and consider all possible paths to decide definitely on the best possible path. However, since the tree can be extremely large, or even infinite, such a method is generally intractable for large (many-state) problems. The alternative is to construct intelligently only part of the tree, i.e., the *search tree* or *subtree*, which includes the most important paths for a given problem. The challenge in the AI search field is determining search techniques that can reliably and efficiently yield the important subtree.

In the IVR problem, the probability from the initial state will generally become

distributed over a few or many final zeroth-order states, the *goal states*. In this paper we focus on the two types of search algorithms that seem best suited to our problem in IVR. Both methods are combinations of beam and best-first searches.¹ A *beam search* considers all possible paths from *every* newly found state whose evaluation function is above a minimum value.⁷ A *best-first* search first considers the most promising of all incomplete paths. Although a beam search can be exhaustive, it can require inordinate amounts of computer time to find the best paths, especially when many couplings exist, as in our model. (The rapid escalation of states that have to be considered is the commonly referred to *combinatorial explosion*.) For this reason we use a compromise wherein a beam search is performed for the first two levels of searching, and then a best-first search is utilized thereafter. We found that using only a best-first search yielded less accurate results. Two search methods are used in the present article, each implemented utilizing the selection rules of the Hamiltonian to allow the algorithm to generate and explore only those states that have non-zero couplings from the state of interest. In AI terminology, the Hamiltonian can be used to form a special operator, the *successor operator*, which, applied to a chosen state, yields all states that can be directly reached in a single step from the chosen state. The process of applying the successor operator to the state chosen for consideration next has been termed *expanding* the state.

We use two specific algorithms, i.e., two search methods, for finding acceptable states. The first search algorithm, which will be referred to as the *best complete paths search*, accepts only states that form a complete path to one of a specified set of goal states. A *goal state* in this search method will be defined as one whose energy is within a given energy range of the initial state and whose evaluation function is above a certain minimum value. The intuitive reason for this type of search is that the prepared state (the initial state) has a certain spread σ in energy, which is time-invariant. The zeroth-order basis states, which will have large probability at long times, will be typically close in energy to the initial state. This feature can be

seen from the relationship of time and energy given by the uncertainty principle. In our calculations, a state will be chosen as a goal state if its energy difference from the initial state is less than twice the root mean square of the energy width σ of the wavefunction. Paths can include states that are outside the spread of the wavefunction, but these states are expected to have significant probability only for short times. Such states that are important at early times are frequently referred to in the literature on radiationless transition and IVR as doorway states. In the current best complete paths search, incomplete paths are not accepted, even if they have a higher evaluation function than a complete path. The minimum value of the evaluation function for a goal state was used so that the accepted paths had a reasonable contribution to the actual dynamics. The value was chosen through experience such that the excluded paths did not noticeably change the dynamics. With increasing deviation of the zeroth-order basis from the actual eigenstates of the system, the zeroth-order states that are farther away in energy from the initial state have a greater likelihood of having a significant probability at long times. This behavior could lead to important states' being difficult to find by the best complete paths search algorithm.

In a second search algorithm, which we shall term the *best incomplete paths search*, there is no insistence that acceptable states lead to any one of a specific set of goal states. In the searching, a beam search is again used for the first two levels in the search, and this search is followed by a best-first search for all subsequent steps. However, a goal state is now defined as the state that has the best evaluation function at *each* step of the best-first part of the search. These goal states are the same as the states that are expanded at each step of the best-first search. All states in the path to any such goal state at each step are accepted.

In each of our search algorithms we start from a given zeroth-order initial state and apply the successor operator to determine all states that are coupled to it. We assign a value of the evaluation function to each of these coupled states, states

which we will designate as S_1 . The successor operator is applied to all states in S_1 whose evaluation function is above a minimum value, one at a time. The newly formed states are called S_2 . The evaluation function associated with each path to states in S_2 is assigned. The minimum value in the beam search is chosen through experience such that the states eliminated from consideration have essentially no effect upon the dynamics. A balance is sought between including too many states in the beam search and eliminating states from consideration that may be important to the dynamics. At this point a beam search of the first two levels of the tree has been performed. The states in S_2 are sorted by their evaluation function. Duplicate states, i.e., the same zeroth-order state found from two different paths, are located in S_2 , and the state with lower evaluation function is removed from S_2 . The state in S_2 with the highest (best) evaluation function is removed from S_2 and selected for consideration next. The successor operator is applied to form a set of states, S_3 . The combined set of states of the new S_2 and S_3 are sorted by evaluation function, and duplicates are removed as before. The successor operator is applied to the state with the best evaluation function in $S_2 + S_3$ to form S_4 , and the state chosen to expand is removed from $S_2 + S_3$. All states in the new $(S_2 + S_3)$ and in S_4 are sorted with duplicates removed. The process is repeated until a desired number of states are chosen. These search algorithms are not limited in any way by the length of the path but use the evaluation function to determine the best possible paths to pursue.

An example of our two search algorithms is given below and illustrated in Fig. 1. Both methods in this example consider the same states in their search. In actual applications, the evaluation function and states considered can differ in the two search methods. The states are numbered in the order in which they are found, the first number above the line representing the number of each state and the next number giving the evaluation function for that state. Both searches begin with the initial state #1, and upon expansion by applying the successor operator find the two

states #2,#3 coupled to it which have, say, an evaluation function of 1.5 and 1.0, respectively. The successor operator is applied to state #2 and then to state #3, since they are both above the assumed minimum evaluation function value of 0.5 in the beam search. This procedure yields states #4,#5,#6. The beam search for the first two levels is now complete and the search continues as a best-first search. Of the states that have not yet been expanded (#4,#5,#6), the path to state #4 has the best evaluation function and state #4 is expanded to yield state #7. Let us suppose that state #7 is a duplicate of state #2. Since state #7 reached by the above path has a lower evaluation function than state #2, state #7 is removed from the list of states to be consider. (This removal is represented by the "X".) Of the remaining states not yet expanded (#5,#6), state #5 has the highest evaluation function. Application of the successor operator yields states #8,#9. The procedure up to now applies to both search methods used. We stop the search here for brevity of presentation and illustrate next the process of accepting the states.

The best complete paths search accepts only paths that lead to states that are within $\pm 2\sigma$ of the energy spread of the wavefunction of the initial state (represented by the dotted lines in Fig. 1) and that have at least the minimum value of the evaluation function. States #6,#9 are the only two states found by the search that are within $\pm 2\sigma$ of the initial state. If the minimum acceptable evaluation function to be a goal state is 0.3, only state #6 is a goal state. Since the path leading to state #6 is included, states #1,#3,#6 are accepted.

In the best incomplete paths search, the path is accepted that leads to the state with highest evaluation function among the set of states that have not yet been expanded during the best-first search process. Thus, state #4 with the path of states #1,#2 to state #4 is accepted first, since state #4 has the highest evaluation function of states #4,#5,#6. State #5 is accepted next, since it has the best evaluation function of states #5,#6, which are left after state #4 is expanded and duplicates removed. Since the path of states #1,#2 to state #5 is already accepted

with a higher evaluation function, the states #1,#2 are not included again. Finally, state #8 is accepted since it has the best evaluation function of states #6,#8,#9. Thus, the best incomplete paths search accepts states #1,#2,#4,#5,#8, whereas the best complete paths search accepts states #1,#3,#6.

III. Evaluation Functions

Any evaluation function must be simple enough so that it can be quickly calculated, in order to provide an easy evaluation of the many possible choices of paths. The three evaluation functions below are motivated by perturbative expressions. (A discussion of the perturbative expressions is given at the end of this section.) They heuristically combine terms for both the energy difference from the initial state and the energy difference from the previous state. If the initial state in a path is numbered 1 and the final state is numbered $n + 1$, there are $n - 1$ intermediate states and n links between the initial and final state. Three possible evaluation functions of this type are considered in this paper:

$$\begin{aligned}
 EF_1 &= \left| V_{12} \prod_{i=2}^n \frac{V_{i,i+1}}{\frac{1}{2}(\Delta E_{i,i+1} + \Delta E_{1,i+1})} \right| \\
 EF_2 &= \left| V_{12} \prod_{i=2}^n \frac{V_{i,i+1}}{\sqrt{(\Delta E_{i,i+1} \Delta E_{1,i+1})}} \right| \\
 EF_3 &= \left| V_{12} \frac{1}{\Delta E_{1,n+1}} \prod_{i=2}^n \frac{V_{i,i+1}}{\Delta E_{i,i+1}} \right|, \tag{1}
 \end{aligned}$$

where each factor after the product sign is set equal to unity whenever its magnitude exceeds unity in analogy to an approximately degenerate perturbation theory for the amplitudes. $V_{i,i+1}$ represents the matrix element between the i and $i + 1$ zeroth-order states and $\Delta E_{i,i+1}$ is the analogous energy difference. $\Delta E_{1,i+1}$ is the energy difference between the initial state and state i . The terms after the product sign are included only for n greater than one. (Incidentally, the use of our evaluation function, which is maximized, may be compared with the use of a cost function,

which is minimized.)

Evaluation functions EF_1 and EF_2 give an equal weighting to the two energy differences $\Delta E_{i,i+1}$ and $\Delta E_{1,i+1}$, whereas evaluation function EF_3 includes only the energy difference $\Delta E_{1,i+1}$ between the initial state and the *last* state in the path. These features lead to the property that evaluation functions EF_1 and EF_2 are monotonically decreasing functions of n , whereas EF_3 is not monotonic, since the energy difference from the initial state $\Delta E_{1,n+1}$ is taken only to the last state, $n+1$, in the path, and that state will change with increasing n . This non-monotonic property leads to greater difficulties in using evaluation function EF_3 , because its use is more likely to find paths with an evaluation function higher than that of some state previously chosen in the search. Furthermore, the units for the first step in EF_3 are different from those in all future steps. Because EF_3 generally caused a large reordering of the importance of paths by their evaluation function from level 1 to level 2, the minimum value for the evaluation function EF_3 in the beam search was set equal to zero, but not for the other evaluation functions. When the best complete paths search is performed using EF_3 , the $1/\Delta E_{i,i+1}$ term is deleted in computing the final evaluation function of the *final state*. This deletion is made since no energy preference is given here to one state over another within the spread of the wavefunction. (We also note that the deletion yields a final evaluation function in units of energy, the same units as EF_1 and EF_2 .)

From n^{th} order perturbation theory, one of the matrix elements between state 1 and state n in a path is⁸

$$EF_4 = |V_{\text{eff}}^n| = \left| V_{12} \prod_{i=2}^n \frac{V_{i,i+1}}{\Delta E_{1,i+1}} \right|, \quad (2)$$

when $V_{i,i+1}/\Delta E_{1,i+1}$ is small, and thereby when non-degenerate perturbation theory holds. (In the actual perturbation expression many other terms are actually present.⁸) One choice of the evaluation function would be to use Eq. (2), but with each $V_{i,i+1}/\Delta E_{1,i+1}$ set equal to unity whenever this factor exceeds unity, so as to

simulate very roughly the amplitude in degenerate perturbation theory.

An alternative effective matrix element would be to consider each step in the path as involved in an independent step-by-step perturbation and include only the energy difference between the i and $i + 1$ states:

$$EF_5 = |V_{\text{eff}}^n| = \left| V_{12} \prod_{i=2}^n \frac{V_{i,i+1}}{\Delta E_{i,i+1}} \right|, \quad (3)$$

with each $V_{i,i+1}/\Delta E_{i,i+1}$ being replaced by unity whenever it exceeds unity. The problem encountered with using EF_5 as the evaluation function is that it gives states with optimal evaluation function having no preference to be near the energy of the initial state. In tests of EF_5 , we sometimes found that the states with the largest couplings to the initial state are remote in energy from the initial state. Since all other steps in the path have some energy difference from the previous state in the denominator, the states with the best evaluation function would stay near the energy of the state in the first step, if Eq. (3) were used for the evaluation function. This result would lead to the best incomplete paths search wandering off to energies far from the initial state and to the best complete paths search never or only rarely finding complete paths that return nearly the amount of energy of the initial state in a reasonable amount of computer time.

Evaluation functions EF_1 , EF_2 and EF_3 represent three choices that heuristically combine both the energy difference to the initial state ($\Delta E_{1,i+1}$) and the energy difference to the previous state ($\Delta E_{i,i+1}$) to encourages searching of possibly dynamically important states. This choice combines the advantages of the two perturbation ideas in Eqs. (2) and (3).

IV. Model System

The AI methods were tested on an 11-dimension IVR problem involving a heavy central mass.⁹ The model represents the system $C_a - C_b - M - CD_2 - C_c$, where M is the central mass that can act as a barrier to energy redistribution in the

molecule and C and D denote carbon and deuterium atoms.¹⁰ C_a, C_b and C_c have as effective masses those of CH₃, CH₂ and CD₃, respectively. The Hamiltonian for the system is given by

$$H = H_L + H_R + V_{LR} , \quad (4)$$

where

$$H_L = \frac{1}{2} \sum_{i=1}^2 \sum_{j=1}^2 G_{ij} P_i P_j + \sum_{i=1}^2 D_i (1 - \exp[\alpha_i (r_i - r_i^e)])^2 \quad (5)$$

$$H_R = \frac{1}{2} \sum_{i=3}^{11} \sum_{j=3}^{11} \left[\left(G'_{ij} + \sum_{k=3}^{11} \frac{\partial G'_{ij}}{\partial r_k} r_k \right) P_i P_j \right] + \frac{1}{2} \sum_{i=3}^{11} k_i (r_i - r_i^e)^2 \quad (6)$$

$$V_{LR} = \lambda \frac{\cos \theta}{M} P_2 P_3 . \quad (7)$$

Here, r_i and P_i are the bond-coordinate and momentum, respectively. G_{ij} is the standard Wilson \mathbf{G} matrix¹¹ where its derivatives in Eq. (6) are evaluated at the equilibrium value of the bond-coordinates. The detailed parameters of this model are discussed elsewhere.¹⁰ H_L , the Hamiltonian for the left ligand of the molecule, contained two Morse potentials for a non-bending chain, and that for the right ligand, H_R , contained only harmonic potentials in the present tests. In addition, the kinetic energy coupling in H_R included a first-order correction to the equilibrium \mathbf{G} matrix term, thereby adding a non-quadratic term.¹² In the calculations, H_R was transformed into a normal mode coordinates Hamiltonian.¹¹

The Hamiltonian is written as having left (L) and right (R) contributions, so as to represent the physical notion of approximate separability of the motion of two ligands attached to a relatively heavy central atom. The basis set used in the calculations was the product of a wavefunction of H_L and one of the normal modes of H_R , the latter found when the derivatives of the \mathbf{G} matrix in H_R are omitted. H_L had been “pre-diagonalized” to yield wavefunctions of the left ligand, because of the high energies of excitation used for the left ligand. The λ parameter in V_{LR} allows for the variation of the kinetic coupling between left and right ligands in a

way that mimicked changing the central mass M . The advantage of using λ instead of actually changing the central mass is that the frequencies of the left and right ligands remained unchanged. Thus, a "pure" mass effect is achieved in this model calculation without the possibility of resonances' accidentally being modified.

The system was initially "prepared" in a zeroth-order state that had excess energy only in the left ligand (the initial wave function being a product of a pre-diagonalized state of H_L and the normal mode ground state of H_R). The quantum dynamics of the system was then determined by full matrix diagonalization of the zeroth-order basis set determined by the AI methods. A physical quantity of interest is the amount of energy in the left ligand of the molecule as a function of time because it indicates the amount of IVR occurring between the ligands.

V. Results

The two I search algorithms and the five evaluation functions were compared with the best exact" result, a result that was achievable in a reasonable amount of computer time by imposing a simple energy constraint on the zeroth-order states used in the calculation. In this large "exact" calculation, the basis set consisted of all zeroth-order states within 650 cm^{-1} in energy of the initial state. For the model system and excitations studied, there were then 1112 basis functions. In order to compare the AI methods to the exact result, the search was restricted to the set of the 1112 basis. These calculations were performed so as to compare the quality of different AI methods with the ultimate goal of using the developed techniques without constraint on the basis states chosen, both for this system and other systems. In the present comparison, λ in Eq. (7) is set to 0.5 and 0.1012, to represent masses of twice carbon and tin, respectively, and M in Eq. (7) has the mass of carbon. In the exact calculations, the lighter mass system showed a great dissipation of energy from the left ligand into the right, whereas the heavier system displayed, instead, vibrational quantum beats. Even though the latter

resembled largely an effective two-state problem in an eigenstate representation, it involved many zeroth-order basis states. These two situations, quantum beats and dissipation, represent different dynamical situations and serve to test the robustness of the present AI methods.

In Tables Ia and Ib, the different combinations of AI-search algorithms and evaluation functions are compared for the model system and for the conditions described. For all of these calculations, the AI methods were used to find the same number of basis states for the same initial conditions so that a direct comparison could be made. The number of states chosen was the number required to give an approximate convergence by the better methods (described later in Tables IIa and IIb). Two quantitative measures used to compare the different methods are the long-time average of the energy in the left ligand $\langle E_L \rangle$, and the spread of energies in the left ligand σ_{E_L} , given by

$$\begin{aligned} \langle E_L \rangle &= \lim_{T \rightarrow \infty} \frac{1}{T} \int_0^T E_L(t) dt \\ \langle E_L^2 \rangle &= \lim_{T \rightarrow \infty} \frac{1}{T} \int_0^T E_L^2(t) dt \\ \sigma_{E_L} &= [\langle E_L^2 \rangle - \langle E_L \rangle^2]^{\frac{1}{2}} . \end{aligned} \quad (8)$$

$\langle E_L \rangle$ indicates the average energy in the left ligand and σ_{E_L} is related to the amplitude of the energy fluctuations. An additional quantitative measure for the tin system (Tables Ia and Ib) is the time period τ_{FT} corresponding to the dominant peak in the Fourier transform of $E_L(t)$, since this time period (along with its amplitude) characterizes the dominant oscillation that acts as an *effective* two-state oscillation. (The dominant peak in the transform had a coefficient that was approximately one order of magnitude larger than the next most important peak.) All values in Tables Ia and Ib are given as the absolute value of the percent difference from the exact result. Although none of the methods are totally unacceptable, the best incomplete paths search with evaluation function EF_1 and the best complete paths

with evaluation function EF_3 gave the best overall results and are given at the top of Tables Ia and Ib. These two methods are seen to be the best at reproducing *both* types of dynamical situations. For the best incomplete paths search in Table Ia, the two evaluation functions EF_1 and EF_4 show good results. However, EF_1 gave a substantially better result than EF_4 for $|\% \Delta E_L|$ for the dissipative case and was the method chosen for further analysis in this investigation. The final row of Table Ia contains the results for evaluation function EF_1 , when a pure best-first search was performed for all levels of searching. As previously noted, these results using EF_1 in a pure best-first search are less accurate than those using E_1 in the combined beam search and best-first search in the proposed best incomplete paths search.

In Figs. 2 and 3, plots of the time behavior of the energy in the left ligand are given for the two best AI methods, for the two different dynamical situations given in Tables Ia and Ib and compared with the exact results. The short-time agreement is excellent and the overall agreement reasonable, confirming the quantitative numbers listed in Tables Ia and Ib. In Tables IIa and IIb, the convergence of the two best AI methods are shown as a function of the number of basis functions chosen. It shows that the two methods tend to approach the exact result as the number of basis states is increased for the quantitative measures used in Tables Ia and Ib.

An additional example is given in Table III, using these two best AI methods for the model Hamiltonian where the search for basis sets was not constrained by energy (i.e., where the condition $\Delta E \leq 650 \text{ cm}^{-1}$ was not imposed). No “exact” calculations are given now, since it was not presently computationally practical to include the many thousands of zeroth-order states that are within the range of energies included by the present AI results, when the dynamics is performed by full matrix diagonalization. The parameter λ was varied from 1 to 9.9 to mimic the masses of Sn, Ge, Ti, Si and C (where the central mass M in Eq. (7) is now that of Sn). In Table III the long-time average energy in the left ligand is given. The

agreement of the two different methods is very good, with the largest difference being for carbon, where the zeroth-order basis set is furthest from the eigenstates.

VI. Discussion

The results show that consideration must be given to both the type of search algorithm and the evaluation function used in IVR problems. It is seen in Tables Ia and Ib that the same evaluation function can give very different results when used with a different type of search algorithm. Furthermore, the results show that inclusion of a weighting factor employing both the energy difference from the initial state $\Delta E_{1,i+1}$ and from the previous state $\Delta E_{i,i+1}$ leads to a better AI evaluation function for our problem than the use of either one alone.

Of all the methods presented, the two best AI methods for reproducing *both* types of dynamical situations are listed, as already noted, at the top of Tables Ia and Ib. Even though they give similar qualitative results, implementation of these two methods is quite different. Evaluation function EF_3 can have both increases and decreases in the evaluation function, whereas EF_1 is monotonically decreasing. The variations in the value of EF_3 implies that a better path can be found at a later time in the search process from a path with a lower evaluation function. This situation leads to additional complications in verifying the convergence of the AI method when EF_3 is used. Furthermore, the best complete paths search needs additional AI parameters not present in the best incomplete paths search. One parameter is the minimum acceptable evaluation function for a *final* path, and the other is the assigned energy range for acceptable final states to form paths. It is also shown in Tables IIa and IIb that the best incomplete paths search, for the examples studied, converges more rapidly for most measures of accuracy than the best complete paths search. Additionally, Tables Ia and Ib show that the best incomplete paths search has a lesser dependence on the specific details of the evaluation function used than the best complete paths search. In summary, the

best incomplete paths search was easier to implement, and with it the AI searches were performed more quickly.

One useful feature of the AI method is in finding the states important to the dynamics. Originally, before we considered adopting an AI procedure to IVR, we had found some of the important states in an energy transfer path by considering the overlap (squared) of the wavefunction with each of the basis states as a function of time. By examining these overlaps as a function of time at very short times, six successive important states in a path were found for the $\lambda = 0.1012$ case. The states had greater than one percent overlap at all short-time points examined. However, both AI methods not only found these six states first in their searching, but then proceeded to find states with less than one percent overlap that were important to the dynamics. Without these additional states, the period of oscillation and the amplitude of the fluctuations of the energy in the left ligand as a function of time had an error of approximately 40%. Thus, these two AI methods found states of highest overlap first and then found states with small overlap but dynamically important.

It should be stressed that the AI search is performed within the set of zeroth-order states. Thus, the AI method is not a replacement for an intelligent choice of the model or the zeroth-order description. (Indeed, the A in AI might better denote "automated" rather than "artificial"!) The larger discrepancies between AI methods in Table III for carbon than for the other central atoms may be due to the much larger left/right couplings of the zeroth-order basis, because of the increased breakdown of the separation of variables for the left and right ligands in the case of a light central atom.

One final aspect is the amount of computer time required by the AI method to find the states of importance. Though our codes were not optimized for speed, the best incomplete paths search took 10 to 20 minutes on a VAX 11/780 for the results given in *Table III*. (The best complete paths search took 40 minutes to 3

hours.) Once the AI search was complete, the time to perform the dynamics for the 1000 states was then 150 seconds on a Cray X-MP, a time that may be loosely equated to 30 hours of VAX 11/780 time. Typically, in fact, the time spent doing the AI searches is a small percent of the total computer time needed to solve the problem.

VII. Conclusion

The development of AI search methods is seen to represent a significant step forward in the ability to study IVR problems with many degrees of freedom. The AI technique is a method of distinguishing the important dynamical states from thousands or millions of zeroth-order states. Explicit inclusion of millions of states is beyond the scope of currently available methods.¹³ Furthermore, the computer time necessary for performing the AI methods on higher energy excitations of a molecule is comparable to that in the case of lower molecular energies states, provided the number of possible states searched by the AI method is the same, even though the total number of available states increases exponentially with energy.

In this paper we have systematically compared several possible choices for search algorithms and evaluation functions. These comparisons, made for two common dynamical situations in IVR, quantum beats and dissipation, should prove helpful in the application of AI methods to a variety of IVR problems. The AI methods presented in this paper are implemented in a modular fashion, such that all of the search and decisions sections of the code can be easily used in any type of IVR problem. Only the sections of the code that involve the description of the Hamiltonian and the specific evaluation function desired need to be changed for each specific application. Thus, the current AI methods are not only extremely promising but can be easily applied to a large range of potential applications.

Acknowledgments

We would like to thank Stephen J. Klippenstein for particularly invaluable suggestions and discussions. We also thank Walter Nadler for his help in several aspects of this research as well as Vicente Lopez and Victor Fairen for their important contributions in developing the model Hamiltonian. It is a pleasure to acknowledge the support of the National Science Foundation, the U.S.-Spain Committee for Scientific and Technological Cooperation, and the Office of Naval Research.

References

- ¹ A. Barr and E.A. Feigenbaum, *The Handbook of Artificial Intelligence* (Heuris-Tech Press, Stanford, 1981) Vol I, Ch. II.; N.J. Nilsson, *Problem-Solving Methods in Artificial Intelligence* (McGraw-Hill, New York, 1971) Ch. 1-5; P.H. Winston, *Artificial Intelligence* (Addison-Wesley, Reading, 1984) Ch. 4.
- ² This method is different from the methods in electronic structure where millions of configurations are considered but only the lowest bound state energy is desired. See, for example, I. Shavitt in *Methods of Electronic Structure Theory*, edited by H. F. Schaefer (Plenum, New York, 1977), Ch. 6. Also, see B.O. Roos and P.E.M. Siegbahn, Ch. 7 in the same text.
- ³ J.V. Tietz and S.-I. Chu, Chem. Phys. Letters **101**, 446 (1983); J. Chang and R.E. Wyatt, Chem. Phys. Letters **121** 307 (1985); *ibid.*, J. Chem. Phys. **85**, 1826 (1986); *ibid.*, **85**, 1840 (1986).
- ⁴ J. Chang, N. Moiseyev and R.E. Wyatt, J. Chem. Phys. **84**, 4997 (1986).
- ⁵ G. Jacucci and M. Rasetti, J. Phys. Chem. **91**, 4970 (1987).
- ⁶ B.G. Buchanan and E.A. Feigenbaum in *Reading in Artificial Intelligence*, edited by B.L. Webber and N.J. Nilsson (Tioga Publishing Co., Palo Alto, 1981) pp. 313-322 and references cited therein.
- ⁷ A beam search reduces to a breadth-first search if the minimum value of the

evaluation function is zero.

- ⁸ A. Messiah, *Quantum Mechanics* (North-Holland, Amsterdam, 1963) Vol II, Ch. XVI, §16.
- ⁹ V. Lopez, V. Fairen, S.M. Lederman and R.A. Marcus, *J. Chem. Phys.* **84**, 5494 (1986); S.M. Lederman, V. Lopez, G.A. Voth and R.A. Marcus, *Chem. Phys. Letters* **124**, 93 (1986); V. Lopez and R.A. Marcus, *Chem. Phys. Letters* **93**, 232 (1982).
- ¹⁰ A detailed discussion of this model is in preparation; see S.M. Lederman, V. Lopez, V. Fairen, G.A. Voth, and R.A. Marcus.
- ¹¹ E.B. Wilson, J.C. Decius and P.C. Cross, *Molecular Vibrations* (Dover, New York, 1955).
- ¹² W.H. Green, W.D. Lawrance, C.B. Moore, *J. Chem. Phys.* **86**, 6000 (1987).
- ¹³ Several methods have been proposed for determining the approximate dynamical properties associated with a large calculation. These methods could presumably be used for performing the dynamical calculations on the basis states chosen by the AI methods. See, for example, A. Nauts and R.E. Wyatt, *Phys. Rev. Lett.* **51** 2238 (1983); W. Nadler and R.A. Marcus, *J. Chem. Phys.*, **86**, 6982 (1987); G.A. Voth and R.A. Marcus, *J. Chem. Phys.*, **84**, 2254 (1986).

Table Ia: Comparison of AI evaluation functions for best incomplete paths search^a

Evaluation	$\lambda = 0.1012, 70 \text{ states}^b$			$\lambda = 0.5, 20 \text{ states}^b$	
	$ \% \Delta \langle E_L \rangle ^c$	$ \% \Delta \sigma_{E_L} $	$ \% \Delta \tau_{FT} $	$ \% \Delta \langle E_L \rangle $	$ \% \Delta \sigma_{E_L} $
EF_1	1.7	14	6.6	2.3	14
EF_2	5.9	47	18	3.6	15
EF_3	4.4	35	34	3.1	14
EF_4	1.2	10	4.9	14	15
EF_5	1.4	11	20	0.86	35
EF_1^d	5.8	47	17	11	18

^aValues for “exact” results for $\lambda = 0.1012$ are $\langle E_L \rangle = 3834 \text{ cm}^{-1}$, $\sigma_{E_L} = 337 \text{ cm}^{-1}$, and $\tau_{FT} = 32 \text{ ps}$, where τ_{FT} is the period for the peak with the dominant amplitude in the Fourier transformation of E_L . For $\lambda = 0.5$, the values are $\langle E_L \rangle = 2521 \text{ cm}^{-1}$ and $\sigma_{E_L} = 316 \text{ cm}^{-1}$. The initial energy on the left is 4433 cm^{-1} , which includes a zero-point energy in the left ligand of 972 cm^{-1} . The minimum value in the beam search (except EF_3) was generally $1 \times 10^{-3} \text{ cm}^{-1}$. This compares with the smallest evaluation function for an accepted path, which was generally $1 \times 10^{-2} \text{ cm}^{-1}$ for $\lambda = 0.1012$ and 5.0 cm^{-1} for $\lambda = 0.5$.

^bThe total number of states sometimes varied by one, more or less, so that only complete paths were included.

^cDefined as $100(\langle E_L \rangle - \langle E_L^{\text{exact}} \rangle) / \langle E_L^{\text{exact}} \rangle$, and similarly for $\% \Delta \sigma_{E_L}$ and $\% \Delta \tau_{FT}$.

^dUses a pure best-first search, as discussed in the text.

Table Ib: Comparison of AI evaluation functions for best complete paths search^a

Evaluation	$\lambda = 0.1012, 70 \text{ states}^b$			$\lambda = 0.5, 20 \text{ states}^b$	
	$ \% \Delta \langle E_L \rangle ^c$	$ \% \Delta \sigma_{E_L} $	$ \% \Delta \tau_{FT} $	$ \% \Delta \langle E_L \rangle $	$ \% \Delta \sigma_{E_L} $
EF_3^d	2.2	18	10	3.7	15
EF_1	6.9	56	18	16	3.2
EF_2	6.5	52	19	16	3.2
EF_4	7.3	58	19	30	7.2
EF_5	5.1	41	19	17	12

^{a,b,c}See footnotes of Table Ia.

^dThe minimum value of the evaluation function for a goal state for EF_3 was $7.5 \times 10^{-3} \text{ cm}^{-1}$ for $\lambda = 0.1012$ and 10 cm^{-1} for $\lambda = 0.5$. The values for the other evaluation functions varied by their specific form and numerical value.

Table IIa: Comparison of convergence of two best AI methods as a function of number of basis states chosen for $\lambda = 0.1012$

# Basis	Best Incomplete Paths/ EF_1			Best Complete Paths/ EF_3		
	$\% \Delta \langle E_L \rangle$	$\% \Delta \sigma_{E_L}$	$\% \Delta \tau_{FT}$	$\% \Delta \langle E_L \rangle$	$\% \Delta \sigma_{E_L}$	$\% \Delta \tau_{FT}$
30	1.9	-13	-30	4.0	-30	-38
50	-7.6	61	22	0.72	-38	N.A. ^a
70	-1.7	14	6.6	-2.2	18	10
90	-3.6	1.1	4.6	-2.2	18	9.7

^aMethod fails to give only a single dominant period.

Table IIb: Comparison of convergence of two best AI methods as a function of number of basis states chosen for $\lambda = 0.5$

# Basis	Best Incomplete Paths/ EF_1		Best Complete Paths/ EF_3	
	$\% \Delta \langle E_L \rangle$	$\% \Delta \sigma_{E_L}$	$\% \Delta \langle E_L \rangle$	$\% \Delta \sigma_{E_L}$
10	17	20	14	5.7
20	2.3	14	3.7	15
30	-4.3	6.2	-2.7	12
40	-1.4	3.8	-0.29	11

Table III: Comparison of $\langle E_L \rangle$ for Two Best AI Methods on Model Hamiltonian with 1000 Basis States^a

Mass	Best Incomplete Paths/ EF_1	Best Complete Paths/ EF_3
	$\langle E_L \rangle$	$\langle E_L \rangle$
Sn	4120	4094
Ge	3627	3718 ^b
Ti	3465	3289
Si	2831	2736
C	2829	3226

^aThe initial energy on the left is 4582 cm^{-1} , which includes a zero-point energy in the left ligand of 727 cm^{-1} .

^bAI method was able to find only 717 states in a reasonable amount of computer time (less than 3 hours on a VAX 11/780).

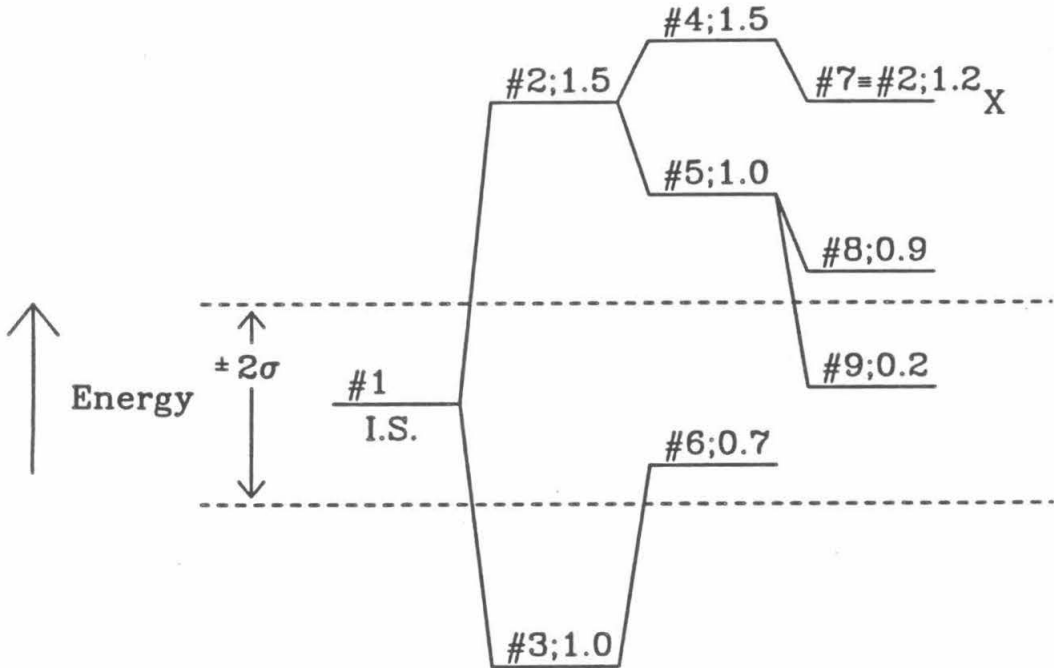


Fig. 1. Sample search tree for the two proposed search algorithms. The first number above each line is the number of the state and the second number the value of its evaluations function. The initial state (#1) has no evaluation function value associated with it. See text for discussion of search.

ENERGY ON LEFT AS A FUNCTION OF TIME FOR $\lambda = 0.1012$

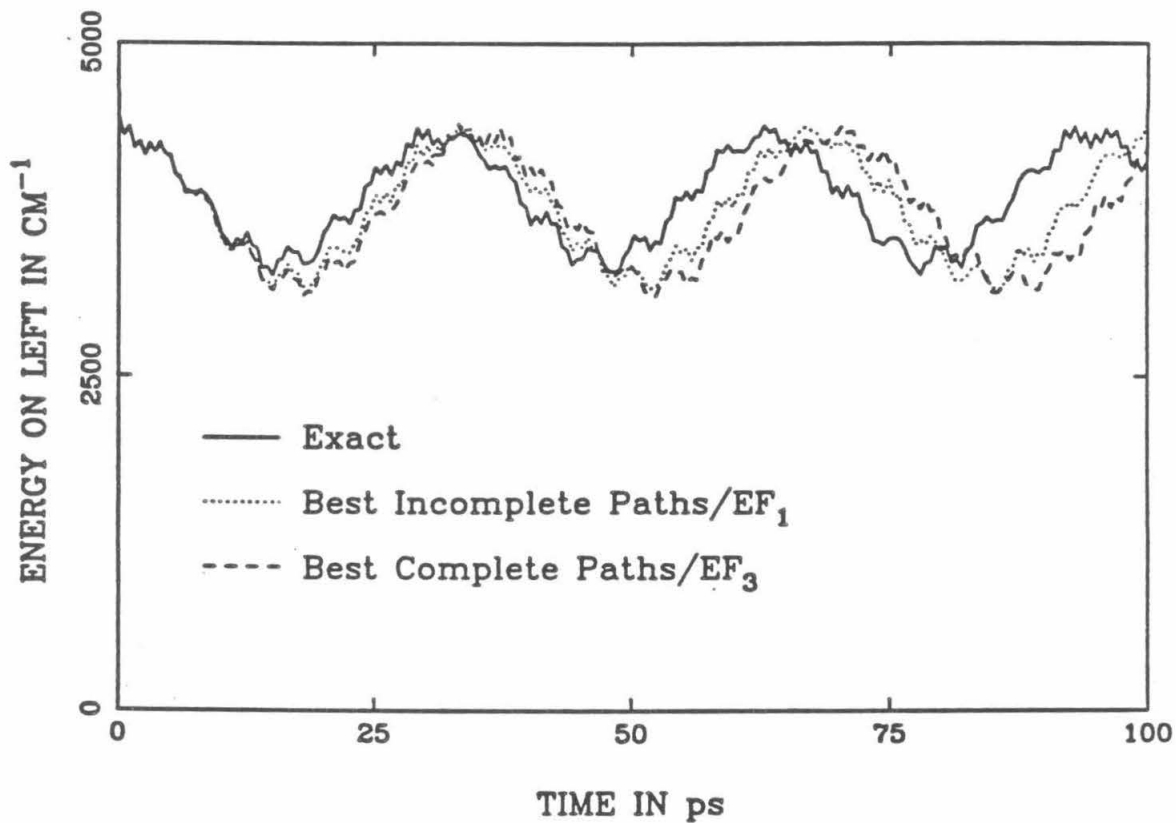


Fig. 2. Comparison of "exact" and two best AI methods for energy on the left as a function of time for $\lambda = 0.1012$ (Sn) for the conditions given in Tables Ia and Ib.

ENERGY ON LEFT AS A FUNCTION OF TIME FOR $\lambda = 0.5$

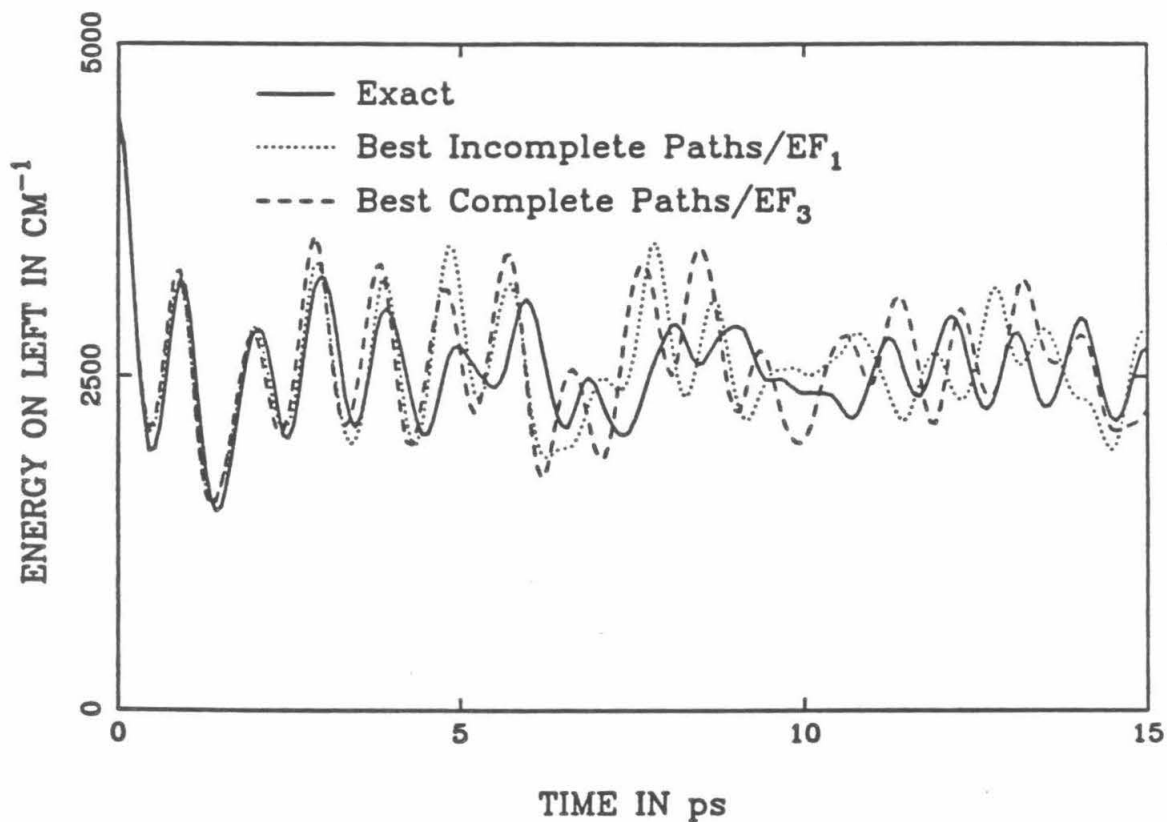


Fig. 3. Comparison of "exact" and two best AI methods for energy on the left as a function of time for $\lambda = 0.5$ (2C) for the conditions given in Tables Ia and Ib.